MODELING AND SIMULATION OF FORCED CIRCULATION EVAPORATION CRYSTALLIZER

Thesis submitted in partial
fulfillment of the requirement
for the degree of

Master of Technology
(Research)
In
Chemical Engineering
By

ANIS BAKHSH
(Roll No – 610CH308)

Under the guidance of

DR. H. M. JENA

2013

NATIONAL INSTITUTE OF TECHNOLOGY
ROURKELA, ODISHA

A

Thesis

On

MODELING AND SIMULATION OF FORCED CIRCULATION EVAPORATION CRYSTALLIZER

Submitted By

Anis Bakhsh

(610CH308)

Under the Supervision of

Dr. H. M. Jena

In partial fulfillment for the award of the Degree of

Master of Technology (Research)
In
Chemical Engineering

Department Of Chemical Engineering

National Institute Of Technology

Rourkela -769008,

Odisha, India

July 2013

Dedicated

To

My Parents& Family members

Department of Chemical Engineering
National Institute of Technology
Rourkela – 769 008,
Odisha, India

CERTIFICATE

This is to Certify that the thesis entitled "**Modeling and Simulation of Forced Circulation Evaporation Crystallizer",** submitted by **Anis Bakhsh,** Roll No. **610CH308** to National institute of technology, Rourkela is a record of bonafide research work under my supervision and is worthy of consideration for the award of the degree of Master of Technology (Research) in Chemical Engineering of the institute. The candidate has fulfilled all prescribed requirements and the thesis, which is based on candidate's own work, has not been submitted elsewhere for a degree or diploma.

Date:
Place: Rourkela

Supervisor: **Dr. H. M. Jena**
Assistant Professor
Department of Chemical Engineering
National Institute of Technology
Rourkela-769008.

Acknowledgement

I take this opportunity to express my profound gratitude and deep regards to my guides Dr. H. M. Jena and Dr. Shabina Khanam for his exemplary guidance, monitoring and constant encouragement throughout the course of this thesis. The blessing, help and guidance given by him time to time shall carry me a long way in the journey of life on which I am about to embark.

I take this opportunity to express my deep sense of gratitude to the members of my Master Scrutiny Committee Prof. P. Rath (HOD), Prof. (Mrs.) Abanti Sahoo of Chemical Engineering Department, Prof. D. Chaira of Material and Metallurgy Engineering Department and Prof. S. Biswas of Mechanical Engineering Department for thoughtful advice during discussion sessions. I am also thankful to Prof. K. C. Biswal, Prof R. K. Singh, Prof. M. Kundu, and other faculty members of department for constant encouragement and good wishes throughout the current work.

I am very much thankful to my senior Akhilesh Pravakaran Khapre, Divya Raja Vathsavai Gaurav Kumar, Rajib Ghosh Chaudhuri, Suman Chaudhuri, Arvind Kumar, Deepti Trimula, Pranati Sahoo, Bodhisattwa Chakraborty, Dhananjay Kumar, and Kailash Krishna Prasad; to my batch mates and friends Sambhurisha Mishra, Prince George, V. Balaji Patro, Rajesh Tripathy, Shivani Sharma, Tapash Ranjan, Manoj Mahapatra, Satya Sunder Mohanti and Rahul Omar to Prasnna Ravi, Sangram Patil and all other juniors for their cordial support, valuable information and guidance which helped me in completing this task through various stages.

Last but not the least, thank to my lovable parents, sister, brother, and sister in law, for incredible love and support and for the believing me unconditionally.

(Anis Bakhsh)

Contents

List of Tables

List of Figures

Nomenclature

a_p	linearized co-efficient for ϕ, -
a_{nb}	linearized co-efficient for ϕ_{nb}, -
A_c	area of a crystal, m^2
$\vec{A}_f$	area of face *f*, m^2
α	liquid (solution) phase, under-relaxation factor, -
α_p	under relaxation factor for pressure, -
β	vapor (gas) phase,-
b	net flow rate into the cell, m^3/s
c, c_i, c_s	concentrations of solute in bulk, interface and saturation, mol/m^3
C_D	drag co-efficient,-
$C_\mu, \sigma_k, \sigma_\epsilon$	coefficient in turbulent parameters,-
C_{1e}, C_{2e}	coefficient in turbulent parameters,-
C_V	mass coefficient,-
$C_{p,q}$	heat capacity at constant pressure, J/kg-K
d_f	diameter of face, m
d_b	diameter of bubble, m
d_s	diameter of solid particles, m
d_{32}	Crystals mean diameter, m
$D_{t,i\alpha}, D_i, D_\alpha$	diffusivities of phases, m^2/s
$\Gamma_\emptyset$	diffusion co-efficient for ϕ, -
ϵ_α	turbulence dissipation rate, m^2/s^3
f	drag function,-
$\vec{F}$	force vector, N
f_i	fraction of phase,-
$\vec{F}_D$	drag force, N

$\vec{F}_{\text{lift}}$	lift force, N
$\vec{F}_{\text{vm}}$	virtual mass force, N
ϕ	total volume fraction of secondary phase
ϕ_α	volume fraction of solution,-
ϕ_β	volume fraction of vapor,-
ϕ_f	value of ϕ convected through face *f*, -
ϕ_i	volume fraction of particle size i,-
ϕ_q, ϕ_p	volume fraction of phases q and p,-
ϕ_s	volume fraction of solid,-
$\nabla\phi$	gradient of ϕ, -
$\nabla.\phi_f$	gradient of ϕ at face *f*,-
$\vec{g}$	acceleration due to gravity, m/s^2
G	growth rate based on particle length, m/s
$G_{k,\alpha}$	production of turbulence kinetic energy, J/m^2
G_V	growth rate based on particle volume, m^2/s
h_{pq}	interphase heat transfer coefficient, W/m^2-K
h_q	enthalpy of phase, J/kg
i	dispersed phases,-
I	identity matrix
J_f	mass flux through face f, kg/m^2
J_f^*	face flux, N/m^2
J_f'	correction factor, -
k_α	turbulence kinetic energy, J/m^2
$k_{i\alpha}$	covariance of the velocities, m/s
k_L	mass transfer coefficient, m/s
κ_q	thermal conductivity of the q phase, W/m-K

k_r	rate constant,-
K_a, K_V	area and volume shape factors,-
K_{pq}	interphase momentum exchange coefficient, kg/s
$K_{\alpha\beta}$	liquid-vapor interphase exchange coefficient, kg/s
$K_{\alpha s}$	liquid-solid interphase exchange coefficient, kg/s
L	length of crystals, m
$L_{t,\alpha}$	length of turbulent eddies, m
L_i	length density of crystals, no. of crystals/m^4
ΔL	crystal size interval, m
λ_q	bulk viscosity of phase *q*, Pa s
m_k	moment,-
m_0, m_1, m_2	zeroth, first and second moments,-
$\dot{m}$	mass transfer rate, kg/m^3-s
m_c	mass of single crystal, kg
$\vec{M}_{i,q}$	interphase force, N
$\vec{M}_{D,pq}$	interphase drag force, N
$\vec{M}_{D,\alpha\beta}$	liquid-vapor interphase drag force, N
$\vec{M}_{D,\alpha s}$	liquid-solid interphase drag force, N
μ_α	viscosity of phase *q*, Pa s
μ_q	viscosity of phase *q*, Pa s
$\mu_{t,\alpha}$	turbulent viscosity, Pa s
n	number density, no. of particles/m^3
nb	neighbour cell, -
$\dot{n}_0$	nucleation rate, no. of particles/m^3-s
N	number of phases
ΔN	number of particles

N_i	number density of crystals, no. of crystals/m^3
N_{face}	number of face enclosing cell
Nu_p	Nusselt number
p	pressure, Pa
p	secondary phase,-
p'	pressure correction, Pa
p^*	guessed pressure, Pa
p'_{C_0}	cell pressure correction, Pa
p_q	pressure of phase *q*, Pa
Pr	Prandtl number
q	phase
$\vec{q}_q$	heat flux, W/m^2
$Q_{i,q}$	interphase heat exchange, W
Re	Reynolds number
ρ_α	density of liquid α, kg/m^3
ρ_β	density of vapor β, kg/m^3
ρ_f	density of ϕ convected through face *f*, kg/m^3
ρ_i	density of dispersed phase, kg/m^3
ρ_q	density of phase *q*, kg/m^3
ρ_s	density of solid particles *s*, kg/m^3
S_q	heat source term, kw/m^3
S_ϕ	source of ϕ per unit volume, -
$\sigma_{i\alpha}$	dispersion Prandtl number
t	time, s
T_p, T_q	temperature of phases, K
$\bar{\bar{\tau}}_\alpha$	stress-strain tensor of liquid α, Pa

$\bar{\bar{\tau}}_q$	stress-strain tensor of phase *q*, Pa
τ_β	particulate (bubbles) relaxation time, s
τ_s	particulate relaxation time, s
$\tau_{t,\alpha}$	characteristic time of the energetic turbulent eddies, s
$\tau_{t,i\alpha}$	integral time, m/s
$\tau_{F,i\alpha}$	particle relaxation time related to inertial force, s
$\vec{u}_{dr}$	drift velocity, m/s
$\vec{u}_{i\alpha}$	relative velocity, m/s
$\vec{u}_q$	velocity of phase *q*, m/s
$\vec{u}_p$	velocity of phase *p*, m/s
$\vec{u}_s$	velocity of solid phase, m/s
$\vec{u}_{pq}, \vec{u}_{qp}$	interphase velocities, m/s
U_t	terminal settling velocity, m/s
$\vec{U}_\alpha$	phase-weighted velocity, m/s
$\vec{U}_i$	dispersed phase-weighted velocity dispersed, m/s
$\vec{v}_f$	velocity of ϕ at face *f*, m/s
V	cell volume, m^3
V, V', V_i	volume of phases, m^3
$\vec{x}$	co-ordinate of the particle position
$\prod_{k_\alpha}, \prod_{\epsilon_\alpha}$	influence of the dispersed phase on the continuous phase,-

Abbreviations

APIs	active pharmaceutical ingredients
CFD	computational fluid dynamic
CSD	crystal size distribution
CV	coefficient of variation
DDT	double draft tube

DT	draft tube
DTM	draft tube magma
DTB	draft tube baffle
FB	fluidized bed
FC	force circulation
FS	fluidized Suspension
FVM	finite volume method
MSMPR	mixed suspension mixed product removal
PBM	population balance model or method
PSD	particle size distribution
QMOM	quadrature method of moments
RTD	residence time distribution
SIMPLE	semi-implicit method for pressure linked equations
STR	stir tank reactor (stirred vessel)
SMM	standard method of moments
VOF	volume of fluid

Abstract

Crystallization is an effective process of forming a solid phase from solution and crystallizer is the equipment used for industrial crystallization operations. There has been a lot of experimental research work carried out for understanding and improving crystallization operations in the past years, several aspects relating to the crystal growth, nucleation, breakage, type of crystallization process, design of crystallizer and scale up of crystallizers. It is difficult to analyze complex hydrodynamic behaviour in crystallizer by experiment. In last decade a good number of works has been carried out using CFD simulation for different types of crystallizers to study the flow dynamics and crystal formation. In present work flow behavior, solid suspension distribution, population density and mean crystal growth studies have been carried out for the forced circulation evaporation crystallizer (FC crystallizer) by CFD simulations using software package; Ansys Fluent 13. The FC crystallizer is a continuously operating mixed suspension mixed product removal (MSMPR) type crystallizer used in salt, sugar and pharmaceutical industries for crystal production. In the present work simulation has been carried out in isothermal and non-isothermal conditions to characterize the hydrodynamics and population balance model to explain the population density. 3D modified computational geometries have been used to observe the vigorous 3D multiphase flow by Eulerian model. The process of crystallization of NaCl from its solution has been used for simulation. NaCl solution and water vapor has been considered as the two phase liquid and gas. Water and solid particles (NaCl) as two phase has been used to see the crystal size distribution. For population density study all three phases: NaCl solution, NaCl crystals, and vapor has been considered. RNG k-ϵ model has been used for turbulent fluctuations of velocities in multiphase phase flow. The present work is carried out under varying conditions of flow rates and inlet positions. From the results it is observed that phase distribution, velocity profiles and pressure is changing with change in flow rates for isothermal and non-isothermal both conditions Increase in inlet height found to affect the vapor distribution. Flow rate and inlet position are affecting the suspension distribution in crystallizer. Better distribution of crystals is seen for higher flow rate of solution and for inlet at higher position. Population density of large crystals and mean crystal size is found to increase with time.

Keywords: phase separation, solid suspension, crystal size distribution, population density, mean crystal size growth, FC crystallizer.

CHAPTER-1

INTRODUCTION AND LITERATURE

Crystallization is the (natural or artificial) process of formation of solid crystals precipitating from a solution, melt or more rarely deposited directly from a gas. It is considered as important and effective solid-fluid separation process (Essemiani et al., 2004). This process occurs due to phase transformation of one or more substances from a liquid, amorphous solid or gaseous condition to a crystalline state (Tangtonsakulwong et al., 2006; Geankoplis, 2007). The recovery of sodium chloride in solid crystalline form from water by using evaporative crystallization phenomena is one of the ancient known separation operations (Wohlk and Hofmann, 1987; Seader et al., 2011). Majority of the industrial crystallization processes carried out from solutions (Perry, 2009). Generally in case of solution crystallization a species crystallizes from its liquid mixture when the solute (species) concentration has become more than its solubility. The term used for this condition of solution is supersaturation, so it is an important factor for crystallization. In crystallization supersaturation can be achieved by the processes such as cooling, evaporation, vacuum, pressure, and reaction, or in some conditions combination of these processes (Geankoplis, 2007). Evaporative crystallization is the most common crystallization process used in maximum industrial crystallizers. In this process the mixture is heated to reach the condition of supersaturation by the evaporation of solvent. Crystallization is required for the manufacturing of a; large range of materials from bulk commodity chemicals to very distinctive chemicals and pharmaceutical products.

1.1. Crystallization processes

There are several processes that can be achieved by crystallization as;

- ***Separation*:** All separation techniques involve formation of another phase from the feed and according to the selected processing conditions relatively easy segregation of the resulting phases occur. Na_2CO_3 (Sodium carbonate) is recovered from a brine by first contacting the brine with CO_2 to form $NaHCO_3$ (Sodium bi carbonate) which has a lower solubility than Na_2CO_3 and it can be readily crystallized. The primary function of crystallization in this process is separation; a high percentage of $NaHCO_3$ is solidified in a form that makes subsequent separation of the crystals from the mother liquor economical with the available pressure drop across filters that separate liquid

and solid, the capacity of the process is determined by the rate at which liquor flow through the cake. The rate is set by the crystal size distribution (CSD) produced in the crystallizer. Separation of a chemical species from a mixture of similar compounds can also be achieved by melt crystallization (cooling melt), which is e.g., an important means of separating "bisphenol A" from the mixture of substances after the reaction. Bisphenol A is crystalized on the inner surface of a tube bundle while the circulated melt flows from top to bottom on the outside of the tubes, the coolant is flowing also from top to bottom (co-current). The crystalline material is recovered by melting the residue is discharged in liquid form; in this batch operation very high purities can be achieved if necessary by additional purification steps like sweating or by further crystallization stages with the product of each previous stage until the desired purity is reached. Stripping stages for the required yield are also possible (Kirk-Othmer, 2008).

- ***Concentration*:** The concentration of fruit juice requires removal of solvent (water) from the natural juice. This concentration is commonly done by evaporation, but the derived juices may lose flavor components during evaporation. In freeze concentration, solvent is crystallized (frozen) in relatively pure form to leave behind a solution with a solute concentration higher than the original mixture. Significant advantages in product taste have been observed in the application of this process to concentration of certain fruit juices (Kirk-Othmer, 2008).
- ***Purification*:** The objective of crystallization also can be purification of a chemical species; well known in examples this respect are sugar and salt. L-isoleucin (an essential amino acid), is separated by crystallization from a fermentation broth that has been filtered and subjected to ion exchange. The recovered crystals contain impurities deleterious to use of the product and these crystals are therefore redissolved and recrystallized to enhance purity (Kirk-Othmer, 2008).
- ***Solidification*:** Production of a product in a form suitable for use and acceptable to the consumer also may be an objective of a crystallization process. For example, the appearance of sucrose (sugar) varies with local customs and deviation from that custom could lead to an unacceptable product. A final crystallization may thus be called for to bring the product appearance into compliance with expectations. Another example, liquid sulfur that has to be solidified and is liquid sulfur that is solidified as pastilles to provide for a free flowing dust free product (Kirk-Othmer, 2008).

- ***Analysis*:** Many analytical procedures calling for determination of molecular structure are aided by crystallization or require that the unknown compound be crystalline (Kirk-Othmer, 2008).

1.2. Advantages and Disadvantages of crystallization

Crystallization offers the various advantages such as;

- Crystallization is important as an industrial process because of the number of materials that are and can be marketed in the form of crystal.
- Pure product (solute) can be recovered in one separation stage. With care in design, product purity greater than 99% can be attained in a single stage of crystallization, separation and washing.
- A solid phase is formed that is subdivided into discrete particles. Generally, conditions are controlled so that the crystals have the desired physical form for direct packaging and sale (Moyers (Jr.) and Rousseau, 2009).
- In terms of energy requirements crystallization requires much less energy for separation than distillation and other commonly used methods of purification.
- It can be performed at relatively low temperatures and on a scale which varies from a few grams up to thousands of tons per day (Kirk-Othmer, 2008).

The major disadvantages of crystallization are;

- Purification more than one component is not normally attainable in one stage.
- The phase behaviour of crystallizing systems prohibits full solute recovery in one stage; thus, the use of additional equipment to remove solute completely from the remaining crystallizer solution is necessary (Moyers (Jr.) and Rousseau, 2009).

1.3. Application of crystallization

Crystallization is an effective separation process which is applied in various process industries as;

- In the food industry, crystallization may serve for the recovery of crystalline products – (sugar, glucose, lactose, citric acid, salt), for the removal of certain undesirable components or for modification of certain food products in order to obtain a desirable structure.

- Crystallization shows the important role in the pharmaceutical industry as it is started from intermediates separation process and the final manufacture step as active pharmaceutical ingredients (APIs).
- The crystallization used to provide the production requirements as crystal size and purity in fertilizer products such as ammonium sulfate, potassium chloride, potassium sulfate and potassium nitrate
- The crystallization process is used in paper and pulp industry for black liquor concentration and in Chloride Removal Process.
- In metal and mining industries crystallization applied to recover inorganic compounds for example, in the refining of nickel from mined ores crystallizers recover fertilizer grade ammonium sulfate generated (Veoila, 2013).

1.4. Process of solution crystallization

Crystallization may be described as a solid–fluid separation process in which crystalline particles are formed from a solution (Seader et al., 2011). A solution is a homogeneous single phase mixture that is formed by the mixing of two or more species. Solutions are normally liquid; however at time, it may be solids and even gases too (Wantha, 2006). Typically the term solution means a liquid solution, consisting of a liquid (solvent) generally water at the conditions, (*T, P*), of the solution, and one or more dissolved species those are solid in their pure form (solute) at the conditions of interest (Bennett, 2000). The term melt means a material that is solid at ambient conditions and is heated until it becomes a molten liquid. Melts may be pure material or they may be a mixture of materials. Crystallization from solution occurs when the solution is supersaturated i.e. it contains more of the dissolved material than could be dissolved by the solvent under normal circumstances. Fig. 1.1 displays the solubility of a general solution by solubility curve where C_s denotes saturation concentration; area under curve is considered as under-saturated (where any crystal present will redissolve). The area above solubility curve is considered as metastable zone in which nucleation does not occur but crystals can grow. In the supersaturated or labile zone, the concentration of the solution is above the solubility curve, spontaneous nucleation and rapid crystal growth occurs and relative supersaturation is defined as,

$$S = (C - C_S) / C_S \tag{1.1}$$

Crystallization at different super-saturation conditions gives poor crystal size distribution (CSD) due to presence of various sizes and shapes of crystals. Therefore, a good crystal size distribution (CSD) can be induced by maintaining the uniform supersaturation throughout the crystallizer and this is achieved by the proper mixing in the crystallizer.

Industrial crystallization from a solution is accomplished in a large range of processing equipment, but a general schematic can be drawn as in Fig. 1.2. If looking at the general period of operation the streams shown may be present, or absent from a particular type of operation.

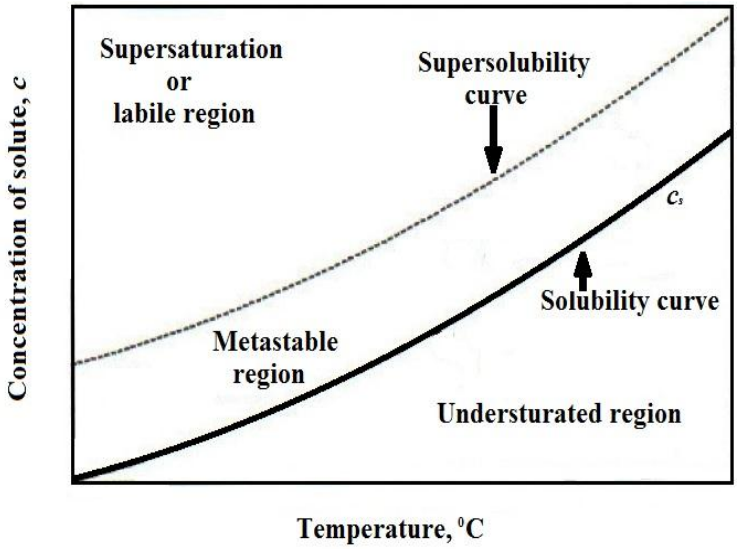

Fig. 1.1. Solubility of a general solution (Bennett, 2000).

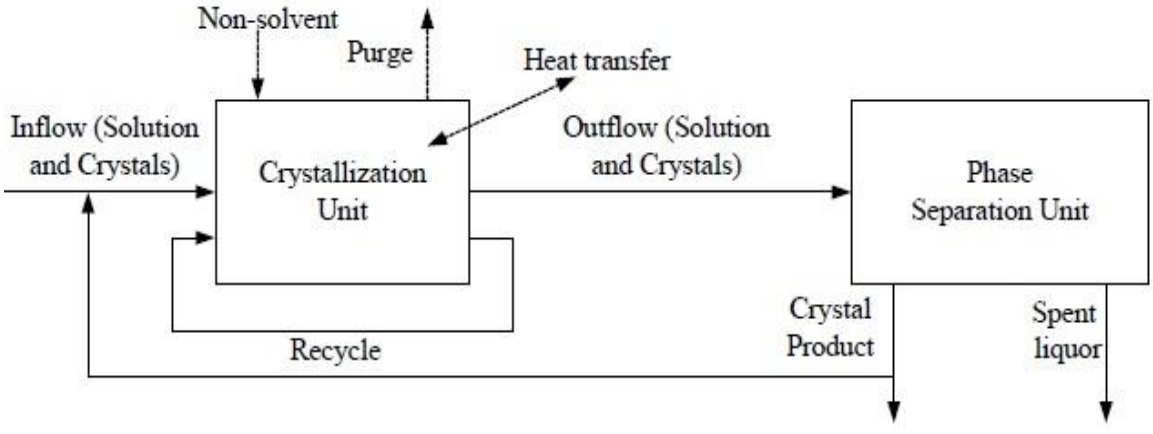

Fig. 1.2. General schematic of a crystallization process (Wantha, 2006).

1.5. Modes of crystallization

The techniques employed to carry out crystallization from solution is referred to as the modes. Various modes for crystallization are;

1.5.1. Crystallization in continuous, steady-state process

Crystallization in continuous, steady state process conditions in a crystallizer is achieved when mass flow rates of the inflow stream and the outflow stream are equal. There is (essentially) no time variation in any of the crystal or fluid properties in the unit. The unit does not operate at equilibrium conditions at any time period (Wantha, 2006).

1.5.2. Crystallization in batch process

In such type of crystallizers, either there is no inflow as well as outflow streams (which is called batch mode) or any one of the two (inflow or outflow) stream does not exits (these are known as semi-batch mode crystallizers). The fluid and physical properties in the vessel will vary with time (unsteady-state) during the batch. The contents of the vessel may be allowed for enough time to reach a state that is very close to the equilibrium condition, or the batch may be completed before this time. This crystallizer is not common for large scale operations since batch crystallizers usually requires larger operating and equipment cost. The main advantages of batch crystallizers are that they can produce a narrow range of product crystal sizes, can sometimes produce slightly more pure products, and are very flexible for plants that produce small quantities of a wide range of products (Wantha, 2006).

1.5.3. Crystallization by seeds

In this method tiny solid particles of solute are added to the feed of the crystallizer to initiate crystallization. The purpose of this operation is to remove the requirement to operate at driving forces high enough to produce nuclei (since crystals already exist in the liquor the nucleation step is not required), or to promote the formation of low numbers of nuclei at low driving forces. Seeding may be performed in both batch as well as continuous crystallizers (Wantha, 2006).

1.5.4. Crystallization by cooling

The crystallization by cooling can be carried out in case where solubility of the solute is steep or when the solubility of solute greatly increases with increase in temperature; $NaNO_3$, $(NH_4)_2CO_3$, $NaClO_3$, KNO_3, etc. are examples of solutes exhibiting this type of solubility (see Fig. 1.3). The simplest example of this process is where the solution is evaporated at high temperature, where the solubility is high (the solution is under-saturated) before being fed to the crystallizer. This feed solution is cooled either via an external jacket or a cooler inside the crystallizer until the crystallizing species becomes

supersaturated (while the amount of solute remains constant), and thus crystal is produced (Mersmann, 2001; Wantha, 2006; GEA Messo, 2011).

1.5.5. Crystallization by evaporation

The crystallization by evaporation can be carried out in cases where solubility of the solute is less conditional i.e. it increases only slightly, remains almost constant, or even decreases with temperature (e.g. NaCl) (see Fig. 1.3). The concepts of this mode are that the under-saturated solution is fed into the crystallizer, and then this feed solution is heated to the boiling point of the solution so that the solvent evaporates. The feed solution is heated via an external jacket, a heater inside the crystallizer and in some cases through an external heat exchanger (Mersmann, 2001; Wantha, 2006; GEA Messo, 2011).

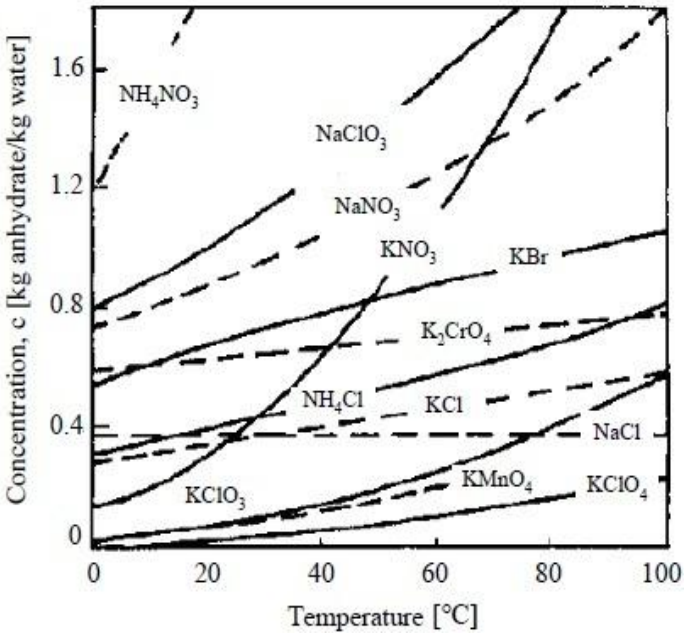

Fig. 1.3. Solubility curves for several components (Mersmann, 2001).

1.5.6. Crystallization under vacuum

In this case the solution is evaporated and cooled simultaneously by decreasing the temperature and pressure. The vacuum is often created above the liquid level and maintained by steam jet compressors (Mersmann, 2001). When the evaporation occurs, the solution loses the energy required to evaporate the solvent (heat of evaporation) causing the solution to cool and become supersaturated (in addition to the supersaturation caused by solvent loss), and thus partially crystallize.

1.5.7. Crystallization by non-solvent (drowning-out)

The supersaturation required for the crystallization is achieved through the addition of a solvent designed to reduce the solubility of the solute, the process is known as a non-solvent or anti-solvent crystallization. The addition of other solutes (other crystallizable species; species not considered as solvents) designed to reduce solubility is known as drowning-out crystallization. Drowning-out crystallization may offer the advantage over other processes of reducing energy consumption (Mersmann, 2001). As the enthalpy of evaporation of drowning-out agents is usually considerably smaller than that for solvent the drowning-out agent can be recovered easily by distillation. This process can be combined with other processes that enable energy to be saved.

1.5.8. Crystallization in pressure

Crystallization under pressure is a process applied when the solubility increases with temperature until it reaches a maximum, after which the solubility decreases as the temperature increases (see Fig. 1.4). This applies to salt solution, such as Na_2SO_4 and Na_2SO_3. This method occurs when aqueous solutions of these salts are held under pressure to avoid evaporation of solvent, and are heated above the temperature of their maximum solubility; at this point nuclei form and grow due to supersaturation (Mersmann, 2001; Wantha, 2006).

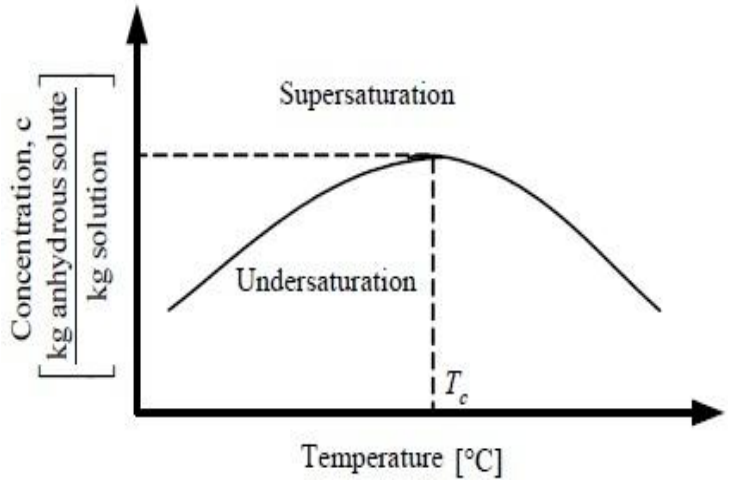

Fig. 1.4. Solubility of the solutions (Wantha, 2006).

1.5.9. Crystallization by reaction (precipitation)

Crystallization by reaction, also called precipitation is carried out by a chemical reaction between two soluble components which results to a less soluble product that is first

achieve saturation and then supersaturation for crystallization. One or more reactants react with one or more components in the liquid phase for homogeneous reaction crystallization, and a reactant is often added in the gas or vapor form for heterogeneous reaction crystallization (Bamforth, 1965; Mersmann, 2001; Wantha, 2006).

1.6. Crystallizer

Crystallizer is the operating equipment applied for crystallization of any material from its solution. These are employed in various process industries like sugar, salt, food, fine chemicals and pharmaceutical. The general classification of crystallizers on the basis of process by which crystallization achieved is shown in Table 1.1 (Geankoplis, 2007).

Table 1.1: Classification of crystallizers

Basis	Type	Example
Mode of operation	Batch crystallizer	Stir-tank crystallizer
	Continuous crystallizer	Swenson-Walker, FC and DTB crystallizers
Method through which supersaturation is occurred	Cooling alone	Agitated tank crystallizers, Swenson-Walker
	Adiabatic evaporation and cooling	Vacuum crystallizers
	Evaporation	Krystal crystallizers, Draft - tube crystallizers

Continuous crystallizers are commonly used for production of chemicals in industries, due to their efficiency of operation, reduction in the requirements for manpower and uniform quality of product (Wohlk and Hofmann, 1987). Some general types of continuous crystallizers are; forced circulation (FC), draft-tube-baffle (DTB), and fluidized-suspension (FS) units used in mixed suspension mixed product removal (MSMPR) mode to produce large size crystals. In MSMPR mode liquid phase and the solid phase are perfectly mixed, and the particle size distribution of the product crystals is the same as in the crystallizer. These crystallizers are designed to modify the crystal size distribution (CSD) by the systems of fines destruction, and clear liquid advance to change the slurry density or product classification (Wantha, 2006).

Industrial crystallizers scale-up and design is the most complicated work in process engineering and there are various facts to observe such as yield, selectivity, purity, and particle size distribution (PSD). The process can simplify for separation with an increase in particle size so the prediction of the PSD is one of the important part of the crystallizer design (Zhu and Wei, 2008). The particle size distribution is commonly modeled by population balance equations as a function of process conditions, crystallizer layout and type of crystallization process. This equation is used to describe the crystal population distribution dynamics. It can be influenced through hydrodynamics, directly linked to flow required for mixing, heat and mass transfer; and solid suspension.

1.7. Crystallizers used in industries

In industries crystallization is essentially a purification and concentration process (Bamforth, 1965) achieved by forming crystals from a solution in a crystallizer. For proper crystallization the suspension must be mixed, and deposition onto the equipment must be avoided by use of a circulating device; stirrer or pump. In the former case, relatively strong attrition occurs, especially of large crystals. Fig. 1.5 shows typical industrial crystallizers. The fluidized bed (FB) crystallizer (see Fig. 1.5 (c)) differs from other crystallizers by the fact that a suspension flow containing only small crystals e.g. under 100 μm; is conducted by the circulation device (pump). Since the larger crystals are heavier than the smaller ones so the small size crystals flow up by the pump and create a fluidized bed, and the large size crystals settle at the bottom tank by the gravitational force and flow out to be the products. Therefore, FB crystallizers generally produce a coarser product than stirred vessel (STR) (see Fig. 1.5 (a)) and forced-circulation (FC) crystallizers (see Fig. 1.5 (b)). The advantage of the FC and the FB over the STR is that the ratio of the heat exchanger surface to the crystallizer volume can be maintained when scaling up the crystallizers due to the external heat exchanger (Mersmann, 2001; Wantha, 2006).

Fig. 1.5 (d) displays a cooling crystallizer with an external heat exchanger. A small flow of warm, concentrated inlet solution is added directly to the much larger circulating flow upstream of the heat exchanger. The supersaturated solution in the heat exchanger enters the crystallization chamber at bottom of the crystallizer and suspends the crystals. Despite the minimal temperature difference allowed usually less than 2 K, between the circulated solution and solvent, high heat flux densities can be obtained. The solid is separated by

enlarging the flow cross-section. The growing crystals sink to lower levels by their rate of sedimentation until they finally reach the product outlet (Mersmann, 2001; Wantha, 2006).

Fig. 1.5 (e) displays an elementary design of evaporative crystallizer with an external heat exchanger which is a heater (Svanoe, 1940); the crystallization process seems similar to the cooling crystallizer but has a different way for obtaining supersaturation that is evaporation rather than cooling (Wantha, 2006). In this design evaporation and crystallizer units are joined together to make crystallization vessel. The crystallization vessel is connected to the heat exchanger by a circulation pump and the fresh solution is fed into this circulation system for crystallization (Mersmann, 2001).

Fig. 1.5 (f) displays outlines of a vacuum cooling crystallizer with distinguish crystallization and evaporation chambers. This does not have a heat exchanger in the crystallizer, and uses an open vessel under atmospheric pressure as the crystallization vessel. Hot saturated feed enters at the suction pump, and mixes with the mother liquor passing through pump, and is then cooled back to the crystallizer temperature by evaporation in the evaporation chamber (Wantha, 2006). The difference in pressure relative to the vacuum part is compensated by the hydrostatic pressure of the liquid (Mersmann, 2001).

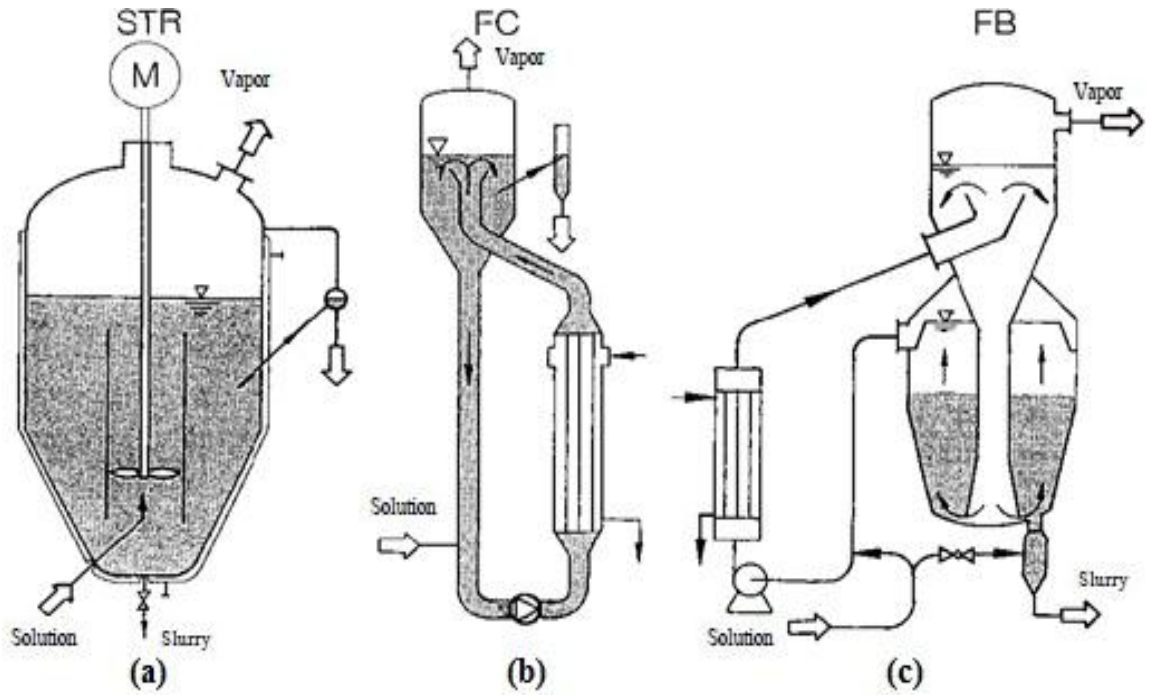

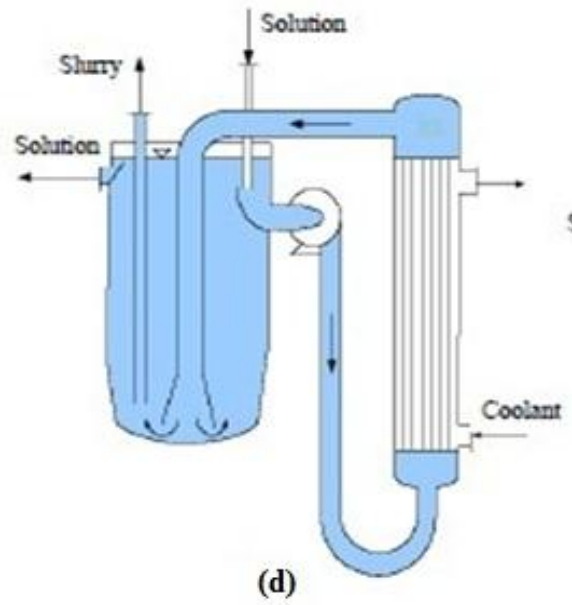
Solution
Slurry
Solution
Coolant

(d)

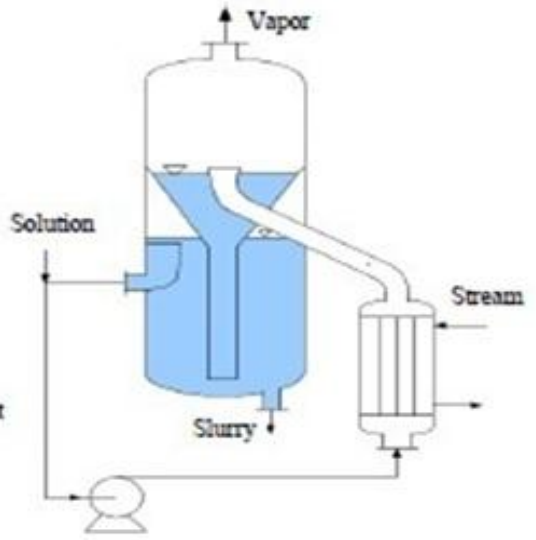
Vapor
Solution
Stream
Slurry

(e)

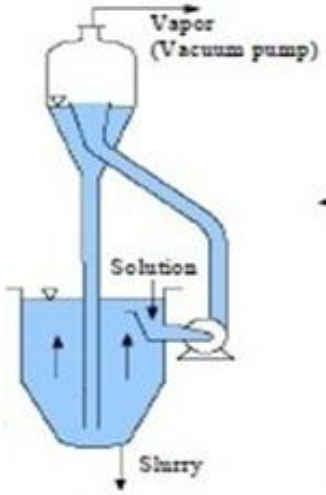
Vapor
(Vacuum pump)
Solution
Slurry

(f)

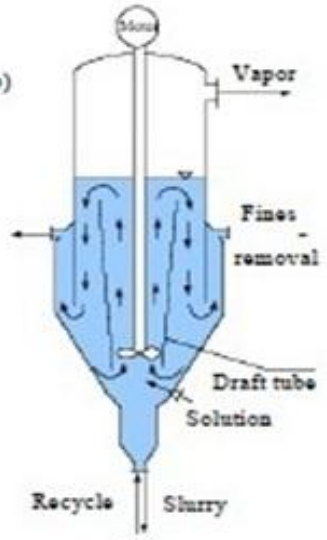
Vapor
Fines
removal
Draft tube
Solution
Recycle
Slurry

(g)

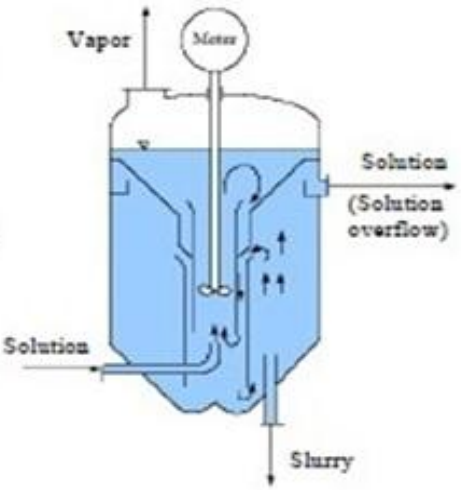
Vapor
Solution
(Solution
overflow)
Solution
Slurry

(h)

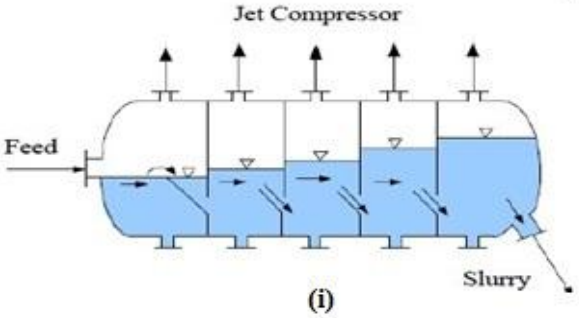
Jet Compressor
Feed
Slurry

(i)

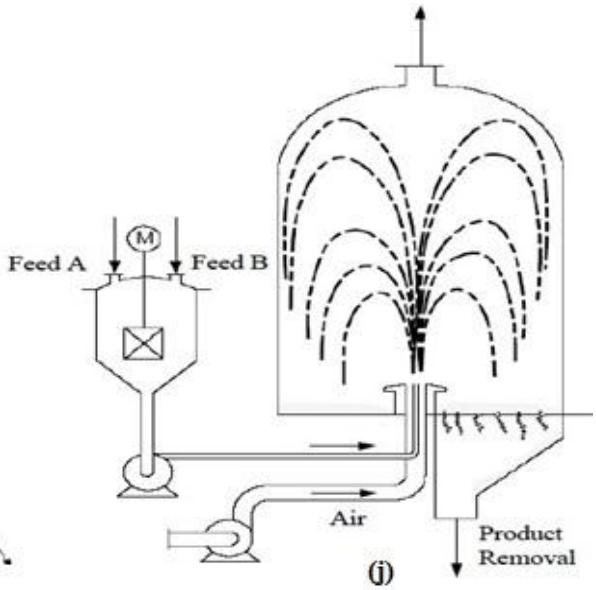
Feed A
Feed B
Air
Product
Removal

(j)

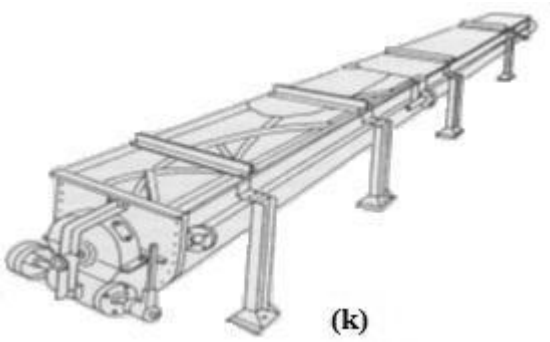

Fig. 1.5. Crystallization equipment for industrial application: (a) stirred vessel; (b) forced circulation crystallizer; (c) fluidized bed crystallizer (d) cooling crystallizer; (e) evaporative crystallizer; (f) vacuum crystallizer; (g) continuously operated vacuum crystallizer with a circulating device; (h) vacuum crystallizer with a circulating device in a tube (i) horizontal five-stage vacuum crystallizer; (j) prilling tower for production calcium nitrate. (k) trough shape crystallizer (Mersmann, 2001; Wantha 2006).

Fig. 1.5 (g) displays design of vacuum crystallizer with upward flow in the inner tapered vertical draft tube and skirt baffle forming a partitioned settling area (Dutta, 2009). A long shaft axial flow type agitator is located near the bottom of draft tube and causes circulation in crystallizer. An elutriating leg is fitted to the bottom cone (Bamforth, 1965). This type of crystallizer is used to produce coarse crystals as product. Fresh heated solution is fed near the draft tube and circulated upward in draft tube by agitator towards boiling surface. The crystals enter the vicinity of the vaporizing surface, where supersaturation is at the highest level. Fines can be removed by an overflow with mother liquid from the top of ring chamber. The coarse part of the narrow crystal size distribution is separated by a screening tube at the lower end of the crystallizer (Mersmann, 2001).

Fig. 1.5 (h) displays diagrammatically a two suspension circulation flow in a fluidized-bed crystallizer, which has two concentric tubes, a bottom tube with a circulating device and an external ejection tube and continuous gap around the crystallizer. A fine product exists primarily in the inner circulation loop, which has a fast upward flow in the inner tube and a high supersaturation value at the evaporation surface. In the external chamber, a classifying fluidized bed is formed and coarse crystals exist; fine crystals are carried away and drawn into the inner circulation via the ejector gap. The overflow above the classifying zone influences the crystal content. Fresh solution is fed directly into the tube. The product is withdrawn from the classifying zone (Mersmann, 2001; Wantha, 2006).

Fig. 1.5 (i) displays design of a continuous multistage vacuum crystallizer in a horizontal position without moving parts. It is suitable for vacuum-cooling crystallization. The evaporation chambers are separated from each other by several partitions. Fresh solution is fed in at the first stage and is cooled continuously from stage to stage. The product is withdrawn from the last stage, which has the lowest pressure. Steam jets maintain the various low pressures. In many cases, the liquid is brought into motion in the individual stage by bubbling gas (air) through the stage (Mersmann, 2001).

Fig. 1.5 (j) displays design outlines of a prilling tower. In this crystallization occur by an air flow which cools the solution and causes the solvent to evaporate. The solid crystals drop to the floor of the prilling tower, from where they are mechanically transported to a cooling drum (Mersmann, 2001; Wantha, 2006).

The final crystallizer is illustrated in Fig. 1.5 (k). This is a long open rectangular U-shaped trough, externally jacketed cooling crystallizer with a spiral agitator. It is a scrapped surface type crystallizer Agitator rotates in such a way that it is as close to the bottom as possible, to scrape the deposition and convey the crystals with mother liquor from one end to other end. Fresh heated solution is fed at one end circulates toward the other end of the crystallizer where an overflow gate for the crystals and mother liquor discharge are provided. It is also called Swenson-Walker crystallizer (Gavhane, 2008).

1.7.1. Forced Circulation Crystallizer

The Forced circulation (FC) crystallizer is displayed in Fig. 1.6. It is most widely used process of crystallization. FC crystallizers are found in sizes ranging from 2' diameter laboratory models to over 40' diameter units for continuous operation. The forced circulation crystallizer in Fig. 1.6 is most common type of crystallizer for the industrial crystallization. Generally in FC crystallizer due to evaporation of solvent, solution concentration increases and solution reaches to the limit of supersaturation where crystallization occurs. Most conventional FC units can be operated at normal conditions, under vacuum, and at slight upper atmospheric pressure.

The FC crystallizer can be dissociated in four major components: the crystallizer vessel, which offers most of the volume determined by the residence time requirements, the circulating pump, which provides the mixing energy, the heat exchanger, which allows energy to the crystallizer in evaporative crystallization operation, and the vacuum equipment, which handles the vapors generated in the crystallizer. Slurry from the

crystallizer vessel is circulated, in plug flow manner, through the heat exchanger, and returned to the crystallizer vessel again, where its supersaturation is relieved by deposition of solute on the crystals present in the slurry. The supersaturation is controlled so as to avoid spontaneous nucleation, by sufficient circulation capacity (GEA Messo, 2011).

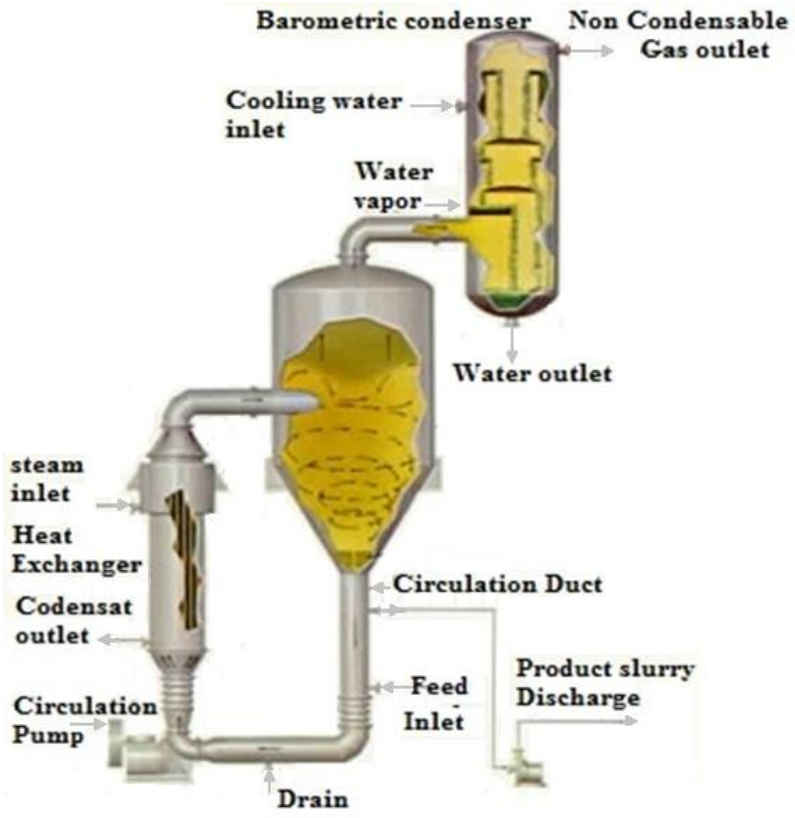

Fig. 1.6. FC Evaporation crystallizer (Swenson, 2013).

The FC crystallizer is normally used for, simple crystallization operations, where large crystal size is not a requirement. The FC design aims to protect the crystal size from reduction from the crystallizer environment by agitation and breaking, but does not have any features to aggressively increase the crystal size. So for fine size crystallization and due to easy operation, FC crystallizer have been used for crystallization of many inorganic salts and other chemicals such as, ammonium sulphate, sodium chloride (salt), trisodium phosphate, potassium nitrate, sodium carbonate monohydrate, potassium sulphate, ammonium chloride, citric acid, sugar etc. (Dutta, 2009; GEA Process, 2013). FC crystallizers can be either single or multiple effects. Usually, they operate from low vacuum to atmosphere pressure. As a rule, these units are used for high evaporation rates and when crystal size is not of the utmost importance or if crystal grows at a fair rate.

Almost any material of construction can be considered for the fabrication of these crystallizers (GEA Process, 2013).

1.8. Crystallizer characteristics

1.8.1. Effect of Hydrodynamics on crystallization

The role of hydrodynamics is one of the key facets in the dynamic behaviour of a crystallization process, importantly in larger scale equipment where uniform flow conditions are difficult to attain. On a macroscopic level the hydrodynamic conditions control the crystal residence time and the circulation time in the crystallizer which affects the solid suspension in the crystallizer. On a microscopic level, the smallest scale flow determines the crystal collisions, causes secondary nucleation by agglomeration and mass transfer for crystal growth. So the study of hydrodynamic conditions can describe flow behaviour, fluid mixing, and particles distribution.

1.8.2. Crystallization mechanisms

The crystallization is a complicated phenomenon of crystal formation and it involves two steps: (1) nucleation and (2) crystal growth. Together, these steps are mentioned as crystallization kinetics. The driving force required for the nucleation and growth of a crystal is mentioned as supersaturation because in saturated or unsaturated solution neither nucleation nor crystal growth is occur (Khanam, 2007; Seader et al., 2011).

Crystal growth involves phase change thermodynamics, solution chemistry, mass transfer, fluid dynamics, and heat transfer. In solution, crystal growth occurs by increasing the solute concentration. This may done by evaporation and cooling to remove solvent (Wantha, 2006). According to the diffusion–reaction theory the crystal growth occurs by the transfer of mass and it can be explained in two steps; first step is convective transport of the solute from the bulk of the supersaturated solution to the surface of a crystal and second step is surface integration or accommodation of the solute molecules in the growing layers of a crystal (Dutta, 2009; Seader et al., 2011). The second step is a first order process whose rate depends on the presence of supersaturation $(c - c_s)$ at the surface of crystal. The crystal growth rate can be determined as

$$\frac{dm_c}{dx} = k_L A_c (c - c_i) = k_r A_c (c_i - c_s) \tag{1.2}$$

Where, m_c is mass of single crystal, A_c is area of a crystal, k_L and k_r are mass transfer coefficient and rate constant and c, c_i and c_s are concentrations of solute in bulk, interface and saturation in this equation.

Nucleation refers to formation of tiny new crystalline entity or crystals from a supersaturated solution. The rate of nucleation is the number of new particles formed per unit time per unit volume of magma or solid free mother liquor. It is very important for controlling crystal size distribution (CSD). The sequence of a crystal formation is as: cluster (nuclei) – embryo – nucleus – crystal (Mersmann, 2001; Khanam, 2007). In nucleation at microscopic scale due to various atomic or molecular processes the atoms or molecules of solute or reactant phase rearrange into a cluster (nuclei) of the product phase, which after more growth take a form of crystal (Cubillas and Michael, 2010).

Nucleation can be classified into primary and secondary nucleation. Primary nucleation is divided into homogeneous mechanisms and heterogeneous mechanisms (Wantha, 2006). The homogeneous nucleation occurs when the system is free of impurities means there is absence of external nucleation sites as dust particles, crystals or solids of that or other solute. Heterogeneous nucleation occurs at a much lower supersaturation and in the presence of impurities such as foreign surfaces which are needed to generate primary nuclei.

Secondary nucleation is the phenomena of formation of new crystals from the existing ones. It is far more significant than primary nucleation in most industrial crystallization units because the vessel is run continuously having solute crystals inside. There few mechanisms of secondary nucleation are mentioned through them it can be possible (Wantha, 2006),

- Contact nuclei are formed from crystal-crystal, crystal-vessel wall, and crystal-impeller contacts that result in the removal of an adsorbed layer from a growing crystal.
- Shear nucleation is a similar method where the adsorbed layer is removed by fluid shear.
- Fracture nucleation is caused by breakage of crystals due to collisions similar to contact method.
- Attrition nuclei are attrition fragments of layer crystals.

- Needle breeding results from the removal of dendritic fragments from a larger crystal.

Miers identified metastable zone first and in later years it is defined as a part of supersaturation zone. The metastable region (as described in Fig. 1.1) on the phase diagram is generally considered as for many substances, where crystal growth occurs, but nucleation does not. Nucleation events may occur only in their own region at higher concentrations. Growth can occur in any supersaturated solution. Fig. 1.7 exhibits that the supersaturation area is larger for primary nucleation than for secondary nucleation, and is highest for homogeneous nucleation (Wantha, 2006).

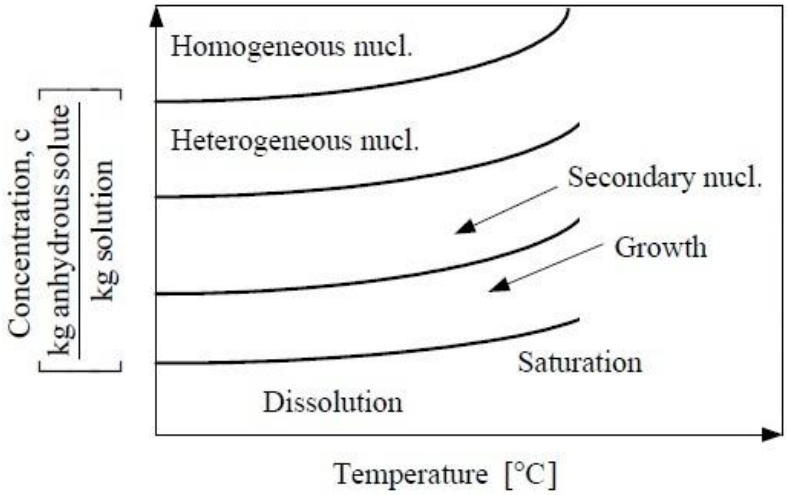

Fig. 1.7. The crystals nucleation and growth regions on a phase diagram (Wantha, 2006).

1.8.3. Crystal size distribution

In a continuous crystallizer, nuclei formed by nucleation remains in the crystallizer for an average period of time and then leaves the crystallizer with the mother liquor. The crystals present in the apparatus at any time are of varying sizes as given by the crystal size distribution. Crystal size distribution is an extremely important quantity in the design and analysis of crystallizers. A narrow size distribution of crystals is always preferred (Dutta, 2009).

1.8.4. Population density

Population balances were presented by Hulburt and Katz but later completely derived for processes of crystallization by Randolph and Larson. The conceptualization of the number balance is based on the number distribution density, $n(L)$, which is derived from the number of particles per unit volume or cubic meters of suspension, N. The number density

n is then derived as the limiting value of the number of particles per unit volume in the crystal size interval ΔL (Mersmann, 2001);

$$n = \lim_{\Delta L \to 0} \frac{\Delta N}{\Delta L} = \frac{dN}{dL} \tag{1.3}$$

1.8.5. Mixing in crystallization

Mixing is the random distribution into and through one another, of two or more initially separated phases (McCab et al., 2005). Crystallization is usually carried out in a suspension, so knowledge of mixing is important to study the crystallization process. Both mixing between fluid and particles, and particles and particles affect the crystallization process. The mixing effect is mainly considered on two scales of mixing; first is considered as macromixing, characterizes residence time distribution, which defines retention time of the elementary volumes, and the other is micromixing, and micromixing that is mixing on the molecular scale which describes product size and size distribution (Tavare, 1994). Successful operations depend on identifying the mixing parameters for the most critical aspects of the process and then evaluating whether those parameters will be satisfactory for the other aspects. The crystallizers normally employed in the fine chemical and pharmaceutical industries are multipurpose vessels with various impellers, baffles, and draft tube configurations. The crystallizers as stir tank in which propeller is used for mixing of solution suspension, draft tube baffle in which agitator and baffles and draft tube is used for mixing. In forced circulation crystallizers mixing energy is occurred through forced circulation of solution by pump. Mixing affects to both primary nucleation and secondary nucleation by attrition breakage these occur due to crystal-crystal impact, crystal-impeller and crystal-wall impact and absorbed layer thickness. Mixing effects on crystal growth can be described by mass transfer rate around the growing crystal, the effect of shear on crystal breakage, dispersion of an antisolvent, Growth rate dispersion and uniformity of crystal suspension (Wantha, 2006).

1.8.6. Particles Settling

The particles separation occur on the basis of size and density in the crystallizer, the particles those have grown and become heavier or dense than liquid they settle down at bottom of crystallizer but fine particles those are lighter in weight remain suspended in solution inside of the crystallizer. The large particles flow out as product with mother liquor and their separation according to size is carried out by screening or through

classifier. Separated small particles recirculate for either growth or dissolving. A dense solid particle present in fluid settles down because of terminal settling velocity. This velocity occurs when the drag force balances the buoyancy and gravitational force of the fluid on the particle.

Correlations for the terminal settling velocity in Newtonian fluids, $U_{t,}$ is calculated by expression

$$\mathbf{U_t} = \sqrt{\frac{4g(\rho_P - \rho)d_p}{3\boldsymbol{C_D}\rho}} \tag{1.4}$$

where g is the gravitational constant which value is 9.81 m/s^2, ρ is the liquid density, ρ_P is the particle density, d_p is the particle diameter, μ is viscosity of liquid, and C_D is the drag coefficient.

The values for $\boldsymbol{C_D}$,

$\boldsymbol{C_D} = 24/Re_p$ for laminar flow

$\boldsymbol{C_D} = 0.44$ for turbulent flow

Where Re_p is Reynolds number $\left(Re_p = d_p U_t, \rho/\mu\right)$

1.9. Methods for analyzing crystallization operation

There are three methods to study crystallization processes; experimental, analytical, and numerical methods.

- Experimental methods are typically high cost methods because of the need to construct a real model of crystallizer
- Analytical methods, the difficulties are based on construction of the mathematical equations and assumptions. The complexity of the geometry of industrial crystallizer makes analytical solutions impossible to achieve.
- Numerical methods are computer aided calculation techniques to find solutions to complex problems. This method reduces cost and time, there is no waste and no risk, it consumes less energy and is safer than compared to the experimental method.

In the field of fluid dynamics problems can be analyzed by computers to obtain velocity, temperature, pressure, and other physical thermodynamic parameters. So this field is called computational fluid dynamics (CFD). This method provides solution of

mathematical models for system involving transport processes. It involves the numerical solution of conservation equations continuity, momentum and energy equations (Mahdi et al., 2009). This allows researchers to understand better the flow process, and to modify or vary design through the computer. Experimentally it is difficult to characterize the hydrodynamic behaviour of a crystallizer and its impact on crystallization kinetics; and find out optimum condition for crystallization. CFD provides better insight into the multiphase dynamics and the local crystallization processes that take place in the crystallizer.

1.9.1. Computational fluid dynamics

CFD uses a range of space and time discretization methods in order to enable a numerical solution to be calculated. The finite volume technique is the maximum used method to discretize the volume in commercial CFD code. Firstly, the volume being investigated is discretized into small tetrahedral elements with nodes at each corner of the element. The information relating to the simulation is stored in the nodes of the elements, and equations of flow can then be applied to each finite volume in the simulation. The information required by the software are the boundary conditions for each of the boundaries of the total volume, flow rate at the inlet, conditions at the outlets, etc., the physical properties of the fluid(s), particles in the system, and the physical model that are required for the system (Tangtonsakulwong et al., 2006; Wantha, 2006).

The availability of high performance computing hardware and the introduction of user-friendly interfaces have led to the development of CFD packages available both for commercial and research purposes. The various general purposes CFD packages in use are PHONICS, CFX, FLUENT, FLOW3D, and STAR-CD etc. Most of these packages are based on the finite volume method and are used to solve fluid flow and heat and mass transfer problems.

1.10. Computational fluid dynamic studies on the crystallizer

Recently, several studies for CFD modeling and simulation of crystallizers have been carried out. A few comprehensive studies are presented as,

Bermingham et al. (1998) have used on-scale approach for the analysis and optimization of crystallizer design (design of DTB, FC, DT) with compartmental modelling a well-known technique in reactor engineering and applied within crystallization since many years as it made easier on-scale design. This approach has been needed due to the

nonlinear dependency of most physical processes as separation and hydrodynamics in crystallization system, on the degree of saturation, energy dissipation, crystal size, and its distribution. From the simulation they have found optimized crystallizer design.

Kramer et al. (2000) have observed that the design of forced circulation crystallizer is not effective for salt crystallization process. For improvement of process model compartmental method has been used to describe the crystallization process of evaporative and cooling suspension crystallizers. The model of a 200-liter evaporative FC crystallizer, with five compartments implemented in the dynamic flow sheeting program, SPEEDUP, and simulate. Simulation has shown large supersaturation profiles presented in the crystallizer and that only a part of the crystallizer volume has been effectively used for the growth of crystals.

Wei et al. (2001) have used CFD to understand reactions, crystallization, mixing, and their interactions in a precipitation process for $BaSO_4$ inside of semibatch crystallizer. By taking moment transformations of the population balances the chemical and crystallization kinetics have been integrated into a CFD solver to describe the generation and transportation of the crystals. The effect of hydrodynamics on the distribution of supersaturation and the crystal size in the stirred tank has been described by the impeller speed and feed location. They have found that numerical predictions are validated with measurements and can be used as an aid in the optimization

Sha et al. (2001) have employed CFX4.2 program to simulate the local particle-size distribution in a multi-fluid flow using the k-ε turbulence model with respect to interface transfer between the particles and the solution. The three dimensional model with sliding grid technique has been used to simulate the transient flow in the mixing tank. The size-dependent classification is calculated based on the local particle-size distribution. The factors that affect the classification function have been discussed. They have found from simulation that the mixing intensity and product removal location and the particle size are the most important factors affecting the classification function.

Rielly et al (2001) have done CFD simulation of the flow in a stirred tank with Lagrangian method to show that flow and mixing in industrial crystallizers has an effect on the kinetics of growth, nucleation and agglomeration and consequently on the crystal size distribution. It has been assumed in population balance modelling that fluid mechanical environment conditions for growing crystals is uniform but practically flow

conditions varied, with change in local velocities, shear rates and energy dissipation rates throughout the vessel. Eulerian and particle Lagrangian statistics have been similar. However, the distribution of slip velocities experienced by the crystals has been strongly dependent on the particle microscale and macroscale Stokes numbers. Results have shown that stirred tanks have not been ideal MSMPR crystallizers for processes where the kinetic rates have been dependent on the local mean and turbulent velocity.

Synowiec et al. (2003) have done simulation for optimization of hydrodynamics in magma crystallizers (CSTR) based on selected parameters; shape of the apparatus bottom, diameter of the stirrer, draft tube location and presence effect on: (i) unit power input distribution, (ii) the average mixing power, and (iii) pumping capacity. Results of CDF simulations have been compared with experiments and literatures; and displayed the effect of the design of crystallizer on energy dissipation rate, axial velocity field and general hydraulic efficiency.

Essemiani et al. (2004) have used CFD technique to show the mixing conditions in a pilot-scale forced-circulation crystallizer by application of VOF model to study the effect of flow rate and aspect ratio on flow conditions and RTD in the crystallizer. The analysis sufficiently has been anticipated the oscillating flow and two-phase gas–liquid interaction at the free surface. Comparison has been carried out between the CFD predictions and models of RTD. The results have been supported the use of CFD methodology as an aid to optimization of commercial-scale FCC design.

Rein et al. (2004) have presented research results for optimization of the vacuum pan design and sugar production by application of modern experimental and numerical techniques (CFD) used for lab scale and full scale crystallizers. The main goals have been to expand and understand the process in sugar crystallizers; development of realistic models for the simulation of the circulation and study the effect of different design parameters. A number of factors; design of cone, flow rates and rate of vaporization influence the operation of vacuum pans have been identified. Some relatively minor changes can be made to improve capacity and performance.

Jones et al. (2005) have applied new computational techniques for the analysis and design of systems for the production of particulate crystals, have become available and the more complex precipitation processes whereby crystallization follows fast chemical reactions have been also analyzed. This progress has been aided by the growing power of the

population balance and kinetic models, computational fluid dynamics (CFD) and mixing theory, respectively. Results have shown that combined population balance and kinetic models, computational fluid dynamics and mixing theory enable prediction and scale-up of crystallization and precipitation systems.

Kougoulos et al. (2006) have worked on improvement of Crystallizer design and scaleup by using a hybrid CFD compartmentalization batch cooling crystallizer model to take into account localized mixing, heat transfer, and fluid hydrodynamics, combined with key process engineering information obtained on a laboratory scale. The population, mass, concentration, and energy balance of each compartment have been modeled in gPROMS separately as a well-mixed MSMPR unit with input and output streams. The results have explained that ability to predict crystallization behaviour on scale-up could reduce batch failures and allow a faster production.

Heath et al. (2006) have employed coupled population balance (PB) and CFD model for continuous stirred tank gibbsite precipitator. Eulerian 2-phases with the population balance for different size of particles has been modelled. The population balance has used to show birth and death of particles based on rates of nucleation, agglomeration and crystal growth. The crystallization time scales are orders of magnitude longer than the flow timescales these tends to homogenize the crystal size and supersaturation throughout the tank. The precipitator due to particles settling at high concentration in the lower part poorly mixed. Simulation for different feed rates and impellor speeds have been carried out in CFX-4, investigated. Results have shown different size crystals distribution based on residence time, supersaturation and solids concentration.

Tangtonsakulwong et al. (2006) have described that Isokinetic withdrawal of solution from research crystallizers has been a key factor in obtaining an effective crystal-size distribution and has been critical for correct analysis of the crystallization process to determine crystallization kinetic parameters such as crystal growth rates, nucleation rates, breakage rates, and agglomeration rates. Isokinetic withdrawal depended upon the characteristics of the flow field in the crystallizer. CFX-5.5.1 has been used for numerical simulation for the fluid flow field in a small-scale (experimental) cylindrical round-bottomed, continuous-flow, cooling crystallizer, for analysis of kinetic parameters in sugar production. The results have showed that the momentum source strongly increased the axial flow velocity but only slightly influences the overall flow pattern, except the flow near the outlet tube.

Zheng et al. (2006) have done simulation to exhibit effect of mixing on the precipitation of $BaSO_4$ in a CSTR for different feed places, feed concentration, draft tube, impeller speed and residence time through solving the standard momentum and mass transport equations coupled with the moment equations of population balance. The simulation results have been validated with the literature data and explaining the distribution of the local supersaturation ratio distribution in the precipitator, mean crystal size and coefficient of variation under different operating conditions. The installation of a draft tube increased the mean crystal size, in general agreement with experimental work in the literature.

Zuoliang et al. (2008) have done CFD simulation to understand the effect of geometry and operation condition on the flow field and suspension density distribution in a fluidized bed crystallizer with total volume of $95m^3$ by. The simulation has been carried out through multi-fluid flow model for different sizes of particles as different phases and different geometries of draft tube have been used. The results have indicated that the liquid velocity field with the draft-tube forms a better circulation. The suspension density distributions for different crystal sizes depended on the feed rates and uniformity of the solid distribution increased with increase in feed rate.

Zhu and Wei (2008) have worked on CFD simulation of batch crystallization of ammonium sulphate. Three types of impellers and two dimensions of tanks have been employed to determine the changes of flow field. CFD code, fluent, has been used to simulate stirred tanks used in the process, and the sliding mesh (SM) method has been adopted to describe the rotating phenomenon. The comparison of the simulation results have showed that a DTB crystallizer with an axial impeller can provide a suitable flow field for a vacuum evaporation crystallization of ammonium sulphate, which can be used as a reference to build an industrial crystallizer.

Al-Rashed et al. (2009) have found a closer look to scale up problem of the Fluidized-Bed crystallizer operation, in particular for solids concentration larger than 10 vol.% by CFD multi-phase method. Data collected using CFD technique, impossible to obtain in any other way, especially for an industrial apparatus, provides the information about the suspension flow behaviour in such crystallizers. In results differences have been found in predictions for laboratory and industrial scale. Those differences have been observed in velocity profiles and distribution of solids in fluidized bed.

Wojcik and Plewik (2009) have modeled fluidized-bed crystallizers with use of the multiphase CFD method with density based solver for the first time. There have been significant differences in predictions of the model and one-phase simulations. There were significant differences in predictions of multiphase model and one-phase model.

Mahdi et al. (2009) have found out through CFD simulations the impacts of the shape of a crystallizer bottom, diameter of the stirrer, its location and presence of the draft tube on: (i) unit power input distribution, (ii) average mixing power and (iii) pumping capacity. Results have indicated the highest value of hydraulic efficiency with an optimal draft tube position between 0.35 and 0.5 hr/dr and an optimal draft tube opening angle in the range of 8^o and 13^o.

Plewik et al. (2010) have applied CFD methods to model a multiphase flow of mono-dispersed suspensions in Draft Tube Magma (DTM), Double Draft Tube (DDT) and Fluidized bed (FL) crystallizers. The geometry of model has been similar to industrial apparatus. The composition of suspensions and their physical properties have been same as in practical cases. The computations showed that axial velocity distribution in the investigated types of crystallizers have been far from optimal. In each case backward circulation loops have been observed.

Sun et al. (2011) in their work have tested a CFD based population balance model in a continuous draft tube baffle (DTB) crystallizer with KCl productivity. In this CFD model, the population balance in DTB crystallizer where 1) nucleation, 2) growth, 3) aggregation, and 4) breakage have been taking place separately has solved by the quadrature method of moments (QMOM).

Rodriguez et al. (2011) have shown modeling of a fluidized-bed crystallizer for seeding and crystals growth using the population balance CFD module. In this work for the simulation two sizes of NaCl seed have been used. They have suggested in results for, decrease the time step size and increase the number of iterations per step to achieve acceptable residual values by simulation. Moreover the effect of supersaturation in the crystal growth rate should be taken account. Furthermore it could be interesting to add a predefined particle size distribution in order to better observe the effect of the initial particle size distribution to the achieved product crystal size.

Al-Rashed et al. (2012) have described scale up of an Oslo fluidized-bed crystallizer with a classification leg using CFD methods for six geometries of volumes: 0.039, 0.33, 2.64,

29, 97, and 230 m^3. Polydispersive suspension of NaCl crystals with the initial concentration equal to 10 vol.% and ten size classes of the crystal diameter from 0.4 to 3 mm have been taken. Simulations have been carried out in Fluent and model two-phase flow, an Eulerian multiphase model has been used with the standard k–ε method. Results have been compared with industrial data and they have been found differences in predictions for laboratory and industrial scale, particularly in velocity profiles and distribution of solids in the fluidized bed.

Ganesan and Tobiska (2012) have employed FEM for solving multi-dimensional population balance systems based on dimensional splitting; in to physical space and internal property variables, where considered balance of fluid velocity, temperature and solute partial density has been as 2-D system, and balance of particle size distribution as 3-D. It has been used for crystallization based on, size independent growth rate without agglomeration and breakage. Simulation performed on different wall temperatures and results have shown the effect of cooling on the crystal growth at different times.

1.11. Scope for CFD analysis of FC crystallizer

Various CFD studies have been carried out for analysis of flow behaviour and its effect on crystallization process in crystallizers. The literature survey reveals work on CFD characterization of forced circulation crystallizer is quite meager although the system is widely used in industry for crystallization of various substances from solution. It can be observed that most of the work has been done for Fluidized bed crystallizer and some for draft tube baffle crystallizer and stir tank crystallizer; with and without draft tube and baffles. It can be observed that generally simulation work has been done using Eulerian multi-phase method in steady and unsteady both conditions using 3D geometries. But in general, multiphase flow in crystallizer is unsteady which cause mixing and turbulence in crystallizer. The study of crystal generation needed to use population balance model (PBM) with CFD, hardly any work on FC crystallizer using PBM is found in literature due to the complexity of this model. In this work an attempt has been made to characterize the hydrodynamics, crystal population density, mean crystal size growth in FC crystallizer. Different inlet positions have been taken to see the effect on hydrodynamic behaviour. In the present work commercial CFD software “ANSYS FLUENT 13” has been used to perform simulation. The finite volume discretization method and unstructured mesh have been used to study the multiphase flow (solution and vapor phases for isothermal and non-isothermal, solid particles and water for solid suspension and solution, solid particles and

vapor in population density conditions) and thermal behaviour in the forced circulation crystallizer. Thus the present work has been carried out with the following main objectives.

1.12. Objectives

The main objectives of the present research work are summarized below;

- To investigate the two-phase (vapor and liquid) flow characteristics in the FC crystallizer.
- To investigate the effect of the different inlet flow rates of solution on the flow characteristics in the Crystallizer.
- To investigate the effect of the position of inlet on the flow characteristics.
- To study the flow profile of liquid and vapor phase in isothermal and non-isothermal conditions.
- To characterize particle size distribution in the solid suspension for different sizes of solid particles and investigate the effect of flow rate and inlet position on particle size distribution.
- To study the effect of flow on particles population density.

1.13. Assumptions of Work

- The work is divided into 4 parts; modelling and simulation of the FC crystallizer using isothermal, non-isothermal, solid particles suspension distribution and population density conditions.
- The FC crystallizer involves three-phase operation but because of dilute solid phase smaller in size which follows the liquid flow neglecting the solid phase simulation of two phases flow; vapor (gas) and solution (liquid) have been carried out in isothermal and non-isothermal conditions but water and solid particles have been used for simulation of solid suspension and all three phases; solution, vapor and crystals have been used in population balance model.
- A water solution with 15 % NaCl as the liquid phase in the crystallizer and water-vapor as the vapor phase has been used. Solid particles in solid suspension simulation and crystals in population density simulation different densities solid materials. The physical properties of these materials are assumed constant.

- Turbulent flow is assumed because the high flow rates in the crystallizer, which normally induces turbulence.
- The FC crystallizer has studied using the CFD modelling software ANSYS FLUENT-13. 3D geometries have been used to account for the 3D multiphase flow.

1.14. Organization of Thesis

This thesis comprises of five chapters v.i.z. Introduction and Literature, Computational Models, Computational Geometry and Solution Methodology, Result and Discussion and Conclusion and Future scope of the work.

- Chapter-1, ***Introduction and Literature*** gives detailed information of the process, equipment, a critical literature review and scope and objective of the present work.
- Chapter-2, ***Computational Model*** discuss about the various computational models used to mathematically describe the system behaviour.
- Chapter-3, ***Computational Geometry and Solution Methodology*** describes about the hardware for simulation, computational geometry and the numerical methods adopted for simulation.
- Chapter-4, ***Results and Discussion*** provides various outcomes of the simulation through graphical representation and discussed in a scientific manner.
- Chapter-5, ***Conclusion and Future Scope*** summarizes the conclusion of the present work and suggestions for further work.

CHAPTER-2

COMPUTATIONAL MODEL

CFD is a powerful tool for the prediction of the fluid dynamics in various types of systems, thus enabling a proper design of such systems. The availability of affordable high performance computing hardware and the introduction of user-friendly interfaces have led to the development of several CFD packages available both for commercial and research purposes. Most of the packages are based on the finite volume method. The Finite Volume Method (FVM) is one of the most versatile discretization techniques used for solving the governing equations for fluid flow. The most compelling features of the FVM are that the resulting solution satisfies the conservation of quantities such as mass and momentum. This is exactly satisfied for any control volume as well as for the whole computation domain. Even a coarse grid solution exhibits exact integral balances (Jena, 2010).

Advances in physical models, numerical analysis and computational power have enabled simulation of the multi-phase flow characteristics in two and three dimensional circumstances. Today, CFD has emerged as a new paradigm for modeling multiphase flow in crystallizers, as seen from the literature review for multi-phase reactors. As described in the objective, the purpose of present study is to investigate numerically the flow behaviour like distribution of phases, flow profiles, pressure change and crystals population density of a multi-phase FC crystallizer.

The FC crystallizer involves operation of three phases; solution as mother liquor, gas as water vapor and solid as crystal, but because of dilute solid phase smaller in size which follows the liquid flow neglecting the solid phase, simulation of two phases flow; vapor (gas) and solution (liquid) have been carried out in isothermal and non-isothermal conditions. For more exact description of flow and distribution in FC crystallizer water and solid particles have been used during simulation solid suspension but three phases have been used in population balance model to study crystals population density. CFD software ANSYS FLUENT 13.0 has been used for modeling and simulation of FC crystallizer.

In computational study selection of appropriate multiphase model play an important role in the simulation result. There are different multiphase models available in commercial software ANSYS FLUENT. In the present work a series of computational models available in FLUENT have been used. The details of various models used in the present work are discussed in the following sections.

2.1. Computational Model for Multiphase Flow

An enormous number of flows occurred in nature and engineering are ordinarily involve a combination of phases. General phases of matter are three; solid, liquid and gas, but in multiphase flow system phases are used in a more comprehensive way. For instance distinct size of solid particles of the identical material can be handled as distinct phases because each group of particles with the identical size will have equal dynamical effect of the flow region. Multiphase flow can be divided in to four types; gas-liquid or liquid-liquid flows; gas-solid flows; liquid-solid flows; and three-phase flows. For resolving a multiphase flow process the primary action is to decide groups who allow a comprehensive way to find-out proper models for every category. Currently there are two methods for the numerical calculation of multiphase flows; the *Euler-Lagrange method* and the *Euler-Euler methods*. In the *Euler-Euler method*, the distinct phases are handled mathematically as interpenetrating continua. Since the volume of a phase cannot be occupied by the other phases, the concept of phasic volume fraction is introduced. These volume fractions are assumed to be continuous functions of space and time and their sum is equal to one. Conservation equations for each phase are derived to obtain a set of equations. These equations are closed by providing constitutive relations that are obtained from empirical information and boundary conditions. For volume averaged information on any hydrodynamic property the Euler-Euler approach is suitable for its simplicity (Wantha, 2006; Ansys Fluent Th., 2009).

2.1.1. The Eulerian Model

There are three different Euler-Euler multiphase models available: the *volume of fluid* (VOF) *model*, the *mixture model*, and the *Eulerian model*.

The *volume of fluid* (VOF) *model* is a surface-tracking technique applied to a fixed Eulerian mesh. It is designed for two or more immiscible fluids. In the VOF model, a single set of momentum equation is shared by the fluids, and the volume fraction of each of the fluids in each computational cell is tracked throughout the domain. *The mixture*

model is designed for two or more phases (fluid or particulate). As in the Eulerian model, the phases are treated as interpenetrating continua, the mixture model solves the mixture momentum equations and relative velocity is used to describe the dispersed phases. The *Eulerian model* solves a set of *n* momentum and continuity equations for every phase. Coupling is carried out via the pressure and interphase exchange coefficients. The mode in which this coupling is treated counts on the types of phases present; fluid- fluid flows are treated distinctly than fluid-solid flows. The momentum exchange between the phases is based on value of the fluid-fluid exchange co-efficient and for solid suspension, the fluid-solid and solid-solid exchange coefficient. An appropriate multiphase model for the multiphase system can be determined from the flow regime. For slug, and stratified free surface flows VOF model are used. For slurry flow, hydro transport, bubbly, droplet, and particle-laden flows in which the phase mix and/or dispersed phase volume fractions exceed 10% either mixture model or Eulerian model are used (Ansys Fluent Th., 2009).

In the present work, an Eulerian multiphase model is adopted where all the phases are treated as continua, interpenetrating and interacting with each other everywhere in the computational domain. The pressure field is assumed to be shared by all the phases.

2.2. Isothermal Simulation

In case of isothermal simulation, user defined mass and momentum sources and phase change are not considered.

2.2.1. Conservation Equations

The motion of each phase is governed by respective mass and momentum conservation equations.

Conservation of mass or continuity equation for phase q is

$$\frac{\partial}{\partial t}\left(\phi_q \rho_q\right) + \nabla \cdot \left(\phi_q \rho_q \vec{u}_q\right) = 0 \tag{2.1}$$

where ρ_q is the density, ϕ_q is the volume fraction and $\vec{u}_q$ is the velocity of phase q; α (NaCl solution) and β (vapor). The volume fractions of both phases satisfy the following condition:

$$\phi_\alpha + \phi_\beta = 1 \tag{2.2}$$

Conservation of momentum for phase q is

$$\frac{\partial}{\partial t}\left(\phi_q \rho_q \vec{u}_q\right) + \nabla \cdot \left(\phi_q \rho_q \vec{u}_q \vec{u}_q\right) = -\phi_q \nabla p + \nabla \cdot \bar{\bar{\tau}}_q + \phi_q \rho_q \vec{g} + \vec{M}_{i,q} \quad (2.3)$$

where p is the pressure shared by all phases, $\bar{\bar{\tau}}_q$ is q^{th} phase stress-strain tensor and $\vec{g}$ is the acceleration due to gravity. $\vec{M}_{i,q}$ is momentum exchange between phases.

Stress-strain tensor for phase q is

$$\bar{\bar{\tau}}_q = \phi_q \mu_q \left(\nabla \vec{u}_q + \nabla \vec{u}_q^T\right) + \phi_q \left(\lambda_q - \frac{2}{2}\mu_q\right) \nabla \cdot \vec{u}_q \bar{\bar{I}} \quad (2.4)$$

where $\mu_q$and λ_q are the shear and bulk viscosity of phase q.

2.2.2. Interphase Momentum Exchange Co-efficient

Interphase momentum exchange, $\vec{M}_{i,q}$ occurs due to interfacial forces acting on each phase due to interaction with another phase q. The inter phase momentum exchange terms $\vec{M}_{i,q}$is composed of a linear combination of different interaction forces between different phases and is generally represented as;

$$\vec{M}_{i,q} = \vec{F}_D + \vec{F}_{\text{lift}} + \vec{F}_{\text{vm}} \quad (2.5)$$

The forces indicated above represent respectively the interphase drag force, lift force, virtual mass force, and turbulence dispersion force. In the present work, the lift force has been neglected as the droplet or bubbles size are less. There is no mass transfer in the system so the virtual mass force has been neglected. Thus the interphase drag force is only needed to be considered (Ansys Fluent Th., 2009; Jena, 2010).

The interfacial force $\vec{M}_{D,pq}$ acting between two phases may arise from several independent physical effects friction, pressure, cohesion, and other factors. The interfacial forces between two phases are equal and opposite, so the conditions that $\vec{M}_{D,pq} = -\vec{M}_{D,qp}$ and $\vec{M}_{D,qq} = 0$ where, subscripts q and p represent various phases. The interphase force term is defined as;

$$\vec{M}_{D,pq} = K_{pq}\left(\vec{u}_p - \vec{u}_q\right) \quad (2.6)$$

where K_{pq} ($=K_{qp}$) is the interphase momentum exchange coefficient.

In the present work, the liquid (solution) phase is considered as a continuous phase and the gas (vapor) phase is treated as dispersed phase. The inter phase drag force between the phases is discussed below.

Liquid-vapor interphase drag force

Liquid-vapor interphase drag force is given by;

$$\vec{M}_{D,\alpha\beta} = K_{\alpha\beta}\left(\vec{u}_\alpha - \vec{u}_\beta\right) \tag{2.7}$$

Liquid-vapor interphase exchange coefficient

Generally in flows there are unequal amounts of two fluids, the predominant fluid should be modeled as the primary fluid, since the dispersing fluid is more likely to form droplets or bubbles modeled as secondary fluid. The exchange coefficient for this type of bubbly, liquid-vapor mixture can be written as;

$$K_{\alpha\beta} = \frac{\phi_\alpha \phi_\beta \rho_\beta f}{\tau_\beta} \tag{2.8}$$

where f the drag function, is defined differently for the different exchange-coefficient models and τ_β, the "particulate (bubbles) relaxation time", is defined as;

$$\tau_\beta = \frac{\rho_\beta d_b^2}{18\mu_\alpha} \tag{2.9}$$

where d_b is the diameter of the bubbles of vapor phase (β). Nearly all definition of f include a drag co-efficient *(C_D)* that is based on the relative Reynolds number (*Re*). It is the drag function that differs among the exchange co-efficient models. For all these situations, K_{pq} should trend to zero. Whenever the primary phase is not present with in the domain, to enforce this *f* is always multiplied by the volume fraction of the primary phase *q* as shown in equation (2.14). In the present study Schiller and Naumann model is used to define the drag function *f*.

$$f = \frac{C_D Re}{24} \tag{2.10}$$

Where

$$C_D = \frac{24}{Re}(1 + 0.15Re^{0.687}), \quad Re \leq 1000 \tag{2.11}$$

$$C_D = 0.44, \qquad Re > 1000 \tag{2.12}$$

The relative Reynolds number is (Wojcik and Plewik, 2009) is defined as;

$$Re = \frac{\rho_\alpha \left|\vec{u}_\alpha - \vec{u}_\beta\right| d_b}{\mu_\alpha} \tag{2.13}$$

2.2.3. Closure laws for Turbulence

For defining the causes of turbulent fluctuations of velocities and scalar quantities in multiphase phase flow; *RNG k-ϵ model* is used (Wei et al., 2001; Essemiani et al., 2004). The *RNG k-ϵ model* is modified version of the *k-ϵ* model and this model depicts improved results for swirl flow (Essemiani et al., 2004). In comparison to single-phase flows, the number of terms to be modeled in the momentum equations in multiphase flows is large, and this makes the modeling of turbulence in multiphase simulations extremely complex. There are three methods for modeling turbulence in multiphase flows within the context of the *k-ϵ* models; mixture turbulence model, dispersed turbulence model and turbulence model for each phase (Ansys Fluent Th., 2009). In present work for the turbulence modeling the *k*-ε dispersed turbulence model has been used;

k-ϵ dispersed turbulence (model is applicable when there is only one primary continuous phase and the others are dispersed dilute secondary phases) In this condition main effect is the primary-phase turbulence on the random motion of the secondary phases. Fluctuating quantities of the secondary phases can therefore be given in terms of the mean characteristics of the primary phase.

For *turbulence in the continuous phase* the eddy viscosity model is used to calculate averaged fluctuating quantities. The Reynolds stress tensor for continuous phase that is liquid (solution), α, take the following form;

$$\bar{\bar{\tau}}_\alpha = -\frac{2}{2}\left(\rho_\alpha k_\alpha + \rho_\alpha \mu_{t,\alpha} \nabla \cdot \vec{U}_\alpha\right)\bar{\bar{I}} + \rho_\alpha \mu_{t,\alpha}\left(\nabla \vec{U}_\alpha + \nabla \vec{U}_\alpha^T\right) \tag{2.14}$$

where $\vec{U}_\alpha$ is the phase-weighted velocity.

The turbulent viscosity $\mu_{t,\alpha}$ is written in terms of the turbulent kinetic energy of phase *q*:

$$\mu_{t,\alpha} = \rho_\alpha C_\mu \frac{k_\alpha^2}{\epsilon_\alpha} \tag{2.15}$$

and a characteristic time of the energetic turbulent eddies is defined as;

$$\tau_{t,\alpha=} \frac{2}{2} C_\mu \frac{k_\alpha}{\epsilon_\alpha} \tag{2.16}$$

Where $\epsilon_\alpha$is the dissipation rate and $C_\mu = 0.085$

The length scale of the turbulent eddies is;

$$L_{t,\alpha} = \sqrt{\frac{2}{2}} C_{\mu} \frac{k_{\alpha}^{2/2}}{\epsilon_{\alpha}} \tag{2.17}$$

The values of $k_{\alpha}$and $\epsilon_{\alpha}$are directly obtained from the differential transport equations for the turbulence kinetic energy and turbulence dissipation rate represented as;

$$\frac{\partial}{\partial t}(\phi_{\alpha}\rho_{\alpha}k_{\alpha}) + \nabla \cdot (\phi_{\alpha}\rho_{\alpha}\vec{U}_{\alpha}k_{\alpha}) = \nabla \cdot \left(\phi_{\alpha}\frac{\mu_{t,\alpha}}{\sigma_k}\nabla k_{\alpha}\right) + \phi_{\alpha}G_{k,\alpha} - \phi_{\alpha}\rho_{\alpha}\epsilon_{\alpha} + \phi_{\alpha}\rho_{\alpha}\prod_{k_{\alpha}} \tag{2.18}$$

and

$$\frac{\partial}{\partial t}(\phi_{\alpha}\rho_{\alpha}\epsilon_{\alpha}) + \nabla \cdot (\phi_{\alpha}\rho_{\alpha}\vec{U}_{\alpha}\epsilon_{\alpha}) = \nabla \cdot \left(\phi_{\alpha}\frac{\mu_{t,\alpha}}{\sigma_{\epsilon}}\nabla \epsilon_{\alpha}\right) + \phi_{\alpha}\frac{\epsilon_{\alpha}}{k_q}(C_{1e}G_{k,\alpha} - C_{2e}\phi_{\alpha}\epsilon_{\alpha}) + \phi_{\alpha}\rho_{\alpha}\prod_{\epsilon_{\alpha}} \tag{2.19}$$

where $\prod_{k_{\alpha}}$and $\prod_{\epsilon_{\alpha}}$represent the influence of the dispersed phase on the continuous phase and $G_{k,\alpha}$ is the production of turbulent kinetic energy. The term $\prod_{k_{\alpha}}$ can be derived from the instantaneous equation of the continuous phase and takes the following form; here *N* represents the number of secondary phases;

$$\prod_{k_{\alpha}} = \sum_{i=1}^{N} \frac{K_{i\alpha}}{\phi_{\alpha}\rho_{\alpha}}(k_{i\alpha} - 2k_{\alpha} + \vec{u}_{i\alpha} \cdot \vec{u}_{dr}) \tag{2.20}$$

where $k_{i\alpha}$ is the covariance of the velocities of the continuous liquid phase α and the dispersed phase *i*, $\vec{u}_{i\alpha}$ is the relative velocity, and $\vec{u}_{dr}$ is the drift velocity.

And $\prod_{\epsilon_{\alpha}}$ is given by;

$$\prod_{\epsilon_{\alpha}} = C_{2e}\frac{\epsilon_q}{k_q}\prod_{k_{\alpha}} \tag{2.21}$$

Where $C_{2e} = 1.2$

Turbulence in the dispersed phase is important factor to evaluate dispersion coefficients, correlation functions, and the turbulent kinetic energy of each dispersed phase from time and length scales that describe the motion. The distinctive particle relaxation time associated to inertial effects working on a dispersed phase *i* is described as;

$$\tau_{F,i\alpha} = \phi_{\alpha}\rho_{\alpha}{K_{i\alpha}}^{-1}\left(\frac{\rho_i}{\rho_{\alpha}} + C_V\right) \tag{2.22}$$

The Lagrangian integral time scale calculated along particle trajectories, mainly affected by the crossing-trajectory effect is defined as;

$$\tau_{t,i\alpha} = \frac{\tau_{t,\alpha}}{\sqrt{\left(1 + C_\beta \xi^2\right)}} \tag{2.23}$$

where

$$\xi = \frac{|\vec{u}_{i\alpha}|\tau_{t,\alpha}}{L_{t,\alpha}} \tag{2.24}$$

and

$$C_\beta = 1.8 - 1.25\cos^2\theta \tag{2.25}$$

where θ is the angle between the mean particle velocity and the mean relative velocity. The ratio between these two characteristic time is written as;

$$\eta_{i\alpha} = \frac{\tau_{t,i\alpha}}{\tau_{F,i\alpha}} \tag{2.26}$$

The turbulence quantities for dispersed phase *i* as follows;

$$k_i = k_\alpha \left(\frac{b^2 + \eta_{i\alpha}}{1 + \eta_{i\alpha}}\right) \tag{2.27}$$

$$k_{i\alpha} = 2k_\alpha \left(\frac{b + \eta_{i\alpha}}{1 + \eta_{i\alpha}}\right) \tag{2.28}$$

$$D_{t,i\alpha} = \frac{1}{2} k_{i\alpha} \tau_{t,i\alpha} \tag{2.29}$$

$$D_i = D_{t,i\alpha} + \left(\frac{2}{2} k_i - b\frac{1}{2} k_{i\alpha}\right) \tau_{t,i\alpha} \tag{2.30}$$

$$b = (1 + C_V)\left(\frac{\rho_i}{\rho_\alpha} + C_V\right)^{-1} \tag{2.31}$$

and $C_V = 0.5$ is the added-mass coefficient.

Interphase turbulent momentum transfer is mainly turbulent drag term for multiphase flow ($K_{i\alpha}(\vec{u}_i - \vec{u}_\alpha)$) is modeled for dispersed phase and continuous phase as;

$$K_{i\alpha}(\vec{u}_i - \vec{u}_\alpha) = K_{i\alpha}\left(\vec{U}_i - \vec{U}_\alpha\right) - K_{i\alpha}\vec{u}_{dr} \tag{2.32}$$

The drift velocity is given by;

$$\vec{u}_{dr} = -\left(\frac{D_i}{\sigma_{i\alpha}\phi_i}\nabla\phi_i - \frac{D_\alpha}{\sigma_{i\alpha}\phi_\alpha}\nabla\phi_\alpha\right) \quad (2.33)$$

Where D_i and D_α are diffusivities and $\sigma_{i\alpha}$ is dispersion Prandtl number in multiphase flow. This is considered that diffusivity values are $D_i = D_\alpha = D_{t,i\alpha}$ and the value of $\sigma_{i\alpha}$ is 0.75.

2.3. Non Isothermal Simulation

In the non-isothermal model, conservation equations, interphase momentum transfer and turbulence model are similar to that of the isothermal model, the heat transfer is the new part added. For the study of multiphase heat transfer in the system, energy conservation and heat transfer equations are included (Wantha, 2006; Ansys Fluent Th., 2009).

2.3.1. Conservation of Energy

To describe the conservation of energy in Eulerian multiphase applications enthalpy equation;

$$\frac{\partial}{\partial t}\left(\phi_q\rho_q h_q\right) + \nabla\cdot\left(\phi_q\rho_q\vec{u}_q h_q\right) = \phi_q\frac{\partial p_q}{\partial t} + \bar{\bar{\tau}}_q:\nabla\vec{u}_q - \nabla\cdot\vec{q}_q + S_q + Q_{i,q} \quad (2.34)$$

where h_q is the specific enthalpy of the phase q, $\vec{q}_q$ is the heat flux, S_q is a source term, $Q_{i,q}$ is the intensity of heat exchange between phases.

2.3.2. Heat Transfer

The internal energy balance for phase q is written in terms of the phase enthalpy, defined by;

$$H_q = \int C_{p,q}dT_q \quad (2.35)$$

Where $C_{p,q}$ is the specific heat at constant pressure of phase q.

2.3.3. The Heat Exchange Coefficient

The heat exchange between the phases must comply with the local balance conditions $Q_{pq} = -Q_{qp}$ and $Q_{qq} = 0$ where, subscripts q and p represent various phases. The rate of energy transfer between the phases is assumed to be a function of the temperature difference;

$$Q_{pq} = h_{pq}\left(T_p - T_q\right) \quad (2.36)$$

where h_{pq}=h_{qp} is the interphase heat transfer coefficient. The heat transfer coefficient is related to the p^{th} phase Nusselt number, Nu_p, by;

$$h_{pq} = \frac{6\kappa_q \phi_q \phi_p \mathrm{Nu}_p}{d_p^2} \tag{2.37}$$

Where κ_q is the thermal conductivity of the q^{th} phase. The Nusselt number is typically determined from the correlation of Ranz and Marshall (Ansys Fluent Th., 2009) given by.

$$\mathrm{Nu}_p = 2.0 + 0.6\mathrm{Re}^{1/2}\mathrm{Pr}^{1/2} \tag{2.38}$$

where $\mathrm{Re}_p$is the relative Reynolds number based on the diameter of the p^{th} phase and the relative velocity $\left|\vec{u}_p - \vec{u}_q\right|$, and Pr is the Prandtl number of the q^{th} phase;

$$\mathrm{Pr} = \frac{C_{pq}\mu_q}{\kappa_q} \tag{2.39}$$

2.4. Solid suspension

Here the solid particles have been considered as secondary phase in place of vapor. The mass conservation equations for both primary (liquid) phase and secondary (solid) phase is similar to the isothermal simulation part and momentum conservation equation is same for primary (liquid) phase but for secondary (solid) phase it is;

$$\frac{\partial}{\partial t}(\phi_s \rho_s \vec{u}_s) + \nabla \cdot (\phi_s \rho_s \vec{u}_s \vec{u}_s) = -\phi_s \nabla p - \nabla . p_s + \nabla . \bar{\bar{\tau}}_s + \phi_s \rho_s \vec{g} + \vec{M}_{i,s} \tag{2.40}$$

The second term in the R.H.S. represents the solids pressure in Eq. (2.40) all other terms are same.

Liquid-solid interphase momentum transfer

Liquid- solid interphase momentum transfer is given by;

$$\vec{M}_{D,\alpha s} = K_{\alpha s}(\vec{u}_\alpha - \vec{u}_s) \tag{2.41}$$

Liquid-solid exchange coefficient $K_{\alpha s}$ (Wojcik and Plewik, 2009) is shown as;

$$K_{\alpha s} = \frac{\phi_s \rho_s f}{\tau_s} \tag{2.42}$$

where f is defined differently for the different exchange-coefficient models and τ_s, the "particulate relaxation time", is defined as;

$$\tau_s = \frac{\rho_s d_s^2}{18\mu_\alpha} \tag{2.43}$$

where $d_s$is the diameter of particles of solid phase *s*. *f* is drag function and include a drag function (C_D) that is based on the relative Reynolds number (*Re*) based on the solid phase.

2.5. Population Balance Method

Various industrial fluid flow processes contain a secondary phase with a size distribution. In a multiphase process the size distribution of particles, considering solid particles, bubbles, or droplets, can occur together with transport and chemical reaction. A group of several processes like nucleation, growth, dispersion, dissolution, aggregation, and breakage producing the dispersion can be important for the evolutionary processes. Thus a balance equation is necessary to describe the changes in the particle population in multiphase flows involving a size distribution, according to conditions with momentum, mass, and energy balances. This balance is ordinarily described as the population balance. Processes where a population balance could work involve crystallization, precipitative reactions from a gas or liquid phase, bubble columns, gas sparging, sprays, fluidized bed polymerization, granulation, liquid-liquid emulsion and separation, and aerosol flows (Ansys Fluent PBM, 2009).

For the effective working of the idea of population balance modeling, a number density function is brought in to account for the particle population. By the help of particle properties such as; particle size, composition etc., different particles in the population can be separated and their nature can be reported.

In ANSYS FLUENT there are three solution methods to the population balance equation: ***The Discrete Method,*** in this method the particle population is discretized into a finite number of size intervals. The advantage of discrete method is to compute the particle size distribution (PSD) directly. Discrete method is also especially effective in the condition of particle sizes limit is according to theory and interval does not exceed than two or three degree of size. These intervals for particle size distribution (PSD) are shown in terms of a set of discrete size classes or bins. Discrete method is computationally expensive when extensive number of spans is required. ***The Standard Method of Moments*** (SMM) is an effective substitution for the discrete population balance method. For the SMM the transport equation for moments of the distribution is derived by transforming the population balance equation. The i^{th} moment is defined by integrating the number density

throughout the particle space weighted with the particle property raised to its i^{th} power. This is normally good for solving a few moment equations; three to six. This leads to a certain decrease in the number of solving equations compared to the discretized method. The SMM is helpful in case of the entire distribution is not required and definite average and total quantities are enough for explanation of the particle distribution. Ordinarily, the zeroth moment shows the total number density, the second moment shows the total surface area per unit volume, and the third moment shows the total mass density. The advantage of this method that it is not expensive computationally. ***The Quadrature Method of Moments*** (QMOM) is not computationally expensive similar to the SMM, but substitutes the exact closure required for SMM by the help of an approximate closure. This allows use of QMOM to a broad range of applications without any limitations. The QMOM is a good replacement for the discrete method when aggregation quantities, rather than an exact PSD, are desired. Its advantages are fewer variables typically only six or eight moments and a dynamic calculation of the size bins.

In the present study discrete method is used to study number of crystals and their population density in the FC crystallizer but SMM is used to study the growth of crystal mean size in the system.

2.5.1. Computational Model for Population Balance

2.5.1.1. The Population Balance Equation (PBE)

The general transport equation for the number density function is given as;

$$\frac{\partial}{\partial t}[n(V,t)] + \nabla \cdot [\vec{u}n(V,t)] + \nabla_V \cdot [G_V n(V,t)] = \frac{1}{2}\int_0^V \phi(V-V',V')\, n(V-V',t)n(V',t)dV' - \int_0^\infty \phi(V,V')\, n(V,t)n(V',t)dV' + \int_{\Omega_V}^{\cdot} pg(V')(V|V')n(V',t)dV' - g(V)n(V,t) \quad (2.44)$$

here the growth function is; $\nabla_V \cdot [G_V n(V,t)]$,

Birth due to aggregation is given by; $\frac{1}{2}\int_0^V \phi(V-V',V')\, n(V-V',t)n(V',t)dV'$,

Death due to aggregation is given by; $\int_0^\infty \phi(V,V')\, n(V,t)n(V',t)dV'$,

Birth due to breakage can be expressed as; $\int_{\Omega_V}^{\cdot} pg(V')(V|V')n(V',t)dV'$

Death due to breakage can be expressed as; $g(V)n(V,t)$

The boundary and initial conditions are given by;

$n(V,t=0)=n_V; \quad n(V=0,t)G_V=\dot{n}_0$

Where $\dot{n}_0$ is the nucleation rate in particles/m^3-s.

2.5.1.2. Particle Growth

The growth rate based on particle volume, G_V, (m^3/s) is defined as;

$$G_V=\frac{\partial V}{\partial t} \tag{2.45}$$

The growth rate based on particle diameter (or length) is defined as;

$$G=\frac{\partial L}{\partial t} \tag{2.46}$$

The volume of a single particle is, $V = K_V L^3$, and thus

$$G_V=\frac{\partial V}{\partial t}=3K_V L^2\frac{\partial L}{\partial t}=3K_V L^2 G \tag{2.47}$$

The surface area of a single particle, A, is defined as $K_a L^2$. Thus for a cube/sphere, $K_a = 6K_V$.

2.5.1.3. Particle Birth by Nucleation

According to the use, intuitive nucleation of particles can occur due to the transfer of molecules from the primary phase. For example, in crystallization from solution, the first step is the phase separation or "birth" of new crystals.

The nucleation rate is defined through a boundary condition as shown by;

$n(V,t=0)=n_V; \quad n(V=0,t)G_V=\dot{n}_0$

2.5.1.4. The Discrete Method

In ANSYS FLUENT for the discrete method the PBE is written in terms of volume fraction of particle size i:

$$\frac{\partial}{\partial t}(\rho_s\phi_i)+\nabla\cdot(\rho_s u_i\phi_i)+\frac{\partial}{\partial V}\left(\frac{G_V\rho_s\phi_i}{V}\right) = \rho_s V_i\left(B_{\mathrm{ag,i}}-D_{\mathrm{ag,i}}+B_{\mathrm{br,i}}-D_{\mathrm{br,i}}\right)+0^i\rho_s V_0\dot{n}_0 \tag{2.48}$$

where ρ_s is the density of the secondary phase and ϕ_i is the volume fraction of particle size i, defined as;

$$\phi_i = N_i V_i \qquad i = 0,1, \dots \dots, N-1 \tag{2.49}$$

Where;

$$N_i(t) = \int_{V_i}^{V_{i+1}} n(V,t)dV \tag{2.50}$$

and V_i is the volume of the particle size i. A fraction of ϕ, called f_i, is introduced as the solution variable. This fraction is defined as;

$$f_i = \frac{\phi_i}{\phi} \tag{2.51}$$

where ϕ is the total volume fraction of the secondary phase. The nucleation rate $\dot{n}_0$ appears in the discretized equation for the volume fraction of the smallest sizeV_0. The term 0^i appears only in the case of the smallest particle size.

The growth rate in Equation 2.48 is discretized as follows;

$$\frac{\partial}{\partial V}\left(\frac{G_V \rho_s \phi_i}{V}\right) = \rho_s V_i \left[\left(\frac{G_{V,i-1} N_{i-1}}{V_i - V_{i-1}}\right) - \left(\frac{G_{V,i} N_i}{V_{i+1} - V_i}\right)\right] \tag{2.52}$$

The volume coordinate is discretized as $V_{i+1}/V_i = 2^q$ where q = 1, 2……..and is referred to as the "ratio factor".

The particle birth and death rates are defined as follows;

$$B_{\text{ag,i}} = \sum_{k=1}^{N}\sum_{j=1}^{N} a_{kj} N_k N_j x_{kj} \xi_{kj} \tag{2.53}$$

$$D_{\text{ag,i}} = \sum_{j=1}^{N} a_{ij} N_i N_j \tag{2.54}$$

$$B_{\text{br,i}} = \sum_{j=i+1}^{N} g(V_j) N_j \beta(V_i \mid V_j) \tag{2.55}$$

$$D_{\text{br,i}} = g(V_i) N_i \tag{2.56}$$

where $a_{ij} = a(V_i \mid V_j)$ and

$$\xi_{kj} = \begin{cases} 1 & for \quad V_i < V_{ag} < V_{i+1}, \ \ where\ i \le N-1 \\ 0 & otherwise \end{cases} \tag{2.57}$$

V_{ag} is the particle volume resulting from the aggregation of particles k and j, and is defined as

$$V_{ag} = [x_{kj}V_i + (1 - x_{kj})V_{i+1}] \tag{2.58}$$

where

$$x_{kj} = \frac{V_{ag} - V_{i+1}}{V_i - V_{i+1}} \tag{2.59}$$

If V_{ag} is greater than or equal to the largest particle size V_N, then the contribution then the contribution to class $N - 1$ is

$$x_{kj} = \frac{V_{ag}}{V_N} \tag{2.60}$$

There is no breakage for the smallest particle class.

2.5.1.5. The Standard Method of Moments (SMM)

The SMM approach is based on taking moments of the PBE. Defining the k^{th} moment as;

$$m_k(\vec{x}, t) = \int_0^\infty n(L; \vec{x}, t)L^k dL \qquad k = 0,1, \ldots, N - 1 \tag{2.61}$$

and assuming constant particle growth, its transport equation can be written as

$$\frac{\partial}{\partial t}(\rho m_k) + \nabla \cdot (\rho \vec{u} m_k) = \rho\left(\bar{B}_{\mathrm{ag,k}} - \bar{D}_{\mathrm{ag,k}} + \bar{B}_{\mathrm{br,k}} - \bar{D}_{\mathrm{br,k}}\right) + 0^k \dot{n}_0 + \mathrm{Growth} \tag{2.62}$$

N is the specified number of moments and $\dot{n}_0$ is the nucleation rate. The growth term is defined as;

$$\mathrm{Growth} \equiv \int_0^\infty k\, L^{k-1} G(L) n(L, t) dL \tag{2.63}$$

and for constant growth is represented as;

$$kGm_{k-1} \tag{2.64}$$

From these moments, the parameters describing the gross properties of particle population can be derived as;

$$N_{\mathrm{total}} = m_0 \tag{2.65}$$

$$L_{\mathrm{total}} = m_1 \tag{2.66}$$

$$A_{\mathrm{total}} = K_a m_2 \tag{2.67}$$

$$V_{\mathrm{total}} = K_V m_3 \tag{2.68}$$

$$d_{32} = \frac{m_3}{m_2} \tag{2.69}$$

These properties are related to the total number, length, area, and volume of solid particles per unit volume of solution suspension. The Sauter mean diameter, d_{32}, is usually used as the mean particle size.

2.5.1.6. Particle Size Distribution from Moments

The number density function *n(L)* is expressed as;

$$n(L) = \exp\left(\sum_{i=1}^{N-1} A_i L^i\right) \tag{2.70}$$

The equation for the k^{th} moment is now written as;

$$m_k = \int_0^{\infty} L^k \exp\left(\sum_{i=1}^{N-1} A_i L^i\right) dL \qquad k = 0,1, \ldots \ldots, N-1 \tag{2.71}$$

Given *N* moments, the coefficients A_i can be found by a globally convergent Newton-Raphson method to reconstruct the particle size distribution.

2.5.1.7. Coupling with Fluid Dynamics

To couple population balance modeling of the secondary phases with the overall fluid dynamics problem, a Sauter mean diameter d_{32} may be used to represent the particle diameter of the secondary phase. The Sauter mean diameter is defined as the ratio of the third moment to the second moment for the SMM. For the discrete method, it is defined as;

$$d_{32} = \frac{\sum N_i L_i^3}{\sum N_i L_i^2} \tag{2.72}$$

2.5.1.8. Mass Transfer Due to Nucleation and Growth

The processes involve the creation, dissolution, or growth of particles such as crystallization, the total volume fraction equation for the particulate phase will have mass source terms due to these phenomena. The momentum equation for the particulate phase will also have mass source terms due to the added mass.

As an example, in crystallization, particles are created by means of nucleation ($\dot{n}_0$), and a growth rate *(G)* can also be specified. The mass transfer rate of formation (in kg/m^3-s) of particles of all sizes is then given by;

$$\dot{m} = 3\rho K_V \int_0^\infty L^2 Gn(L)\, dL \tag{2.73}$$

For the discrete method, the mass transfer rate due to growth can be written as;

$$\dot{m} = \rho \int_0^\infty Gn(L)\, dL$$

or

$$\dot{m} = \rho \sum_i G_{V,i} N_i \tag{2.74}$$

If the nucleation rate is included in the total mass transfer, then the mass transfer becomes;

$$\dot{m} = \rho V_0 \dot{n}_0 + \sum_i \rho G_{V,i} N_i \tag{2.75}$$

For the SMM, only a size-independent growth rate is available. Hence, the mass transfer rate can be written as;

$$\dot{m} = \frac{1}{2} \rho K_a G m_2 \tag{2.76}$$

For both the SMM mass transfer due to nucleation is negligible, and is not taken into account.

CHAPTER-3

COMPUTATIONAL GEOMETRY AND SOLUTION METHODOLOGY

3.1. Introduction

This chapter provides the information on various computational geometries of FC crystallizer used for simulation, hardware used and solution methods adopted for simulation in the present work. The process of the CFD simulation is divided as; geometry creation, mesh creation, choosing models, physical properties, boundary conditions, solver and post-processing. The mathematical models used in the study are described in chapter 2.

In the present work, three dimensional (3D) computational geometries with different inlet position of a FC crystallizer have been considered for simulation. The changes in inlet position have been done to see the effect of inlet position on the flow behaviour in the crystallizer.

The hardware used for simulation is a computer with intel core i5, 3.3 GHz processor and 4 GB of RAM with microsoft windows 7 professional version 2009 as operating system. Commercial software ANSYS FLUENT 13, ANSYS Workbench 13, has been used for CFD simulation.

3.2. Computational Geometry

The first step in CFD study is the flow geometry creation where the computational domain of the physical system is created. In the present work the computational geometry of FC crystallizer has been generated using Design Modeler in ANSYS Workbench.13. The computational geometry of FC crystallizer used for numerical simulation is a model of the pilot scale FC crystallizer, used by Essemiani et al. (2004) for their simulation work. Modifications in inlet and vapor outlet position have been done to see the main effect on flow behaviour (Bamforth, 1965).

The FC crystallizer (Fig. 3.1) used for the study is cylindrical in shape with conical bottom and semi spherical head. Internal diameter of crystallizer is 0.8 m and total height 2.13 m. The height of conical bottom and semi spherical head is 0.3 m and cone angle is 45^0. Inlet

is single (tangential) of diameter 0.154 m but outlets are different, liquid outlet at bottom of cone of diameter 0.2 m and vapor outlet at top of head of diameter 0.09 m.

The semi spherical head is for proper out flow of vapor and disengagement of entrained droplets, bottom is conical at 45^0 which help in smooth out flow and less deposition of solid substance and height of main body increases hold up and cylindrical structure avoids deposition (Dutta, 2009). Inlet is tangential because in industries this type of inlet is also used (Bamforth, 1965) and causes less turbulence.

Fig. 3.2 shows the computational geometries of FC crystallizer used for simulation studies. Fig. 3.2 (a) shows the computational geometry used for simulation in isothermal, non-isothermal condition and for population density study and is likely the physical unit. Fig. 3.2 (b) represents the computational geometry used for solid suspension simulation in which vapor outlet has not been considered because only water and solid particles have been used to see the description of flow and solid distribution.

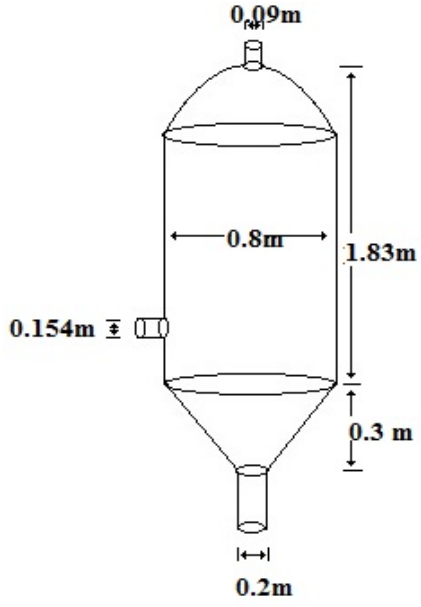

Fig. 3.1. Schematic representation of force circulation crystallizer.

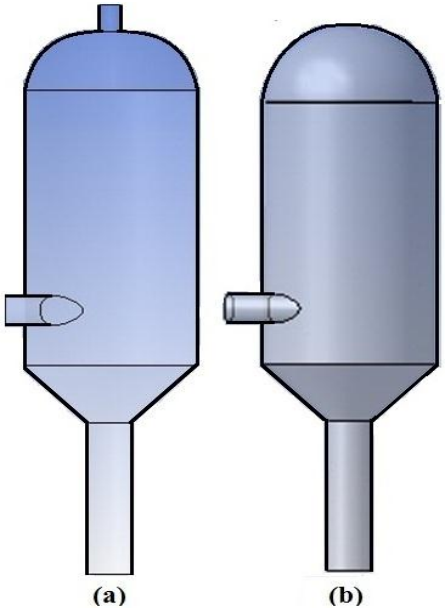

Fig. 3.2. Computational 3D geometries of FC crystallizer for simulation (a) Isothermal, Non–isothermal and population density simulation, (b) Solid suspension simulation.

Four different inlet positions at 0.5 m, 0.7 m, 0.9 m and 1.1 m above the bottom of the cone have been used for both the computational geometries to carry out simulation except for the population density study, in which only main computational geometry (with inlet positions at 0.5 m) has been used.

3.3. Mesh

Mesh creation is the subdivision of main computation flow domain in to number of smaller, non-overlapping subdomains on which flow equations are solved. In the present work mesh for computational geometries has been created by the program FLUENT-Mesh in ANSYS Workbench 13. First step the boundaries (2D regions) has been defined for the computational geometries. These regions include the solution inlet, product outlet, vapor outlet, and walls. Initially 2D mesh on the boundaries of the crystallizer geometry has been created and then this mesh has been extrapolated into the body of the geometry. The volume of the crystallizer tank has been divided into a set of discrete subdomains, computational cells, or control volumes using mesh. The mesh can contain elements of many shapes and size.

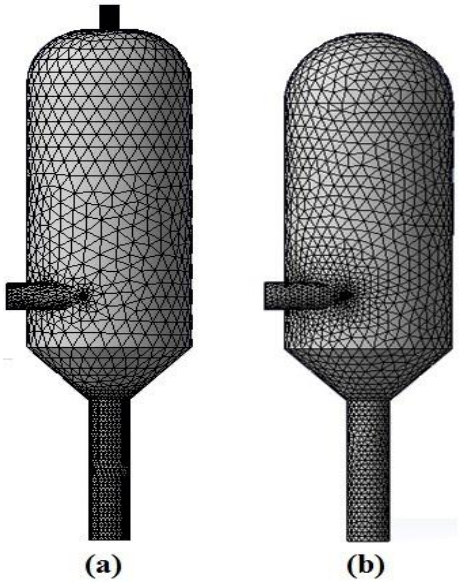

Fig. 3.3. Mesh of forced circulation crystallizer used for different simulation work (a) Isothermal, Non–isothermal and population density simulation, (b) Solid suspension simulation.

Unstructured tetrahedral meshing has been done for both computational geometries of FC crystallizer and is displayed in Fig. 3.3. Fig. 3.3 (a) shows unstructured tetrahedral mesh of the computational geometry used for simulation in isothermal, non-isothermal condition and for population density analyses. Fig. 3.3 (b) shows unstructured tetrahedral meshing of the computational geometry used for solid suspension simulation. The number of nodes and elements for different geometries are shown in table 3.1.

3.4. Physical properties

The physical properties of dilute solution with NaCl [liquid], water-vapor [vapor] and solid particles for simulation are presented in Table 3.2. All properties of water-vapor are available in ANSYS FLUENT 13 and all properties of water solution with NaCl at 298 K have been taken from Essemiani et al. (2004).

Table 3.1: Number of nodes and elements presents in the mesh of different geometries.

Isothermal and Non-Isothermal model		
Geometry	**Number of Nodes**	**Number of elements**
Inlet at 0.5 m	9679	47232
Inlet at 0.7 m	9641	46955
Inlet at 0.9 m	8984	43152
Inlet at 1.1 m	9584	46850
Solid suspension model (without vapor outlet)		
Inlet at 0.5 m	7209	34317
Inlet at 0.7 m	8955	42952
Inlet at 0.9 m	9050	43426
Inlet at 1.1 m	8921	42730
Population balance model		
Inlet at 0.5 m	15496	76268

3.5. Boundary conditions

Boundary conditions are specifications of properties or conditions on the surface of domains and are required to fully define the flow simulation. The fluid boundary conditions are available for the present work in ANSYS FLUENT 13 as; inlet, outlet and wall.

Inlet boundary condition used is mass flow rate for liquid and vapor and outlet boundary condition is mass out flow but for population balance model inlet boundary condition is

velocity inlet and outlet is defined as pressure outlet. Temperature condition is isothermal except for non-isothermal simulation and population balance. Wall boundary conditions are no slip and adiabatic (no heat exchange from wall). The vapor mass flow rate is used in proportion to the solution mass flow rate for maintaining stoichiometric vapor volumetric concentration. Operating conditions used in the present study are listed in Table 3.2 (Essemiani et al., 2004; Dutta, 2009);

Table 3.2: Properties of the system and operating conditions

Isothermal and Non-Isothermal simulation		
Physical properties	**Phases**	
	Liquid (15% NaCl solution)	**Vapor**
Density, kg/m^3	1063	0.59
Viscosity, kg/s-m	0.0013	0.0000124
Surface tension, N/m	0.077	-
Thermal conductivity, W/m-K	6.48	0.025
Mass flow rates, kg/s	27.5, 47.8, 67.5, 87.5	0.0102, 0.0176, 0.0249, 0.0324
Operating pressure, k Pa	101.325	
Temperature, K	379.5 (Non-Isothermal simulation)	
Heat, kW/m^3	3000 (for solution)	
Solid suspension simulation		
	Liquid phase (water)	**Solid particles (second phase)**
Density, kg/m^3	998	2600
Particles sizes, μm	50, 500, 900	
Liquid mass flow rates, kg/s	27.5, 47.5, 67.5, 87.5	
Operating pressure, k Pa	101.325	

Population balance simulation		
	Liquid (15% NaCl solution)	**Crystals**
Density, kg/m^3	1063	2156
Liquid inlet velocity, m/s	2.4	
Crystals sizes (5 - sizes), m	0.0002 to 3.2e^{-05}	
Volume shape factor	0.523	
Nucleation Rate, No. of nuclei/m^3-s	3.2e^8	
Growth Rate, m/s	3.33e^{-8}	

3.6. Solution Methodology

Solution methodology used in the present work is described as,

Discretization and solution: Control-volume based technique has been adopted to convert a general scalar transport equation to an algebraic equation that has been solved numerically by integrating the transport equation about each control volume obtaining a discrete equation that expresses the conservation law on a control-volume basis;

$$\int \frac{\partial \rho \phi}{\partial t}.dV + \oint \rho \phi \vec{v} dA = \oint \Gamma_\phi . \nabla \phi . d\vec{A} + \int_V S_\phi dV \tag{3.1}$$

Where ρ, density, $\vec{v}$, velocity vector, $\Gamma_\emptyset$, diffusion co-efficient for ϕ, $\nabla\phi$, gradient of ϕ and S_ϕ, source of ϕ per unit volume. This is applied to each cell in the computational domain.

Discretized form of equation (3.1) by considering the unsteady conservation equation of a scalar quantity ϕ and for a given cell, is given as;

$$\frac{\partial \rho \phi}{\partial t} V + \sum_f^{N_{face}} \rho_f \vec{v}_f \phi_f \vec{A}_f = \sum_f^{N_{face}} \Gamma_\phi . \nabla . \phi_f + S_\phi \tag{3.2}$$

Where N_{face}, number of face enclosing cell, ϕ_f, value of ϕ convected through face *f*, $\rho_f \vec{v}_f \phi_f \vec{A}_f$, mass flux through face, $\vec{A}_f$, area of face *f*, $\nabla . \phi_f$, gradient of ϕ at face *f* and V, cell volume.

The discretized scalar transport equation contains unknown scalar variable ϕ at the cell center as well as the unknown value in the surrounding neighbor cells. The equation is non-linear with respect to these variables and linearized form of equation (3.2) used is written as;

$$a_p\phi = \sum_{nb} a_{nb}\phi_{nb} + b \tag{3.3}$$

nb is the neighbor cell, and $a_p$and a_{nb} are the linearized co-efficient for ϕ and ϕ_{nb} .

The number of neighbor for each cell depends on a mesh topology, but typically equals the number of faces enclosing the cell. This results in a set of algebraic equations with sparse co-efficient matrix. These linear systems of scalar equation have been solved using a point implicit (Gauss-Seidel) linear equation solver in conjunction with an algebraic multigrid (AMG) method.

Discretization Scheme: The default discrete values of the scalar ϕ at the cell center (C_0 and C_1 in Fig. 3.4*)* available in ANSYS FLUENT have been used. Face values ϕ_f required for the convection term in equation (3.2) and have been interpolated from the cell center value and are accomplished using an upwind scheme. Upwinding means that the face value ϕ_f is derived from quantities in the cell upstream or "upwind", relative to the direction of the normal velocity v_n. ANSYS FLUENT has several upwind schemes: first-order upwind, second order upwind, power law, and QUICK.

In the present work first-order upwind scheme is used for first order accuracy. Quantities at cell faces have been determined by assuming that the cell-center values of any field variable represent a cell-average value and hold throughout the entire cell; the face quantities are identical to the cell quantities. The face value ϕ_f has been set equal to the cell-center value of ϕ in the upstream cell.

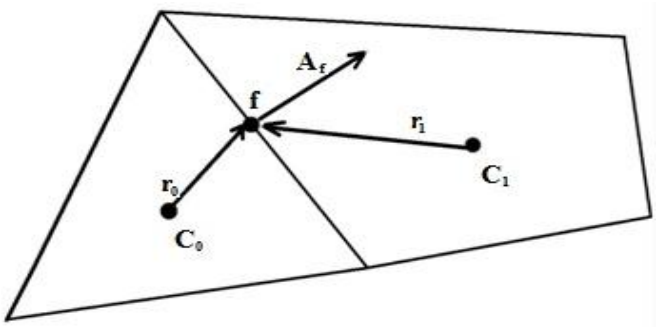

Fig. 3.4. Control volume used to illustrate discretization of a scalar transport equation.

$$\phi_{f,sou} = \phi + \nabla.\phi\vec{r} \tag{3.4}$$

Evaluation of gradient and derivative: Gradient is needed not only for constructing values of a scalar at the cell faces, but also computing secondary diffusion terms and velocity derivatives. The gradient $\nabla.\phi$ of a given variable ϕ has been used to discretize the convection and diffusion term in the flow conservation equation. The gradients have been computed from least square cell-based method (Ansys Fluent User Guide 2009).

Pressure-Velocity Coupling: In the present work SIMPLE algorithm has been used for pressure-velocity coupling which solves the flow problem in segregated manner.

SIMPLE (Semi-Implicit Method for Pressure Linked Equations) algorithm uses a relation between velocity and pressure corrections to enforce mass-conservation and to obtain pressure field. The momentum equation has been solved using a guessed pressure field; p^*, the resulting face flux; J_f^* (from equation for J_f);

$$J_f^* = \vec{J}_f^* + d_f\left(p_{C_0} - p_{C_1}^*\right) \tag{3.5}$$

does not satisfy the continuity equation. Consequently, a correction J_f' has been added to the face flux J_f^* so that the corrected face flux, J_f;

$$J_f = J_f^* + J_f' \tag{3.6}$$

satisfies the continuity equation. The SIMPLE algorithm postulate that J_f' be written as;

$$J_f' = d_f\left(p_{C_0}' - p_{C_1}'\right) \tag{3.7}$$

where p_{C_0}' is the cell pressure correction.

The SIMPLE algorithm substitutes the flux correction equations into discrete continuity equation to obtain a discrete equation for the pressure correction p' in the cell.

$$a_p p' = \sum_{nb} a_{nb} p_{nb}' + b \tag{3.8}$$

where the source term b is the net flow rate into the cell.

$$b = \sum_{f}^{N_{face}} J_f^* A_f \tag{3.9}$$

The pressure-correction equation has been solved using the AMG method. Once the solution is obtained, the cell pressure and the face flux are corrected using;

$$p = p^* + \alpha_p p' \tag{3.10}$$

$$J_f = J_f^* + d_f\left(p'_{C_0} - p'_{C_1}\right) \tag{3.11}$$

where α_p is the under relaxation factor for pressure. The corrected face flux, J_f satisfy the discrete continuity equation.

Under-relaxation of factors: Because of non-linearity of the equation set, it is necessary to control the change of ϕ. This is typically achieved by under-relaxation of variable, which reduces the changes of ϕ produced during each iteration. In a simple form, the new value of the variable ϕ within a cell depend upon the old value; ϕ_{old}, the computed change in ϕ, $\Delta\phi$, and the under-relaxation factor α, as follow;

$$\phi = \phi_{old} + \alpha\Delta\phi \tag{3.12}$$

The under-relaxation parameters for all variables used in the present study analysis are: pressure = 0.1 – 0.3, density = 1, body forces = 1, momentum = 0.1- 0.7, volume fraction = 0.5, turbulent kinetic energy = 0.8, turbulent dissipation rate = 0.8 and turbulent viscosity = 1.

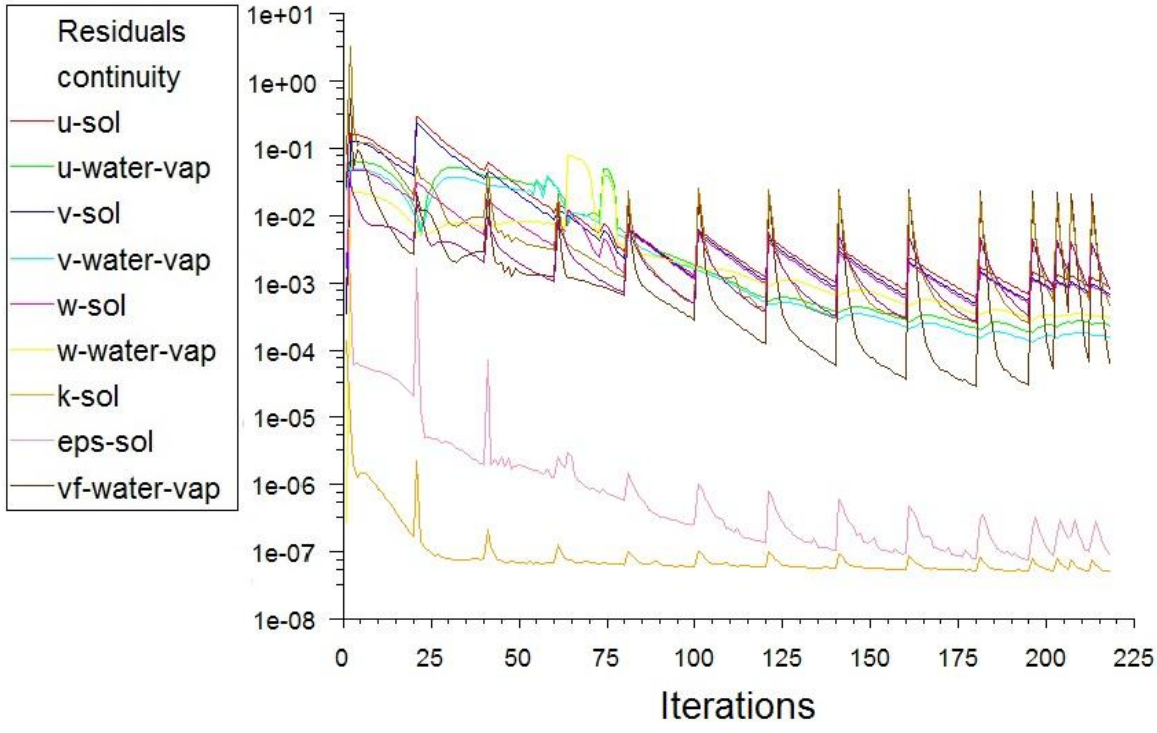

Fig. 3.5. Plot of residuals with the progress of simulation.

For all the numerical simulations the time step size of 0.01 s has been used and 20 iterations are used for per time step. The convergence criteria for all the numerical

simulations are based on monitoring the mass flow residual and the value of $1.0e^{-03}$ was set as converged value. The residual plot of the progress of the simulation is shown in Fig. 3.5.

CHAPTER-4

RESULTS AND DISCUSSION

The numerical results of CFD simulation for various computational geometries of FC Crystallizer solved with different numerical models to characterize various process parameters (as detailed in previous chapters 2 & 3) has been presented in this chapter. Simulations for all cases have been carried out till the quasi steady state is achieved i.e. the volume averaged flow variables are time independent. This has been achieved by monitoring the vapor and solution volume fractions. Fig. 4.1 shows the vapor volume fraction varying with physical time of simulation. At quasi steady state the vapor has completely dispersed in the vessel. It can be observed from Fig. 4.1 that complete distribution of vapor is seen around 110 s of physical time of simulation and there is no variation till 120 s. Simulations continued for 150 s and the averages over the last 30 s has been used in the analysis. Once the fully developed quasi-steady state is reached, the averaged quantities in terms of time, axial and radial direction have been calculated.

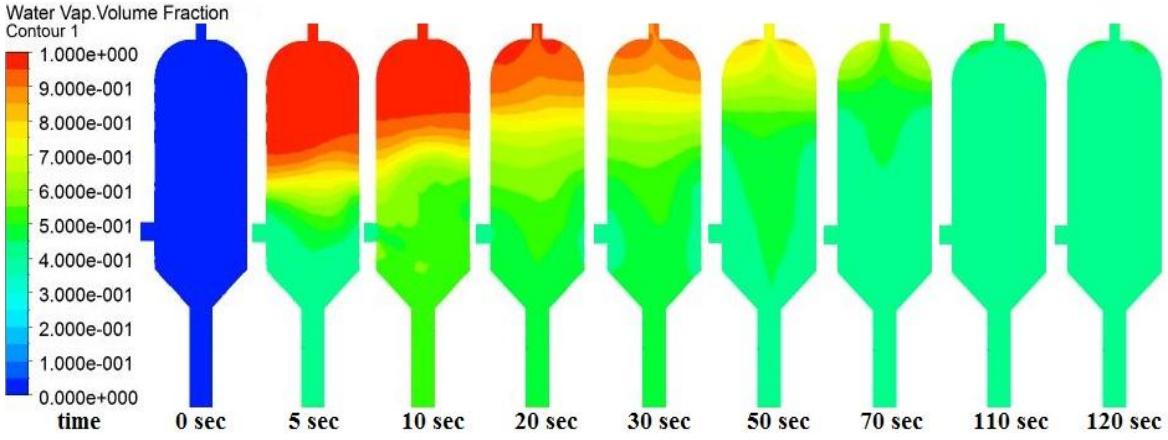

Fig. 4.1. Contours of vapor volume fraction at different physical time of simulation for liquid and vapor mass flow rates of 27.5 kg/s and 0.0102 kg/s respectively with inlet position of 0.5 m.

The results have been represented by means of contour, vector and x-y plots. The results of simulation are divided in to sections based on the model used for simulation. The parameters studied include; phase volume fraction, phase velocity, pressure variation in the vessel, crystal population density, mean crystal growth and crystal size distribution. These results of simulation are analyzed, discussed and comparisons are made for the results obtained in the present study with those available in literature. As hardly any CFD work on FC Crystallizer is seen in literature, some-times the comparison has been made

with results obtained from similar systems relevant to the parameter under discussion. For example, as in the present study tangential inlet for the FC Crystallizer has been used the flow velocity pattern has been compared with the flow pattern occurred in hydro-cyclone.

4.1. Isothermal Simulation

The temperature in crystallizer during crystallization is maintained near boiling temperature of solution to evaporate solvent and large difference does not occur in temperature of due to release of heat of crystallization from solution to vapor phase, thus isothermal condition for crystallization can be assumed without significant error (Wantha, 2006). In this section the vapor is assumed to form in an external heat exchanger before being fed into the crystallizer. This situation has been modeled by an isothermal process in order to reduce the computation time and model complexity. The systems studied for isothermal simulation are detailed in Table 3.2 (chapter-3).

4.1.1. Flow dynamics

Flow dynamics study is important for any flow process because it involves calculating various flow properties of the fluid, such as forces, mass flow rates, velocity and pressure as functions of space and time. Fig. 4.1 shows the contours of volume fraction of vapor inside the FC Crystallizer for the liquid mass flow rate of 27.5 kg/s and vapor mass flow rate of 0.0102 kg/s at inlet position of 0.5 m. From Fig. 4.1 it is observed that the volume fraction of vapor is gradually dispersed, as the simulation proceeds and finally dispersed completely in the entire vessel. In any crystallizer, solution concentration distribution is an important factor for crystallization process because uniform concentration distribution supports the nucleation and growth of crystals. Fig. 4.2 shows the solution volume fraction that solution volume fraction is not uniform through-out the crystallizer; it is more near the wall because of centrifugal force by swirl flow.

Fluid velocity is an important characteristic of the hydrodynamic study because changes in fluid velocity affect the phase distribution. Fig. 4.3 shows contour of solution velocity inside the FC crystallizer for mass flow rate of 27.5 kg/s. The solution velocity magnitude is found to be higher near the wall; it is because of tangential inlet which induces circular motion of the fluid. The velocity at the center is low and increase with radius but it is zero at the wall because of no-slip boundary condition for the solid wall. The circular motion increase holding time of solution which is good for crystal growth. Fig. 4.4 shows plot of solution axial velocity varying in radial direction at different heights. From the Fig. 4.4, it

is found that solution axial velocity pattern is same for all heights, but the magnitude of linear flow velocity decrease with height. It may be because of gravitational force. The solution velocity profile obtained in the present study is different from the one obtained by Essemiani et al. (2004). The difference in flow profile may be due to tangential inlet in the present work which is normal in the work of Essemiani et al. (2004). It can be observed from Figs. 4.3 and 4.4 that a low velocity zone for all phases has been formed at center of the FC crystallizer due to circular motion similar to flow profile in hydrocyclone and cyclone separators (Leeuwner and Eksteen, 2008).

Fig. 4.5 shows the plot of the axial velocity profile of solution and vapor varying radially at height of 0.5 m. It is observed that the velocity profile of vapor is same to that of solution, which is because of higher solution density and mass flow rate of solution compared to that of vapor. The vapor flows along with the liquid as an entrapped phase. The vapor phase follows the path of the solution.

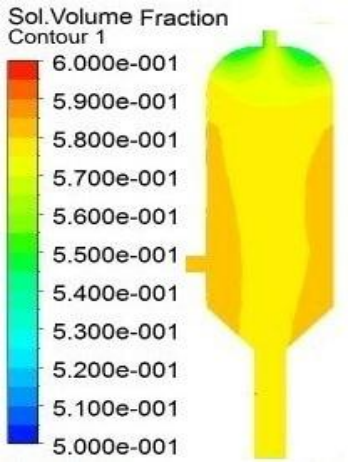

Fig. 4.2. Contour of solution volume fraction at solution mass flow rate of 27.5 kg/s with inlet position of 0.5 m.

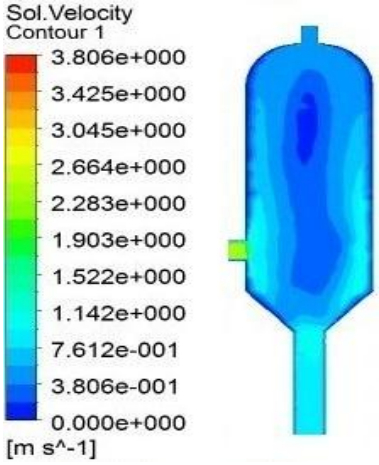

Fig. 4.3. Contour of solution velocity at solution mass flow rate of 27.5 kg/s with inlet position of 0.5 m.

Generally velocity vector exhibits flow direction, velocity magnitude and flow patterns. Fig. 4.6 shows the cross sectional view of velocity vectors of solution at different axial positions. These velocity vectors confirm that flow of solution is circular in pattern (swirl flow) and low velocity zone is forming at the center and the position of low velocity zone position found to change from top to bottom, not coinciding with the geometrical center. Fig. 4.7 represents the velocity vector in central vertical plane; from it can be observed that flow is turbulent, vertices are formed near of the wall and cone; and disturbance is occur due to mixing between downward low velocity center stream of solution with

upward flow stream in the upper region. Fluid flow is twisted, curved and it is not axially symmetric due to the center of circular flow is disturbing the outflow. For cyclone separator Wang et al., (2003) have found non axis symmetric and twisted flow pattern.

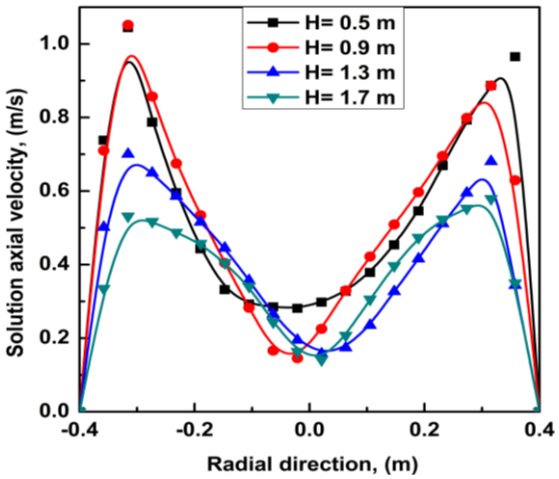

Fig. 4.4. Variation of solution axial velocity in radial direction for mass flow rate of 27.5 kg/s at inlet position of 0.5 m.

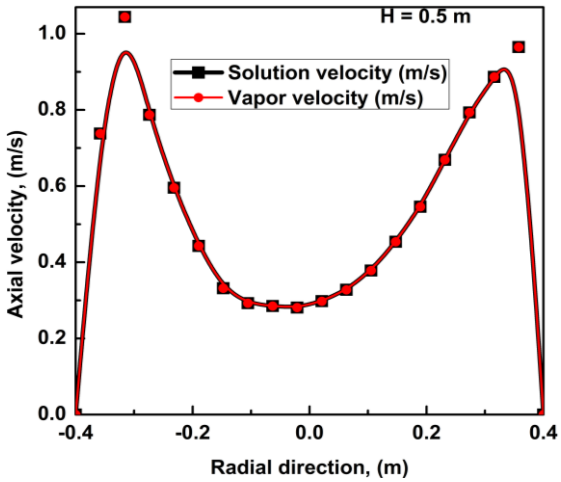

Fig. 4.5. Plot of solution and vapor velocities varying in radial direction for solution and vapor mass flow rates 27.5 and 0.0102 kg/s at inlet height of 0.5 m.

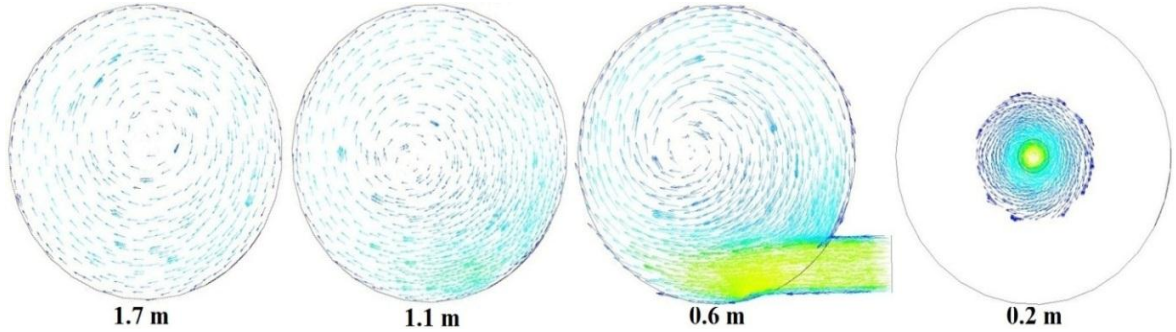

Fig. 4.6. Velocity vector of solution at different cross-sections along axial direction.

Pressure variation is not significant and does not affect the crystallization (except vacuum which cause crystallization at low temperature) but in the hydrodynamics study pressure is an important factor, because due to pressure difference flow varies. Fig. 4.8 shows the contour of pressure. Solution pressure is less at the top and increases towards the bottom, this satisfies the hydrostatic condition. Similarly pressure change from vapor outlet to bulk solution oulet has been observed by Wantha (2006) for DTB crystallizer.

4.1.2. Effect of inlet flow rates

Flow rate contributes an important part in phase distribution for crystallizer. The axial velocity distribution avoids the particles accumulation. It brings on an even solid

suspension distribution and uniform supersaturation in the whole crystallizer. High flow rate induces turbulent flow which exhibits unpredictable motion with a violent exchange of momentum and locally circulating currents. This vigorous circular current forms circular loops (vortices) which causes non uniform low velocity profile in vessel.

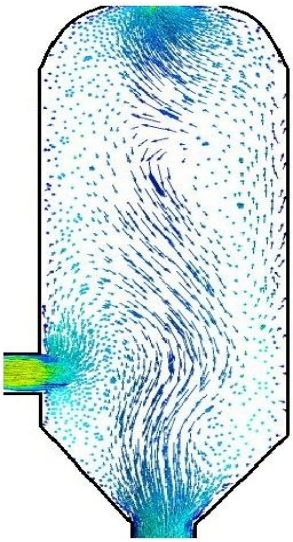

Fig. 4.7. Velocity vector at central vertical plane for solution mass flow rate of 27.5 kg/s and position of inlet at 0.5 m.

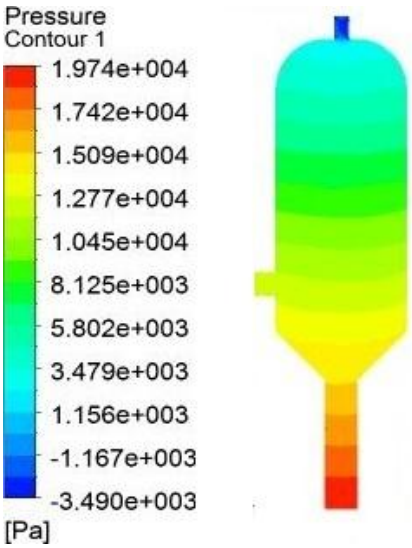

Fig. 4.8. Contour plot of Pressure at central vertical plane for solution mass flow rate of 27.5 kg/s and vapor mass flow rate of 0.0102 kg/s at inlet position of 0.5m.

Fig. 4.9 shows the contour of the solution velocity in FC crystallizer at different solution mass flow rates. The flow field is found to be more undistributed with increase in flow rate of solution and low velocity zone has covered (expanded) more area at high flow rate. In case of hydrocyclone Zahra (2012) has observed expansion in negative velocity core both ways axially and radially with increase in inlet velocity. Due to tangential inlet of solution in the present work, the velocity magnitude is found to be more than achieved for the same flow rate by Essemiani et al. (2004) for normal inlet (Fig. 4.10 (b)).

Fig. 4.10 (a) shows velocity vector of the solution in FC crystallizer at different solution mass flow rates. It is observed that flow is become more turbulent and axially non symmetrical with increase in flow rate of solution. It is due to the mixing in downward flowing low velocity center stream and upward flow stream. Due to tangential inlet of solution in the present work, the circular loop is small and not affecting inlet stream for same flow rate case of Essemiani et al. (2004) for normal inlet (Fig. 4.10 (b)).

Fig. 4.11 shows solution volume fraction distribution. It is observed from the plot that solution volume fraction is completely distributed in the whole crystallizer but it is higher

near the wall. Flow rates are affecting the solution volume fraction distribution in the crystallizer, with increase in flow rate the solution volumetric concentration become more distributed towards upside and increased near of wall in crystallizer, this may be due to increase in centrifugal force with increase in flow rate. The Uniform distribution of solution concentration in crystallizer supports uniform growth of crystals.

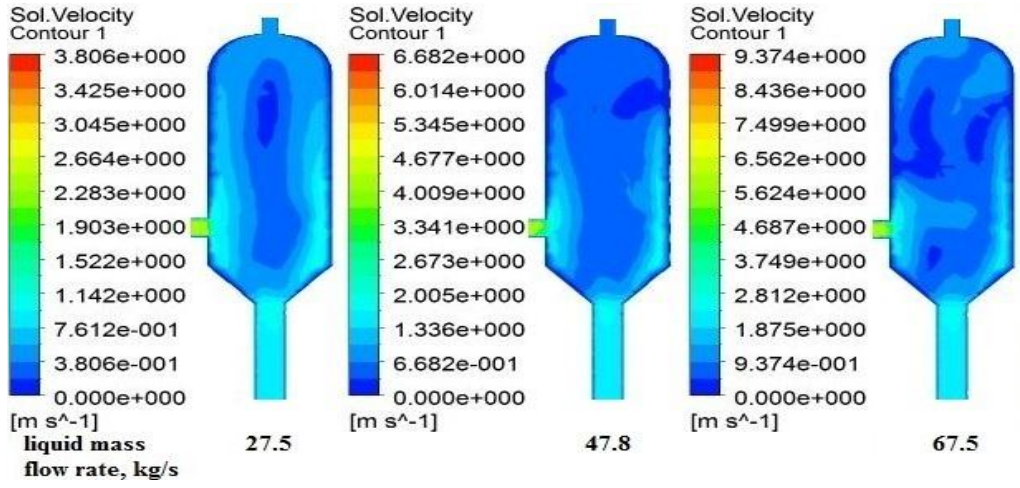

(a) (b) (c)

Fig. 4.9. Velocity contours for solution mass flow rates; (a) 27.5 kg/s, (b) 47.8 kg/s and (c) 67.5 kg/s for inlet position 0.5 m.

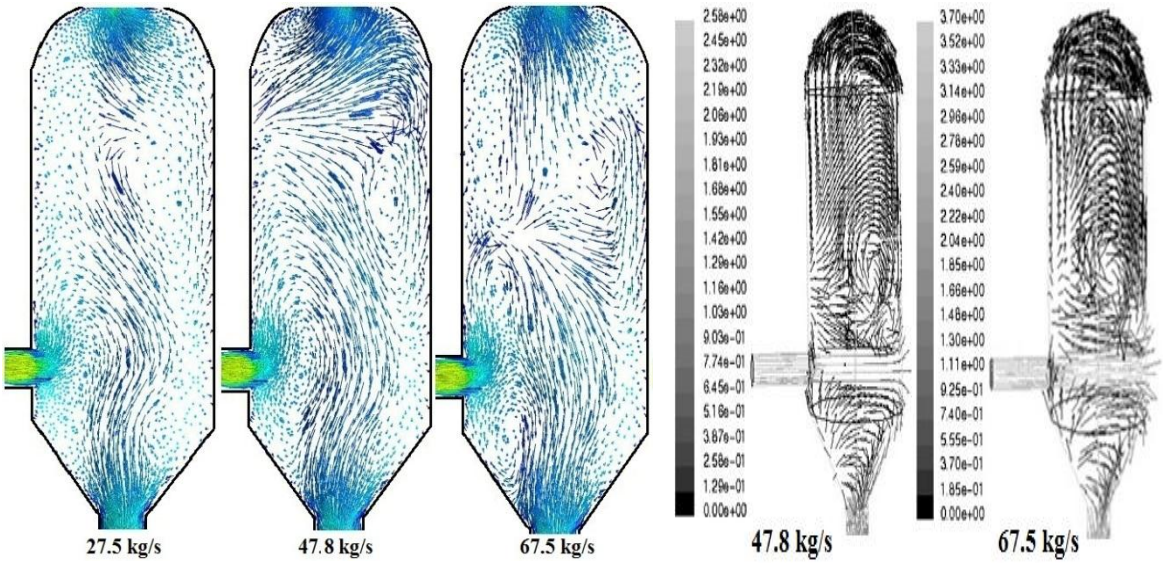

(a) (b)

Fig. 4.10. Velocity vectors for (a) solution mass flow rates; 27.5 kg/s, 47.8 kg/s and 67.5 kg/s for inlet position 0.5 m in present work and (b) Essemiani et al. (2004) for flow rates 47.8 kg/s and 67.5 kg/s.

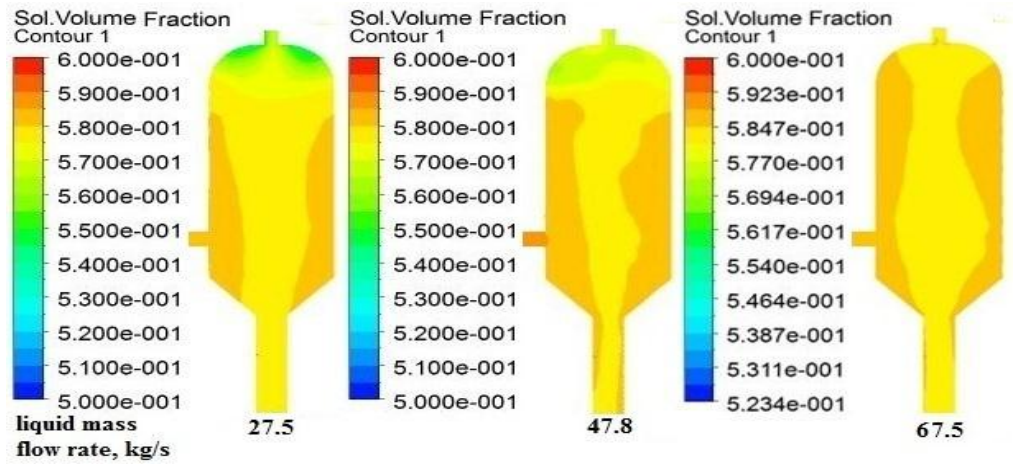

(a) **(b)** **(c)**

Fig. 4.11. Vertical central plane solution volume fraction for solution mass flow rates; (a) 27.5 kg/s, (b) 47.8 kg/s and (c) 67.5 kg/s for inlet position of 0.5 m.

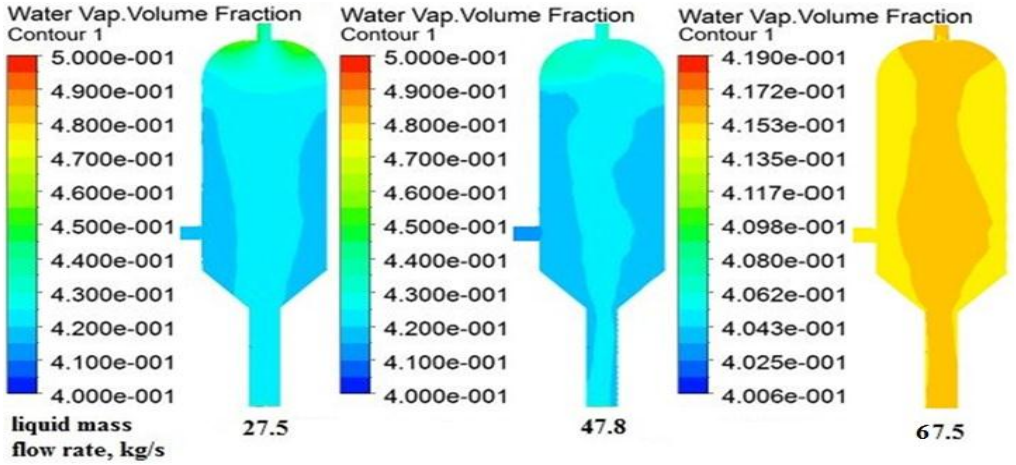

(a) **(b)** **(c)**

Fig. 4.12. Vapor volume fraction for solution mass flow rates (a) 27.5 kg/s, (b) 47.8 kg/s and (c) 67.5 kg/s for inlet position of 0.5 m.

Fig. 4.12 shows vapor volume fraction distribution (magnified scale of contour). It is observed from the plot that vapor volume fraction is completely distributed in the whole crystallizer but it is just opposite of solution volume fraction distribution which is higher in center and increasing with increase in solution flow rates, this may be due to centrifugal force showing phase separation (not complete). It is found by Leeuwner and Eksteen (2008) that air core is formed due to circular flow in hydrocyclone.

Fig. 4.13 shows the contours of solution pressure distribution axially for different solution mass flow rates in FC crystallizer. Solution pressure is changing according to the

hydrostatic conditions, with increase in mass flow rate of solution (dense phase) the solution pressure is found to increase in the cryastallizer.

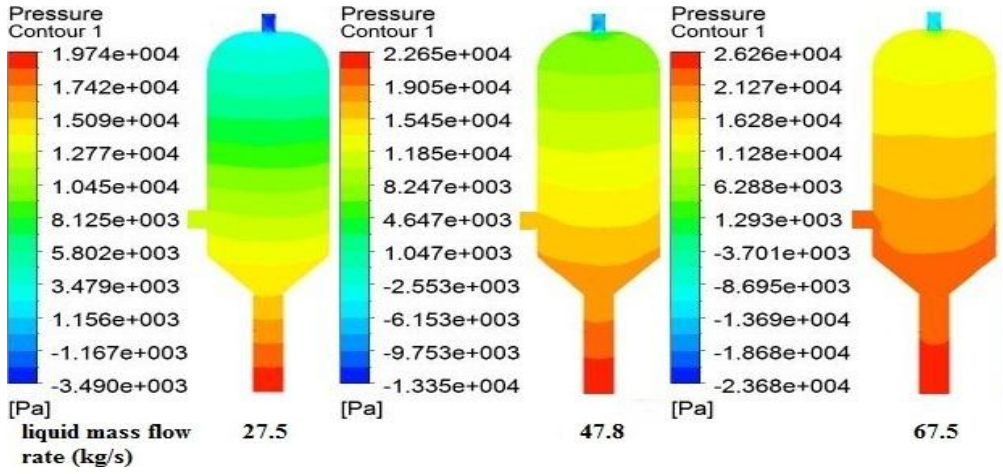

(a) (b) (c)

Fig. 4.13. Pressure contours for solution at different mass flow rates (a) 27.5 kg/s, (b) 47.8 kg/s and (c) 67.5 kg/s for inlet position 0.5 m.

4.1.3. Effect of Inlet position on flow distribution

The flow dynamics and statics change with height mainly due to the gravitational force, so the effect of inlet position by CFD has been observed. The effect of inlet position studied by Wei et al. (2001) for precipitation in semi batch crystallizer and found it support crystal size distribution. Essemiani et al. (2004) have found dead-zone formed due to turbulent flow with inlet height its size increases in the crystallizer.

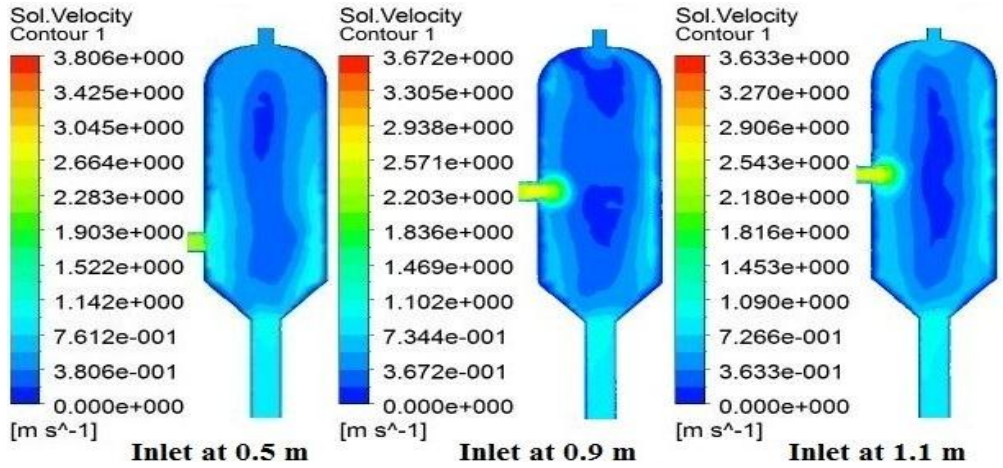

(a) (b) (c)

Fig. 4.14. Velocity contours for solution mass rate of 27.5 kg/s at inlet positions (a) 0.5 m, (b) 0.9 m and (c) 1.1m.

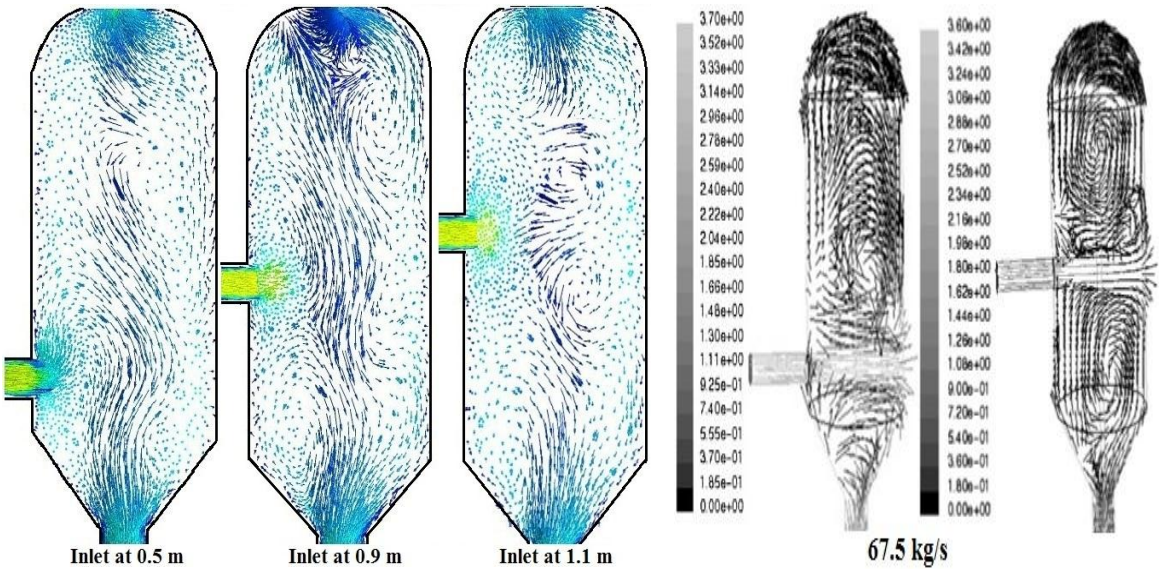

(a) **(b)**

Fig. 4.15. Velocity vectors (a) solution mass flow rate 27.5 kg/s at inlet positions; 0.5 m, 0.9 m and 1.1m, (b) Essemiani et al. (2004) for flow rates 67.5 kg/s at 0.5 m and 0.9 m.

Fig. 4.15 (a) shows velocity vector of the solution in FC crystallizer at solution mass flow rate of 27.5 kg/s for different inlet positions. It is observed that turbulence in flow is increasing with inlet height. It is due to the mixing between downward flowing low velocity center stream and upward flow stream but for inlet at 1.1m this mixing affecting inlet flow and two circulation loops are forming. In the present work at flow rate 27.5 kg/s for all inlet positions, the velocity magnitude is found to be same achieved for the flow rate 67.5 kg/s by Essemiani et al. (2004) for normal inlet but the circular loops are small in size (Fig. 4.15 (b)).

Figs. 4.16 (a) and (b) show solution and vapor volume fraction (magnified scale of contour) distribution at different inlet positions for solution mass flow rate of 27.5 kg/s and vapor mass flow rate of 0.0102 kg/s. It is observed from the plot that volume fraction of both phases completely distributed in the whole crystallizer but it is higher near the wall for solution phase and higher in center for the vapor phase, and with increase in inlet height distribution of both phases has increased in their respective zone, this may be due to centrifugal force by swirl flow. It is found that with increase in level of inlet the maximum vapor volume fraction decreases and the vapor is well distributed in whole of the crystallizer. For lower inlet position the vapor is found to be more at the top of the crystallizer. Vapor separation increases crystallization but non uniform distribution of solution concentration affect the crystal growth.

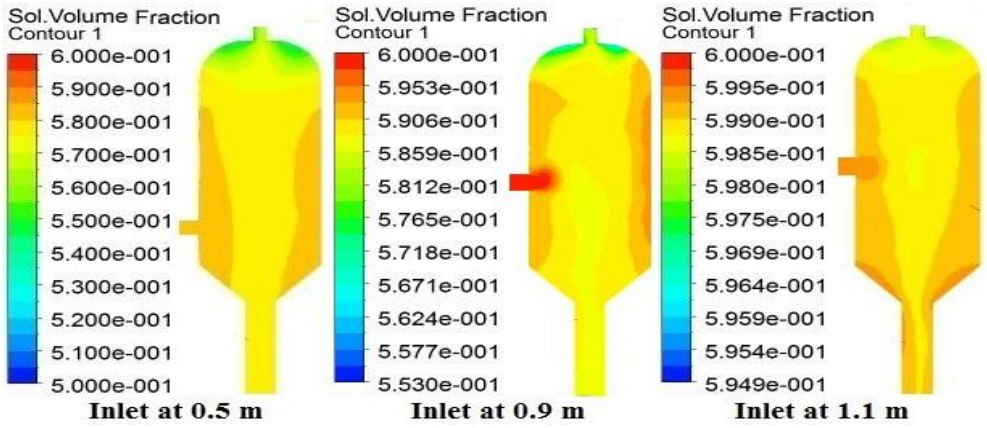

(a)

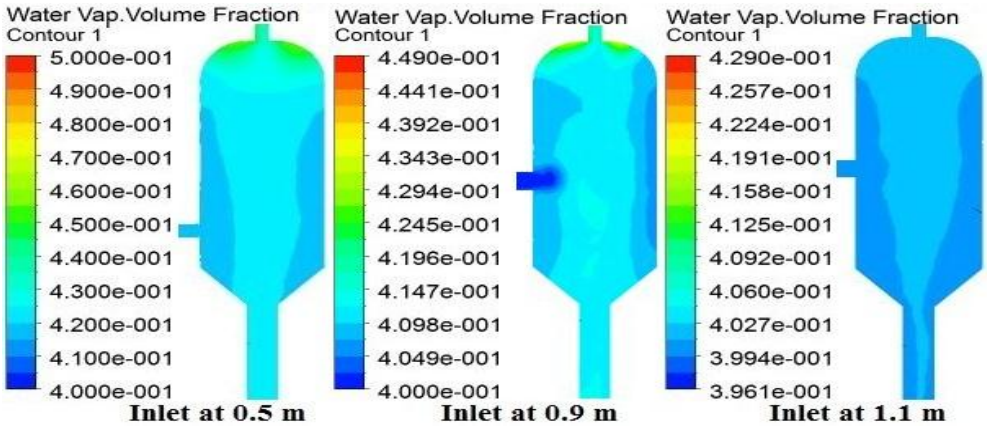

(b)

Fig. 4.16. Contours of; (a) solution volume fraction and (b) vapor volume fraction, for solution and vapor mass flow rates of 27.5 kg/s and 0.0102 kg/s at different inlet positions 0.5 m, 0.9 m and 1.1 m.

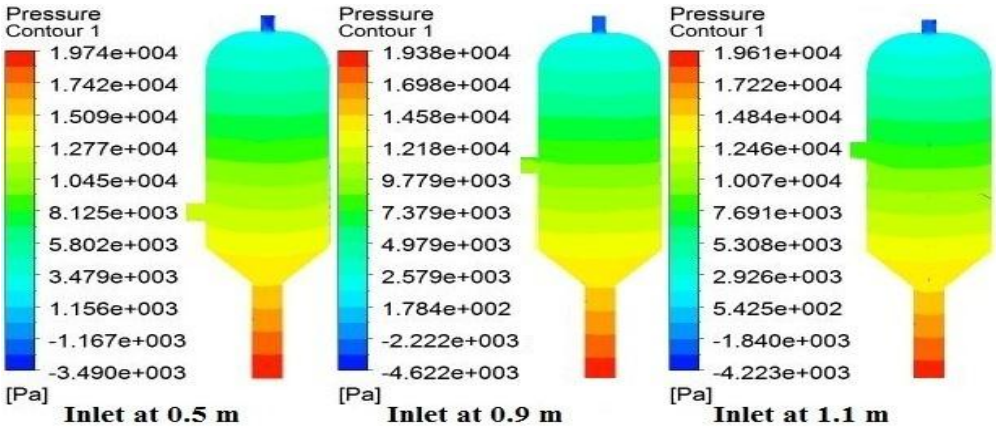

(a) (b) (c)

Fig. 4.17. Pressure contours for solution mass flow rate of 27.5 kg/s at inlet positions (a) 0.5 m, (b) 0.9 m and (c) 1.1m.

Fig. 4.17 shows solution pressure distribution with increase in inlet height and it is found from the contour scale that axial difference of solution static pressure is increased with inlet height. With increase in the level of inlet position, the minimum pressure is lowered but the maximum pressure gradually increases.

4.2. Non-isothermal Simulation

In the present work the temperature of feed solution used is 379.5 K (boiling temperature of solution). A low heat of 3000 kW/m^3 is given to feed solution and observed how the solution temperature varies in the system. Vapor phase is considered as isothermal phase so the vapor temperature is constant at the boiling temperature (saturated vapor temperature, 380.5 K). This is quite realistic: the evaporation produces a saturated vapor, and this will not undergo significant cooling before leaving the body of the FC crystallizer. This study is not much different from isothermal simulation case except the thermal condition of crystallizer is analyzed through temperature profiles of the solution phase. Cases studied in this section are considered with no mass transfer and without any reaction.

4.2.1. Flow dynamics

Flow dynamics is crucial for non-isothermal simulation because it includes calculation of temperature with other properties of the fluid, such as forces, velocity, and pressure, as functions of space and time. In crystallization supersaturation level depend on the quantity of solvent is transformed into vapor phase. The distribution of vapor volume fraction in crystallizer for the solution and vapor mass flow rates of 27.5 kg/s and 0.0102 kg/s at inlet position 0.5 m is shown in Fig. 4.18 (a) for non-isothermal simulation. It is seen that the vapor volume fraction gradually increases from feed to the top of the crystallizer and the vapor is completely separating from solution and interphase or free surface is formed. This may be due to that the heated vapor (light phase) is not following solution phase and is separating. The more separation of vapor (solvent evaporation) more is the crystallization.

Fig. 4.18 (b) shows solution volume fraction in crystallizer for solution and vapor mass flow rates of 27.5 kg/s and 0.0102 kg/s, it exhibits that solution volume fraction is decreased in the top region where the vapor volume fraction is large than the whole crystallizer, this may be due to temperature and density difference for which phase separation occur. Similarly solution and vapor phase separation is observed by Wantha (2006) in the DTB crystallizer. The increase in separation of vapor increases solution

supersaturation which is good for growth of crystal size.

Fig. 4.19 shows variation of solution axial velocity in radial direction at different heights. The solution velocity magnitude is found be zero at the wall because of no-slip boundary condition. The variation of solution velocity along the radius is not uniform as it was observed for isothermal simulation. It may be because of flow of the vapor in some specific zone which changes with time. Solution velocity affects crystal size distribution in the system and undistributed velocity affects it.

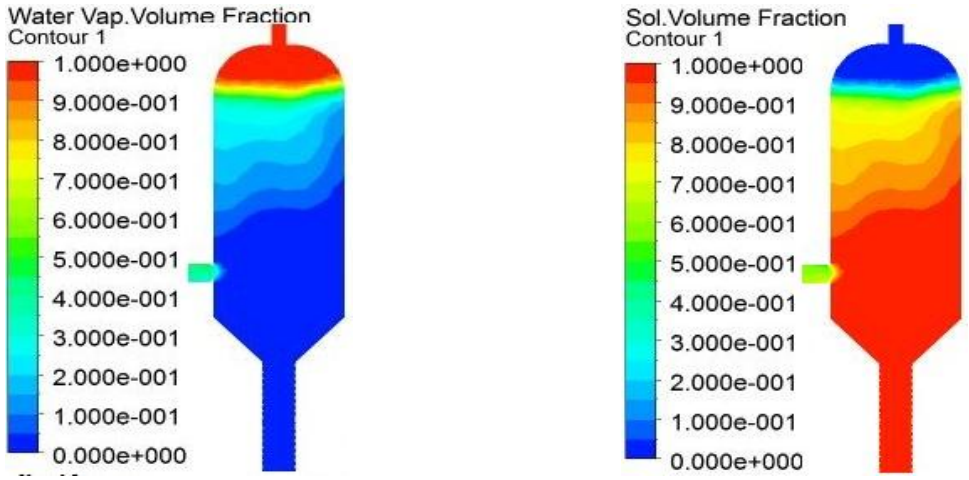

(a) **(b)**

Fig. 4.18. Contour of volume fraction; (a) vapor (b) solution at vapor and solution mass flow rates of 0.0102 kg/s and 27.5 kg/s for inlet position at 0.5 m.

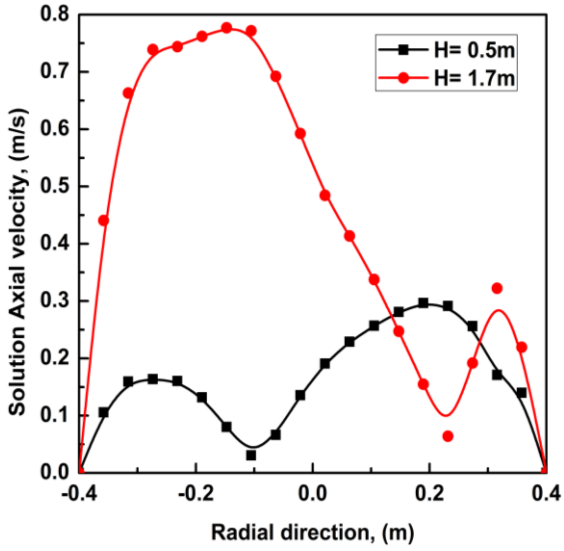

Fig. 4.19. Radial variation of solution velocity at different axial positions for mass flow rate of 27.5 kg/s and inlet position at 0.5 m.

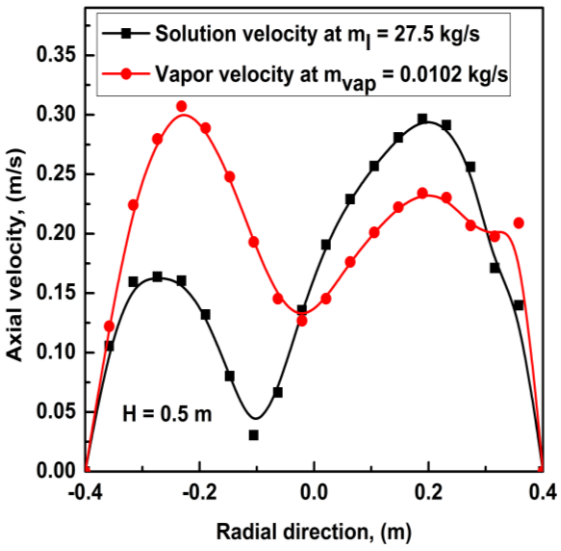

Fig. 4.20. Plot of solution and vapor velocity for solution and vapor mass flow rates of 27.5 and 0.0102 kg/s with feed inlet at 0.5 m.

Fig. 4.20 shows the plot of the axial velocity profile of solution and vapor varying radially at height 0.5 m of FC crystallizer. From the plot it is observed that the velocity magnitude of vapor and solution phase change with position and are reversed i.e. when the solution velocity is high, the vapor velocity at that location is low, and this is because of inventory. The change in flow profile may be due to separation of heated phases and vapor is not completely following the path of solution.

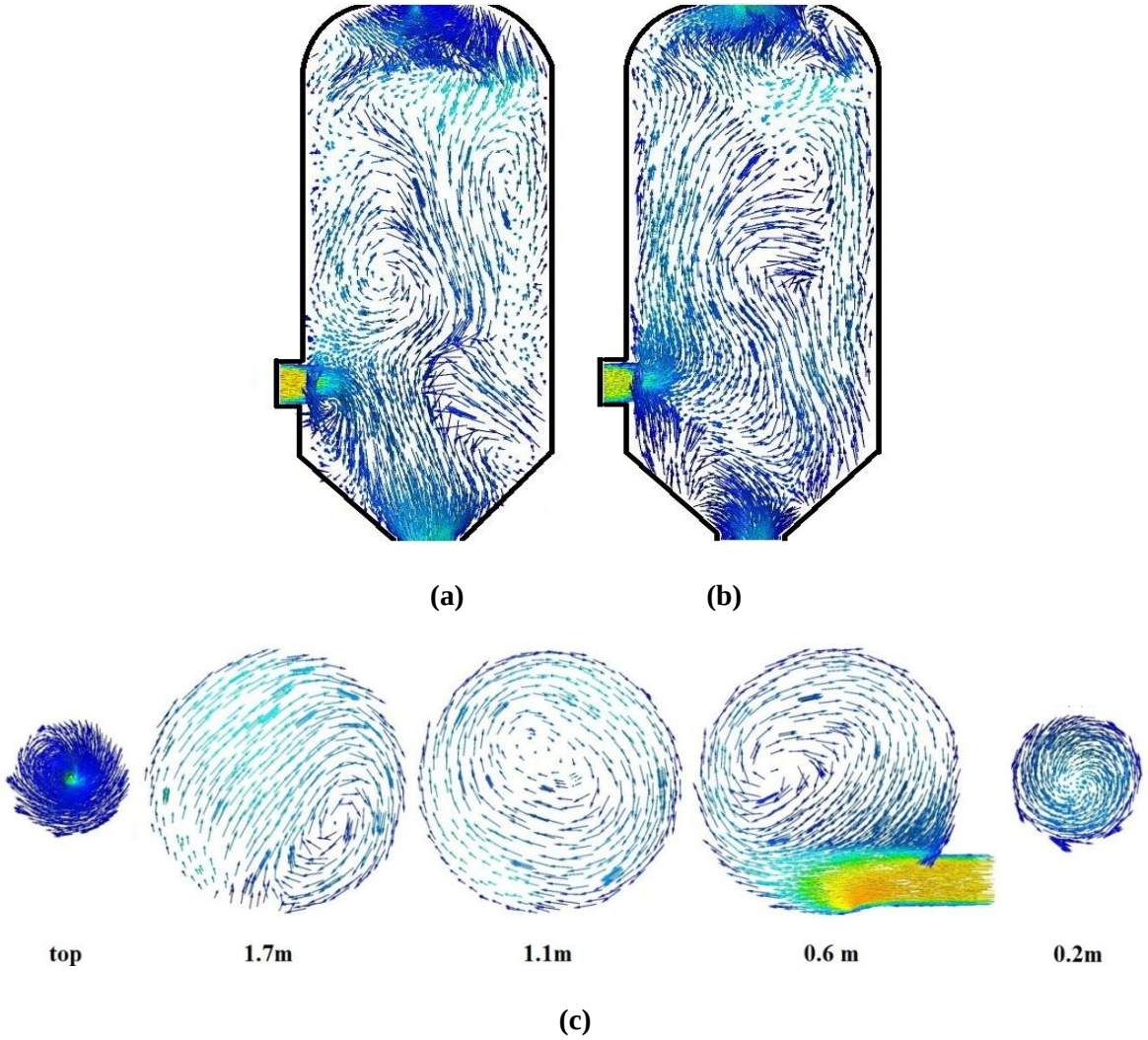

Fig. 4.21. Velocity vectors of (a) solution and (b) vapor at central vertical plane, (c) solution, at different horizontal cross-sections with inlet at 0.5 m, solution mass flow rate of 27.5 kg/s and vapor mass flow rate of 0.0102 kg/s.

Velocity vector shows flow direction and patterns. Figs. 4.21 (a) and (b) show velocity vectors central vertical region for solution at mass flow rate of 27.5 kg/s and vapor at mass flow rate of 0.0102 kg/s, Fig. 4.21 confirms that the overall solution flow direction is downward and vapor flow direction is upward although it varies locally. Both solution and vapor flow field is opposite but for both phases in between fluid flow circulation loops are

formed and their flow direction is clock wise and anticlockwise. Circulation loops are major factor of in proper distribution and energy loss in the flow. Fig. 4.21 (c) shows velocity vectors of solution in cross sectional planes at different axial positions from top to the bottom, it is found that solution is forming circular pattern (swirl flow); and a low velocity center zone is forming and its position changing from top to the bottom of the crystallizer not coinciding to the geometrical center. Flow is twisted and non- symmetric axially and affects the outflow. Wang et al. (2003) have found non axis symmetric and twisted flow pattern which disturbing inlet flow in cyclone separator.

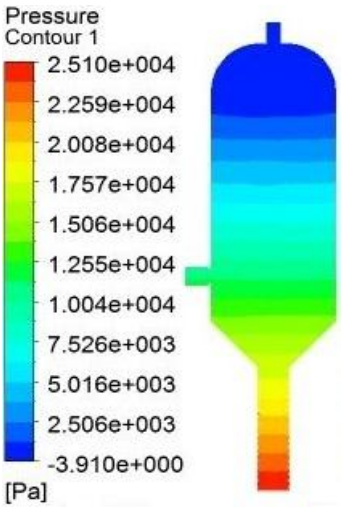

Fig. 4.22. Contour of pressure for solution mass flow rate 27.5 kg/s at inlet position 0.5 m.

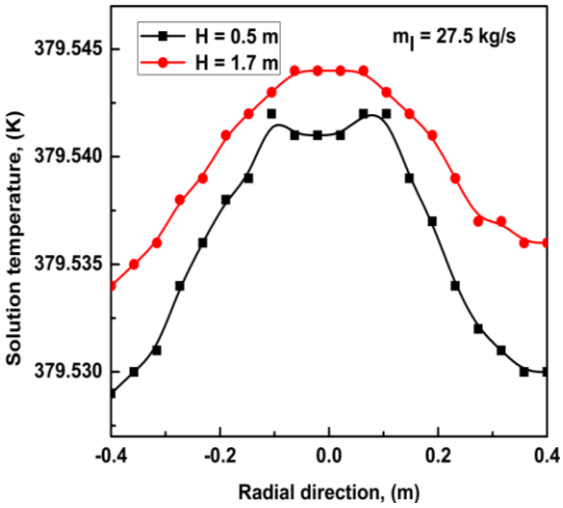

Fig. 4.23. Variation of solution temperature for solution mass flow rate of 27.5 kg/s at inlet position of 0.5 m.

Pressure affect vaporization, at low pressure it increases, in the present work vaporization is not considered but due to heated phase some effect is seen on pressure. Fig. 4.22 shows pressure contour for solution phase for solution mass flow rate 27.5 kg/s and its axial distribution along the crystallizer. The pressure variation is according to the hydrostatic law and incareses from top to the bottom. But pressure is too low in upper zone; this is due to the occupation of the region entirely by the vapor phase after phase separation.

Fig. 4.23 shows radial distribution of solution temperature at two different heights in the FC crystallizer for solution mass flow rate 27.5 kg/s. The solution temperature is less at the wall and gradually increases to the center. At lower height a flat temperature zone is observed for the system. The temperature is found to be more at 1.7 m height that it is at 0.5 m, the temperature is more at the surface where phases separate. This may be due to the fact that in crystallization boiling occur at free surface where by evaporation phases

separates which leads to supersaturation for nucleation and crystal growth (Wantha, 2006); near of it temperature remain high. In crystallization process temperature gradient is a main driving force in maintaining supersaturation to form crystals.

4.2.2. Effect of inlet flow rates

The effect of inlet flow rate of solution and vapor phase on flow behaviour is studied in presence of heated phases. Fig. 4.24 shows contour of vapor volume fraction at different vapor and solution mass flow rates. It is seen from the Fig. 4.24 that in the top region where vapor and solution separation occurs, an interphase or free surface is formed and vapor is occupying full space above the interface. This vapor space is shrinking with increase in mass flow rates of the phases due to increase in level of the solution in the crystallizer. Due to increase in flow rate circular motion is become more intense, vapor distribution in crystallizer is increased and vapor core in center due to swirl motion is started to form, which extends to the bottom with increase in the flow rate. Thus higher flow rate affect the vapor separation. The pattern of the vapor core is same as the one observed in case of hydrocyclone (Leeuwner and Eksteen, 2008; Zahra, 2012).

The deformation of the free surface induces a wave (due to turbulent flow), the force caused by the wave should be taken into account for the structure design (Essemiani et al., 2004). Fig. 4.25 shows the contour plot of solution volume fraction at different solution and vapor flow rates. In the present simulation the free surface formed is found to be at higher height than the one obtained by Essemiani et al. (2004) for normal inlet position. Free surface is not seen at higher flow rates. For flow rate 27.5 kg/s free surface deformation is less than 7 cm which is more in the work of Essemiani et al. (2004).

Figs. 4.26 (a) and (b) show the plot of the solution and vapor axial velocity profile varying radially at height of 0.5 m in the FC crystallizer. From the figures it is observed that the velocity profile of vapor is same to that of the solution velocity profile for all flow rates. At the wall the velocity is zero and near to the wall the velocity is maximum and decreases to the center. At low flow rate (27.5 kg/s) the velocity magnitudes of vapor and the solution phases are different, but for all higher flow rates (47.8, 67.5 and 87.5 kg/s) the velocity magnitudes of the phases are found to be almost same. This indicates that the solution phase forces the vapor to follow the path of the solution. For lower vapor and solution mass flow rate the vapor is completely separated from the solution.

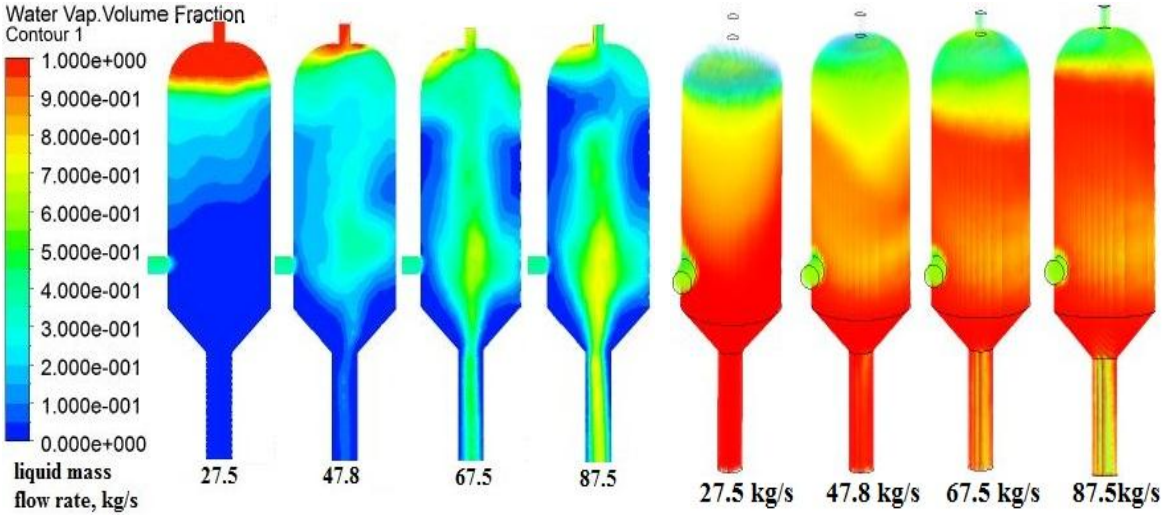

Fig.4.24. Contour of vapor volume fraction for different solution mass flow rates with inlet at 0.5 m.

Fig.4.25. Contour showing solution deformed free surface for solution mass flow rates of 27.5, 47.5, 67.5, and 87.5 kg/s for inlet at 0.5m.

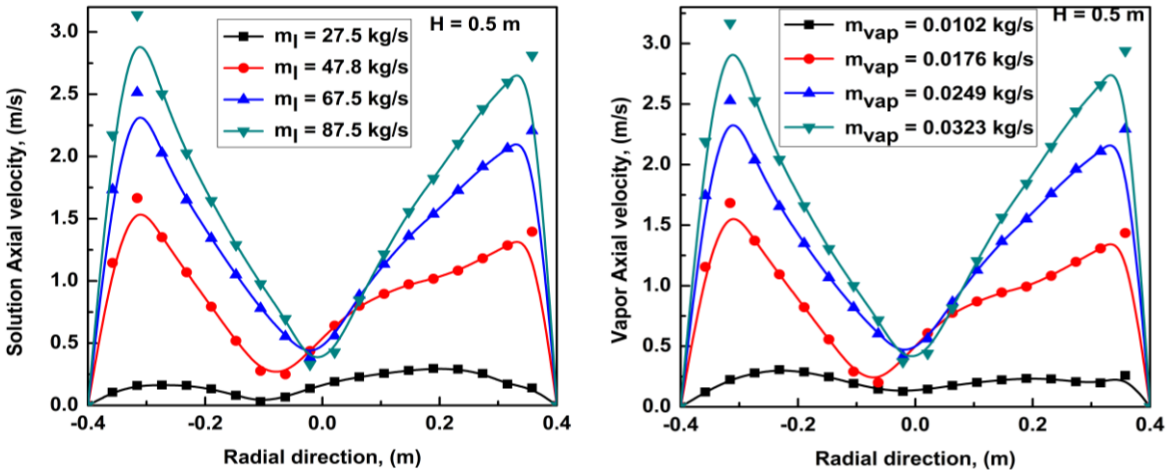

(a) **(b)**

Fig. 4.26. Plot of phase velocity (a) solution and (b) vapor with inlet at 0.5 m for solution mass flow rates of 27.5, 47.5, 67.5, 87.5 kg/s; and vapor mass flow rates of 0.0102, 0.0176, 0.0249 and 0.0323 kg/s.

Fig. 4.27 shows the contours of solution pressure distribution axially for different solution mass flow rates in FC crystallizer. With increase in mass flow rate of solution (dense phase) the pressure is found to increase in the cryastallizer.

Fig. 4.28 shows heated solution axial temperature distribution radially for different solution mass flow rates in FC crystallizer. With increase in mass flow rate of solution the temperature is found to decrease in the cryastallizer, it may be due to the fixed heating rate

per unit volume of solution in the crystallizer. When the solution rate is high the residence time of the solution in the crystallizer is less and the temperature rise for the solution is also less. Decrease in temperature decrease the evaporation which affects supersaturation for crystallization.

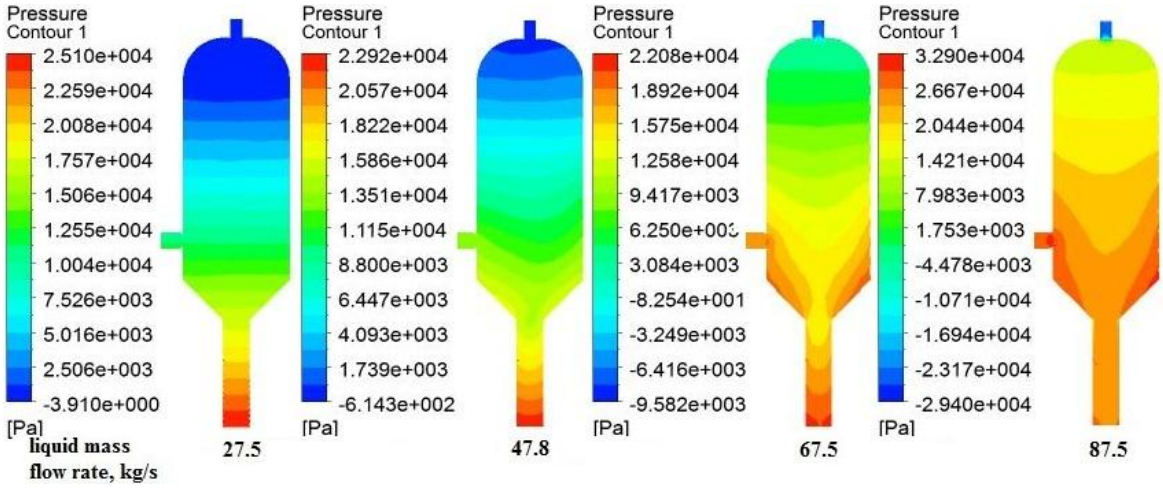

(a) **(b)** **(c)** **(d)**

Fig. 4.27. Pressure contours for solution mass flow rates (a) 27.5 kg/s, (b) 47.5 kg/s, (c) 67.5 and (d) 87.5 kg/s for inlet position at 0.5 m.

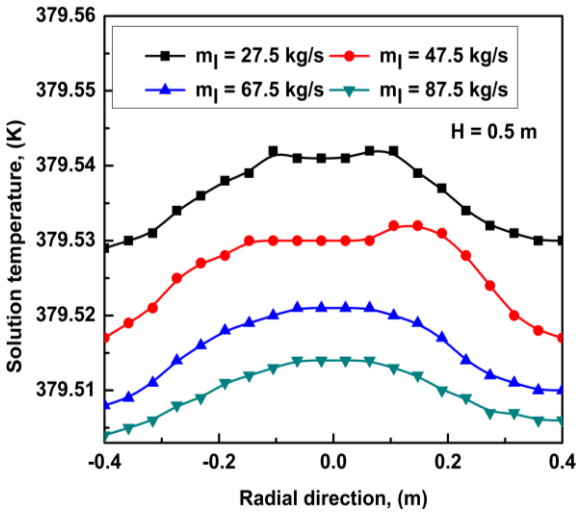

Fig. 4.28. Solution temperature at height 0.5m for solution mass flow rates of 27.5, 47.5, 67.5 and 87.5 kg/s.

4.2.3. Effect of Inlet position on flow distribution

With variation in feed position the flow properties such as velocity, phase distribution, pressure and temperature are expected to vary because of inventory, gravitational and centrifugal forces. The effect of inlet positions for non isothermal flow simulation is presented here.

Fig. 4.29 shows vapor volume fraction distribution at vapor mass flow rate of 0.0102 kg/s for different inlet positions in FC crystallizer. It is observed from the plot that vapor volume fraction is separating from solution at the inter phase or free surface in crystallizer. With increase in inlet height interphase is shifted towards the vapor out let and upper space occupied by vapor is shrunk.

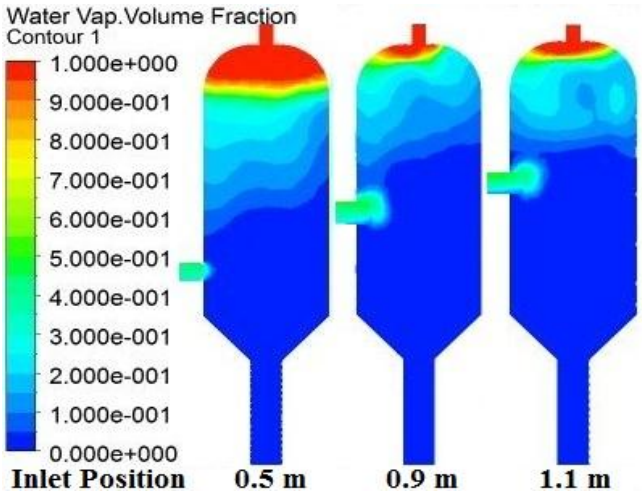

Fig. 4.29. Contours of vapor volume fraction for vapor and solution mass flow rate of 0.0102 kg/s and 27.5 kg/s at different inlet positions of ; 0.5 m, 0.9 m and 1.1 m.

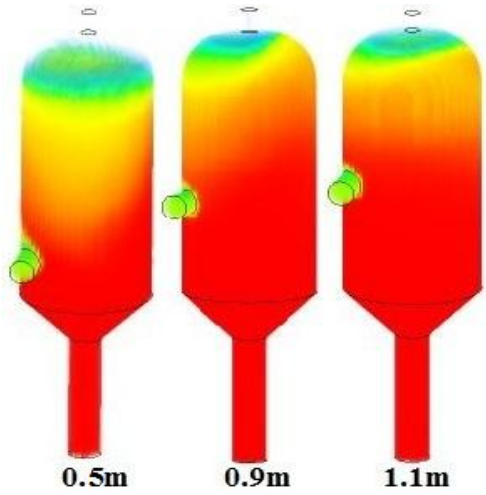

Fig. 4.30. Solution deformed surface for mass flow rate 27.5 kg/s and inlet at 0.5m, 0.9 m and 1.1 m.

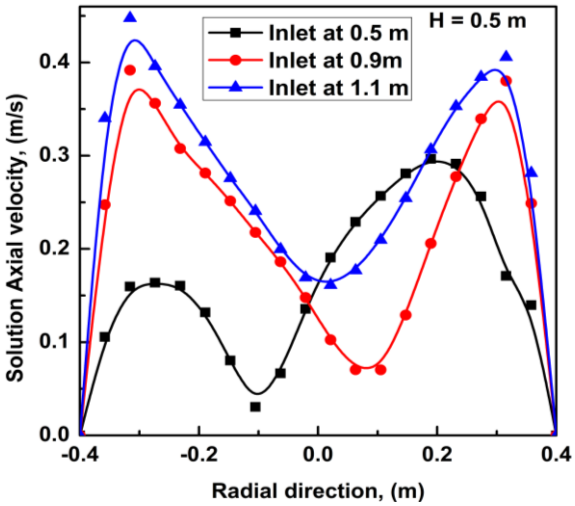

Fig. 4.31. Solution velocity profile at height 0.5m for solution mass flow rate 27.5 kg/s at inlet positions of; 0.5 m, 0.9 m and 1.1m.

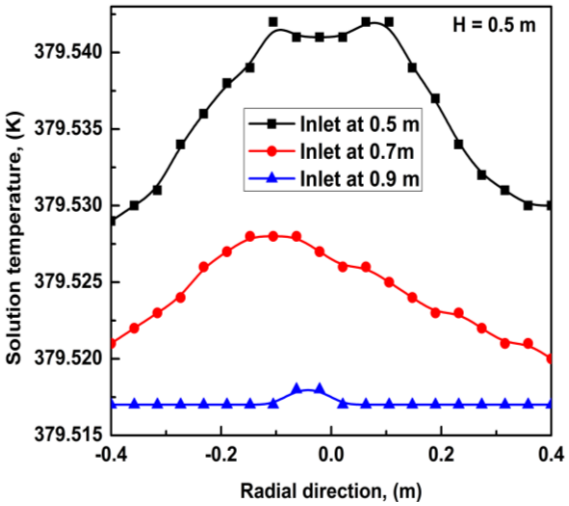

Fig. 4.32. Solution temperature at height of 0.5m for solution mass flow rate of 27.5 kg/s at inlet positions, 0.5 m, 0.7 m and 0.9 m.

Fig. 4.30 shows free surface deformation. Essemiani et al. (2004) for the normal inlet have found high deformation up to 20 cm, whereas in the present study the maximum

deformation found to be 7 cm. With increase of inlet height for the same flow rate of feed free surface is found to move towards the vapor outlet and it is not horizontal.

Fig. 4.31 shows the variation of solution axial velocity in radial direction at different inlet positions for solution mass flow rate of 27.5 kg/s in FC crystallizer. The solution velocity magnitude is found to be higher near the wall (but zero at the wall) for all heights; it is because of tangential inlets which cause circular motion of fluid. With increase in inlet height the velocity magnitude increases but a non-uniform radial variation is seen. The circular motion, increase holding time of solution which is good for crystal growth.

Fig. 4.32 shows heated solution axial temperature distribution radially for solution mass flow rate of 27.5 kg/s at different inlet positions in FC crystallizer. With increase in inlet height of solution, the temperature is found to decrease in the cryastallizer, it may be due to decrease in volume fraction of the solution and increase in the volume fraction of the vapor in that region.

Fig. 4.33 shows solution pressure distribution with increase in inlet height. It is found from contour scale that axial difference of solution static pressure is increased with inlet height. Also the maximum solution is found to increase with the elevation of inlet position.

4.3. Comparison of Isothermal and Non-isothermal flow

Comparison between isothermal and non-isothermal flow is carried out at solution mass flow rate of 27.5 kg/s and inlet position at 0.5m. Fig. 4.34 (a) shows comparison of solution volume fraction. In case of isothermal simulation, solution volume fraction is completely distributed in whole crystallizer with vapor phase and the higher volumetric concentration is present near the wall but in non-isothermal simulation solution phases are separating and the vapor phase is completely found in the upper zone and interphase is forming. Fig. 4.34 (b) shows that pressure drop in non-isothermal simulation is more than in case of isothermal simulation it may be because of separation of vapor from solution occupying upper region for non-isothermal case, but in isothermal simulation vapor is completely dispersed in the whole crystallizer. Comparison shows that non-isothermal simulation is more effective in flow and separation of the phases than isothermal simulation.

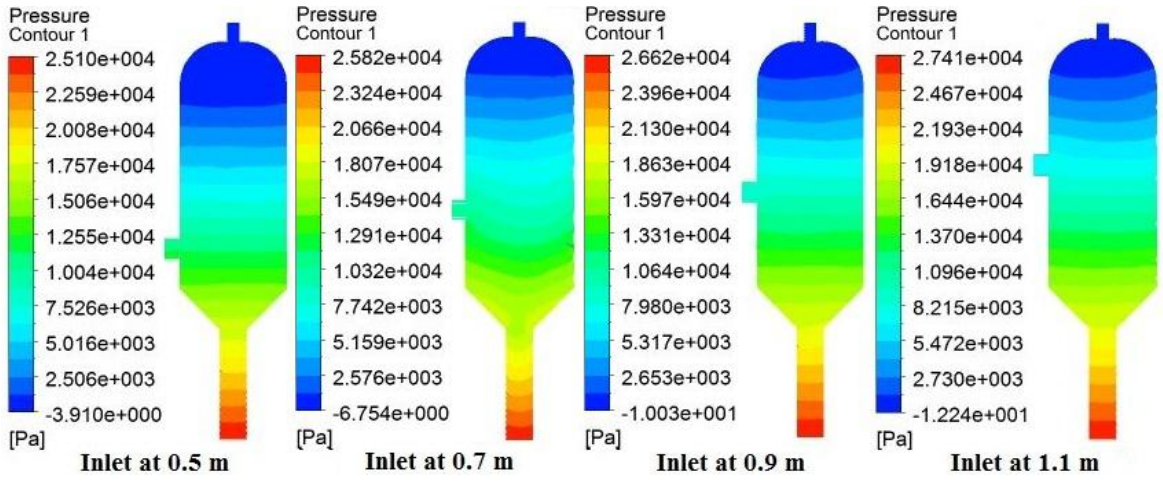

(a) (b) (c) (d)

Fig. 4.33. Pressure contours for liquid mass flow rate 27.5 kg/s at different inlet positions, (a) 0.5 m, (b) 0.7 m, (c) 0.9 m and (d) 1.1 m kg/s.

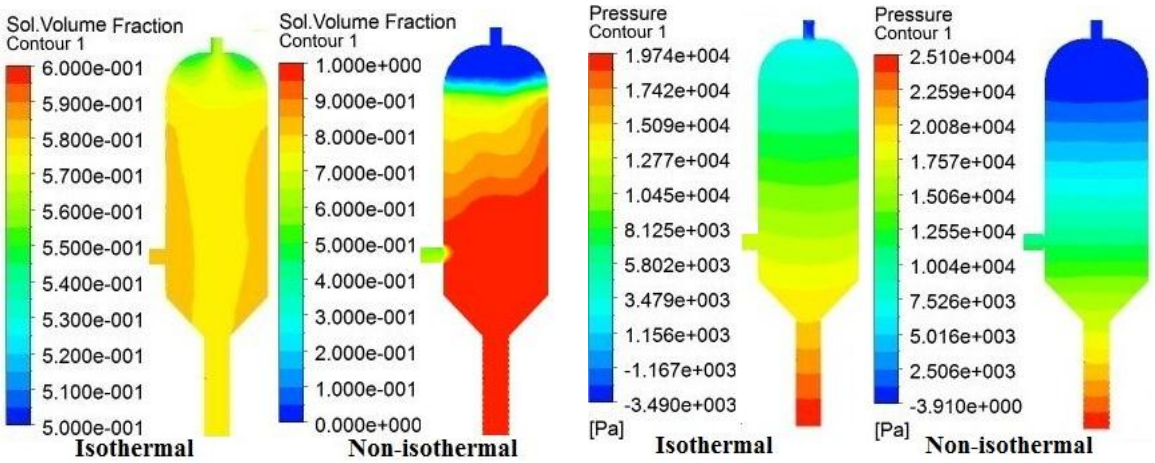

(a) (b)

Fig.4.34. Comparison of isothermal and non-isothermal simulation for solution mass flow rate of 27.5 kg/s; (a) solution volume fraction and (b) pressure.

4.4. Solid suspension in crystallizer

A good number of work is seen in literature on the CFD study of solid suspension distribution for crystallization process in last one decade by using various types of tanks and crystallizers (Sha et al., 2001; Zuoliang et al., 2008; Wojcik and Plewik, 2009; Mahdi et al., 2009; Plewik et al., 2010; Al-Rashed et al., 2012). There is no work seen in literature for the FC crystallizer. In the present work CFD study has been carried out to characterize the solid suspension distribution in forced circulation (FC) crystallizer. For simulation two phases (water and solid particles) have been considered and the simulation results are shown as contour plots and line diagrams.

4.4.1. Solid suspension behaviour for different particle sizes

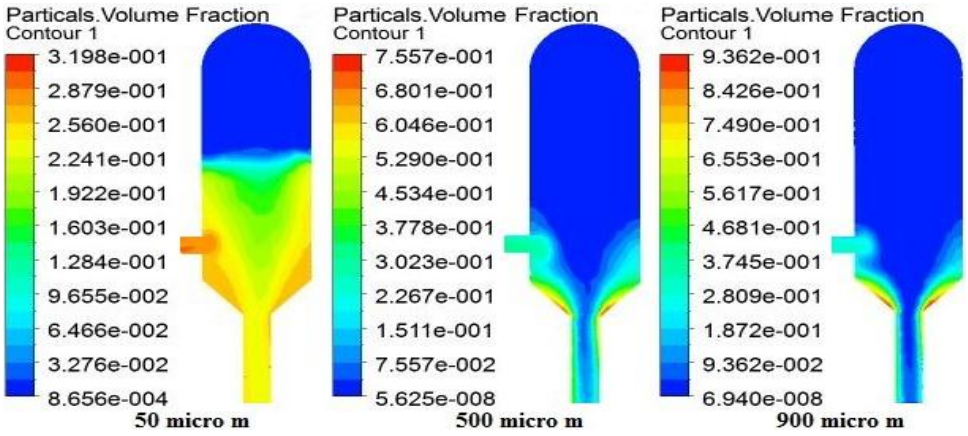

Fig.4.35. Contour of volume fraction for different size of solid particles with liquid mass flow rate of 27.5 kg/s at inlet position of 0.5m.

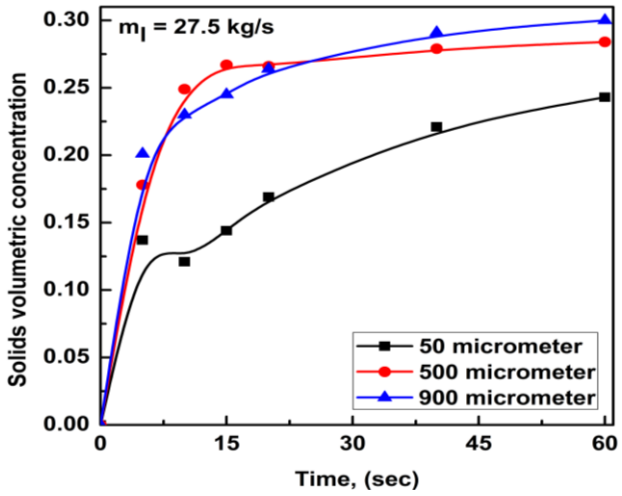

Fig. 4.36. Particles volumetric concentration at solution outlet.

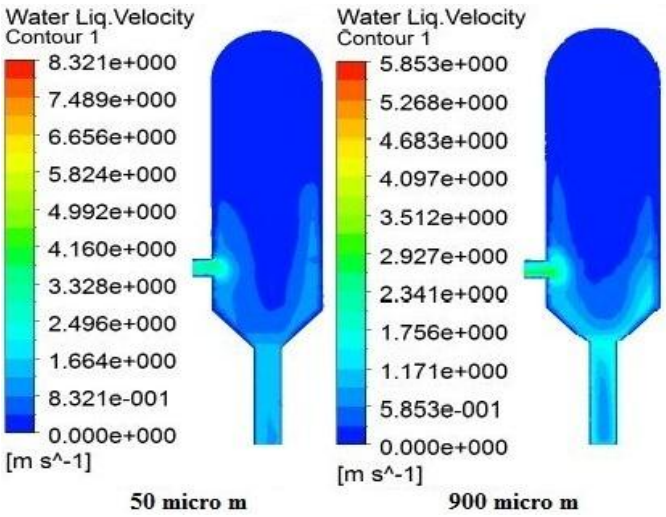

Fig. 4.37. Contour of solution velocity for different size of particles with liquid mass flow rate of 27.5 kg/s at inlet position of 0.5m.

Three different sizes of particles are used in monodisperse flow condition for solid suspension characteristic study. The particle sizes used in the study has been used by Sha et al. (2001) in case of stirred tank crystallizer simulation. Fig. 4.35 shows volumetric concentration distribution for all three different sizes of particles at liquid mass flow rate of 27.5 kg/s in FC crystallizer. The small size particles (50 μm) are more suspended and covering more area in the crystallizer than larger sizes (500 and 900 μm). The concentration of particles are not uniform, it is more at the bottom section and the wall. This is because of gravity and centrifugal forces. 50 μm size particles are present at the center in small volumetric fraction, the concentration of large particles are negligible at the center region. Large particles are mostly seen at the bottom near the cone wall. Sha et al. (2001) have observed similar distribution in case of stirred tank crystallizer.

Fig. 4.36 shows volumetric concentration of solid particles at solution outlet increases with time for every size particles. The figure also depicts large particles volumetric concentration is higher than the volumetric concentration of smaller size particles.

Liquid velocity is an important factor for solid particles distribution; In Fig. 4.37 contours of liquid velocity are shown for every size particles and it is found that velocity is varying with particle size. Maximum liquid velocity in the crystallizer is found to be more for smaller size particle than the larger one.

4.4.2. Solid suspension in crystallizer at different flow rates

Study the effect of the inlet flow rate on the solid suspension characteristics is most important for the crystallizer design and operation. Fig. 4.38 shows solid suspension at different flow rates in FC crystallizer. The particles circulation area is expanded when the flow rate is increased. The small size particles 50 μm, are suspended well and circulating in the large area and their concentration is increasing with increase in the flow rate. In case of the large size particles, 500 μm and 900 μm, their volumetric concentration is negligible in upper and center region at low flow rate but with increase in flow rate their suspension area and concentration in upper region is increased. It means that the crystals with large size can be suspended well for growth at high flow rates. If the crystallizer operated at higher flow rate due to increase in particles holding time, large size crystals with uniform distribution can obtain. Zuoliang et al. (2008) using FB crystallizer for different flow rate have found that there is increase in solid suspension with increase in flow rate. They have also found that small size crystals are more distributed.

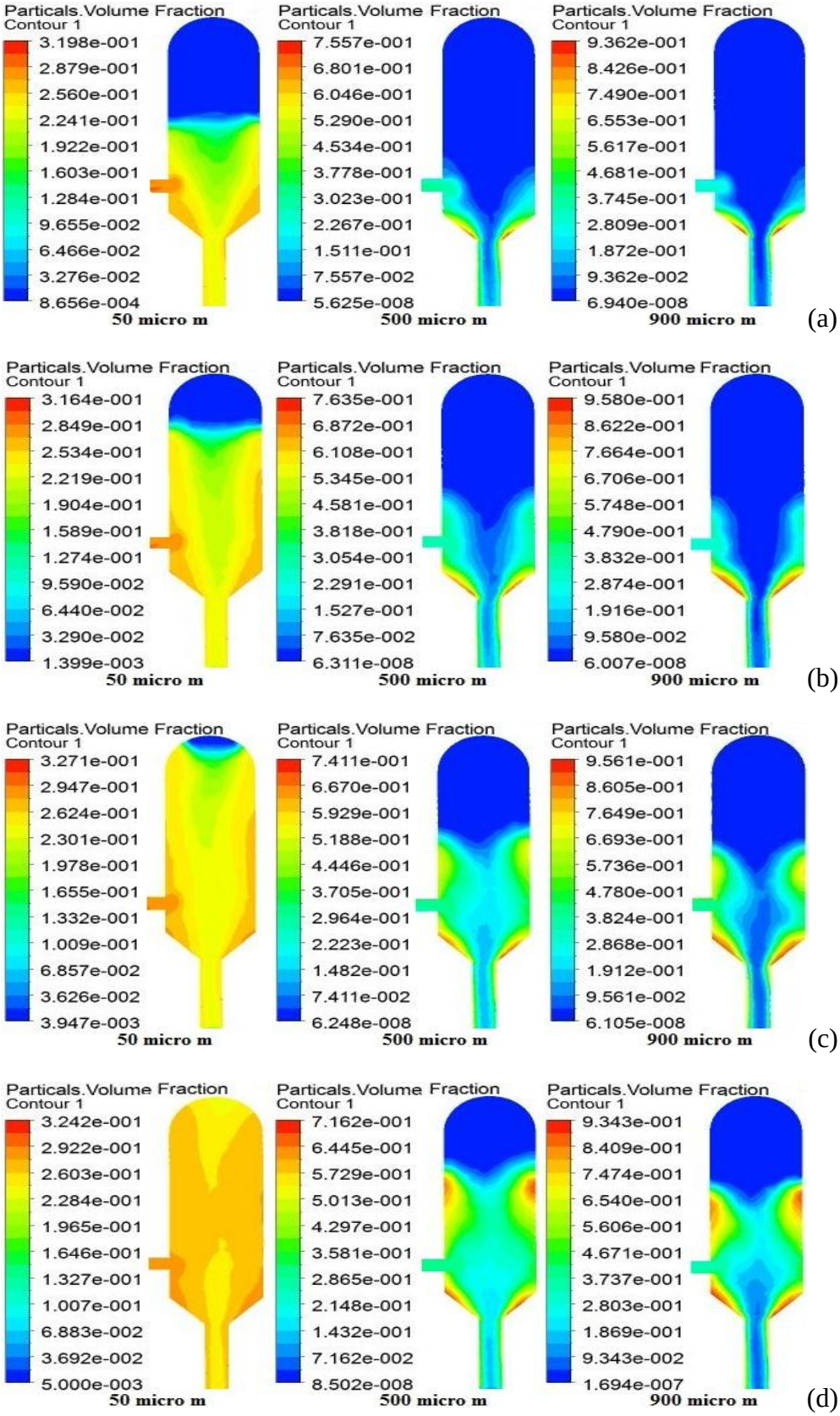

Fig. 4.38. Contours of volume fraction for different sizes particles and liquid mass flow rates (a) 27.5 kg/s, (b) 47.5 kg/s, (c) 67.5 kg/s and (d) 87.5 kg/s for inlet position of 0.5 m.

4.4.3. Solid suspension in crystallizer at different inlet positions

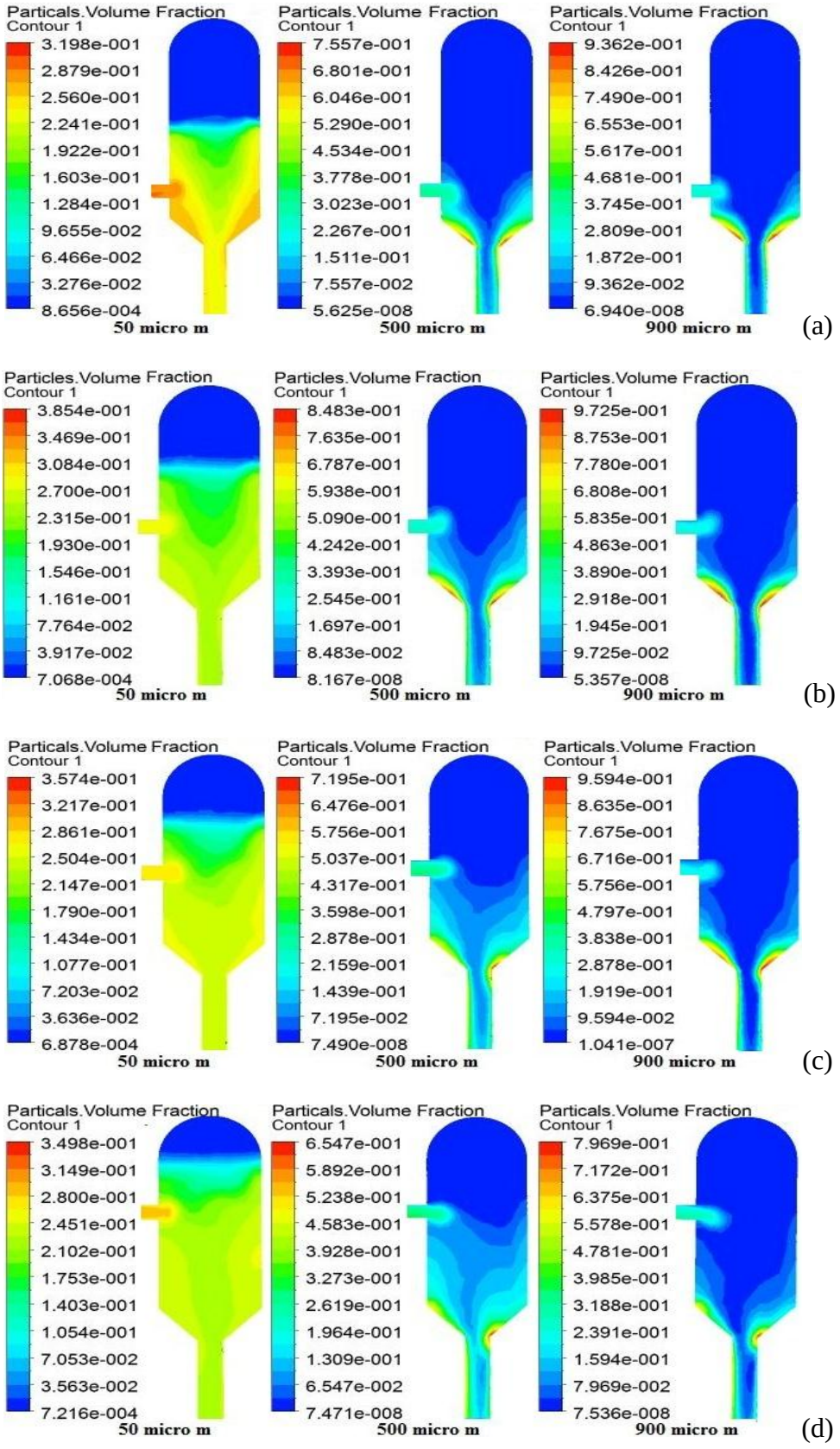

Fig. 4.39. Contours of volume fraction at different inlet positions and sizes of particles for liquid mass flow rate 27.5 kg/s at inlet positions; (a) 0.5 m, (b) 0.7 m, (c) 0.9 m and (d) 1.1m.

The effect of inlet position on solid suspension dynamics has been studied in the present work by varying inlet position at four levels. Fig. 4.39 shows volumetric concentration distribution for all three different sizes of particles at liquid mass flow rate of 27.5 kg/s for different inlet positions in FC crystallizer. It is found that with increase in inlet position there is better distribution of particles and there is increase in suspension level in the crystallizer. This is increases particles local circulation area and duration of stay in the crystallizer. The volumetric concentration distribution has become uniform for small size particles than for large size particles with same inlet height. The local circulation of the crystal results in more nucleation and affect the final product size (Zuoliang et al., 2008).

4.5. Population density

Using population balance model, population density study has been carried out for crystals of different sizes. The simulation results are shown in the form of line diagrams and contour plots. Fig. 4.40 shows crystals number density (number of crystals per unit volume of solution) for crystals of 5 different sizes and it is observed that for each size of crystal, the variation in number density is different. According to theory, in crystallization process small size crystals form early by nucleation in supersaturated solution at given temperature and by contact nucleation or surface growth they form large size crystals (Dutta, 2009). Similarly in the present work in Fig. 4.40 the quantity of large size crystals gradually increase with time. Number of smaller size crystals initially increase then decrease. Smaller the size of crystal less is the time period of increase in number density, this may be because in supersaturated solution initially by nucleation, large amount of tiny new crystals formed but after some time during growth of crystals, supersaturation decrease the solute mass transfer from solution for growth of large crystals so smaller sizes crystals start to dissolve to maintain supersaturation (Khanam, 2007). Also the decrease in the number density of smaller particles is because of conversion of smaller particles to larger ones during the crystallization process.

Crystal's **population density** (length density or population density function) is a function of crystal length that is described as; the number of particles per unit volume of concentrated solution per unit particle length (Ansys Fluent PBM, 2009).

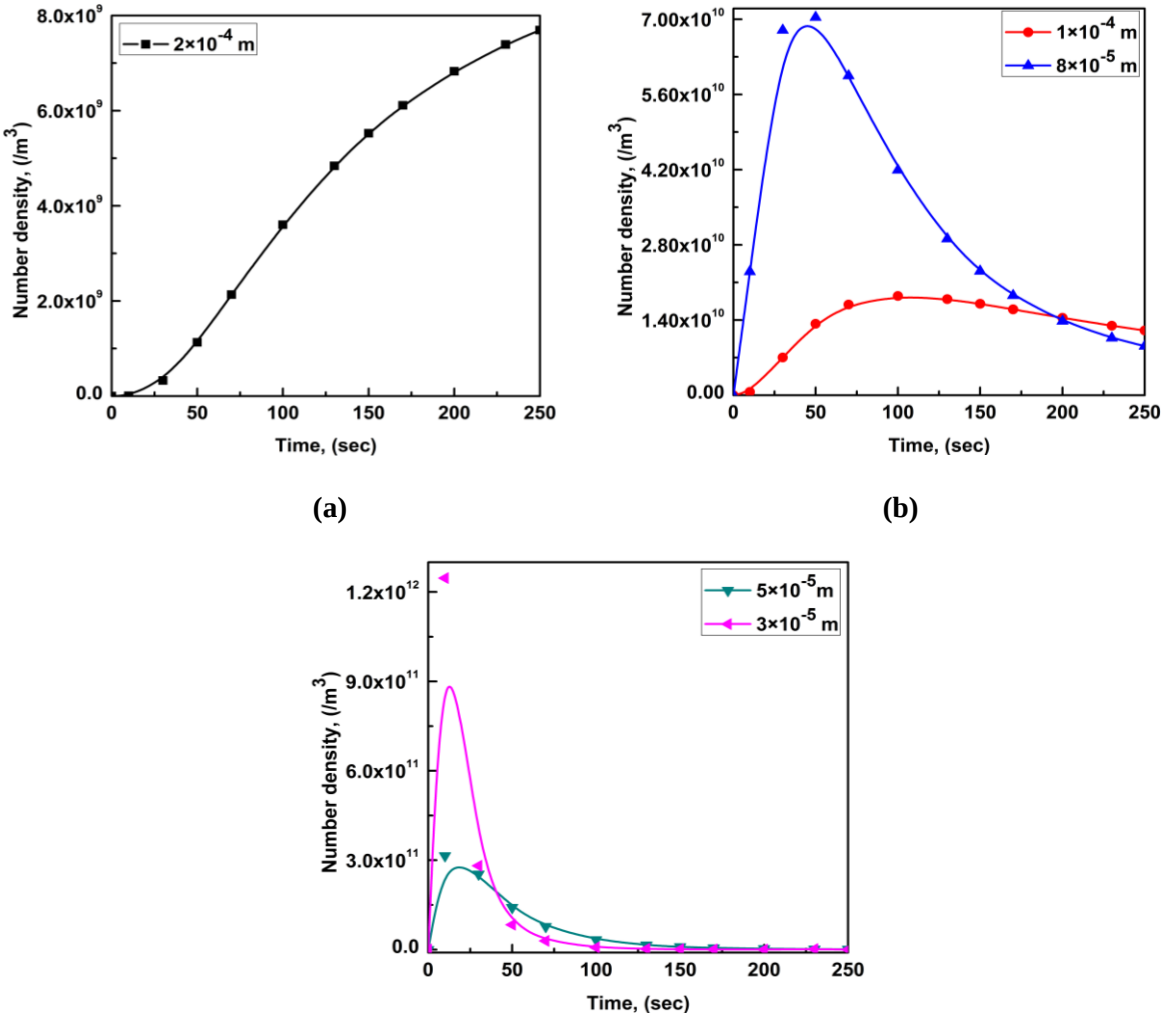

Fig. 4.40. Crystals number density in solution for crystals of different size, (a) 2×10^{-4} m, (b) 1×10^{-4} m and 8×10^{-5} m; and (c) 5×10^{-5} m and 3×10^{-5} m.

Fig. 4.41 shows the variation in population density of different size crystals with respect to time. Similar to the number density profile, the population density of large size crystals have been found gradually increase with time but for the smaller size crystals there is initial increase then decrease in population density is seen.

Fig.4.42 shows contours of crystals (product) volume fraction distribution for all sizes crystals and vapor volume fraction obtained from population balance model simulation. Formed (product) crystals are suspended in crystallizer and shows increase in volume fraction from top to the bottom. Vapor formed during crystallization is separating from solution and reaching the vapor outlet.

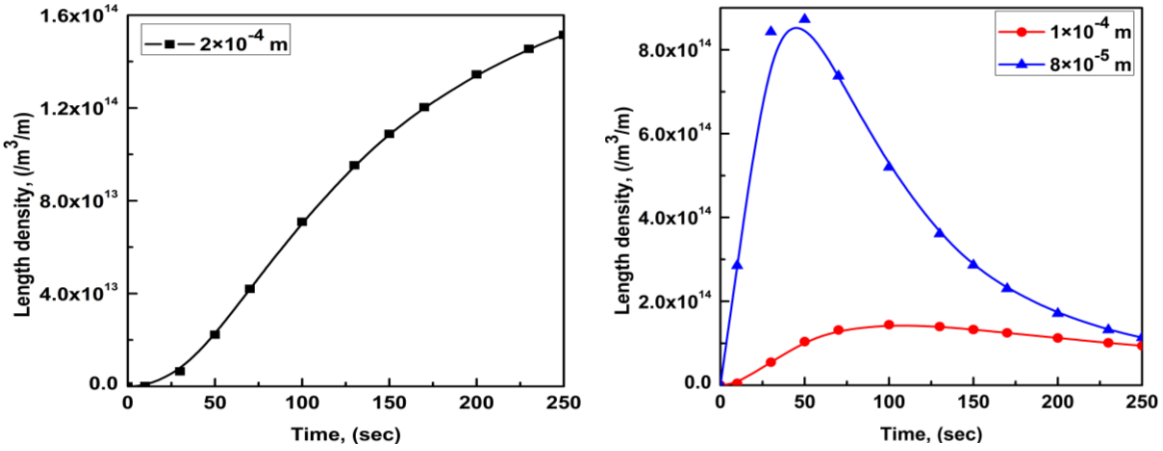

(a) (b)

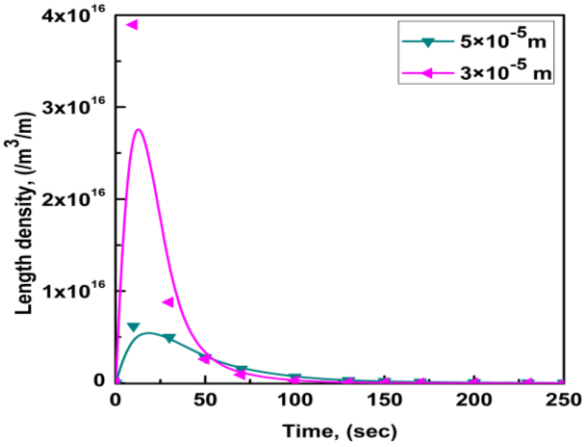

(c)

Fig. 4.41. Population (length) density of crystals in solution for crystals of different size, (a) 2×10^{-4} m, (b) 1×10^{-4} m and 8×10^{-5} m; and (c) 5×10^{-5} m and 3×10^{-5} m.

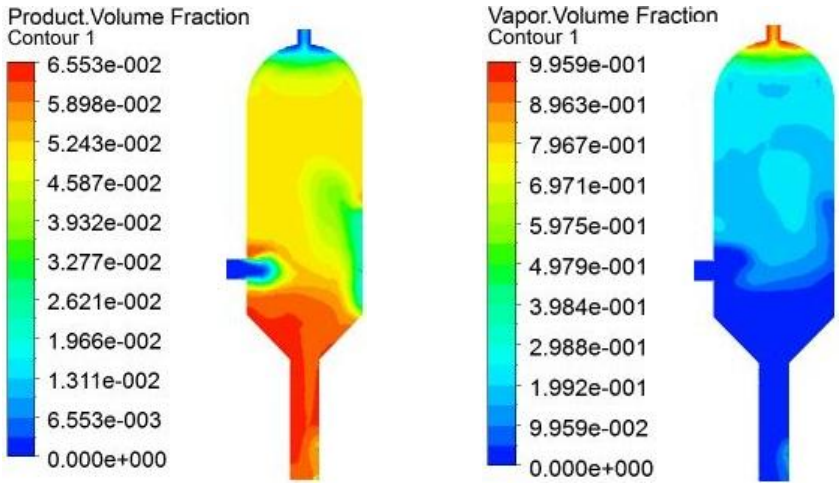

(a) (b

Fig. 4.42. Contours of (a) product volume fraction (b) vapor volume fraction at inlet position of 0.5 m.

Fig. 4.43 shows the co efficient of variance which is calculated by, (Zhang et al., 2009)

$$C.V. = \sqrt{\frac{\bar{m}_0 \bar{m}_2}{\bar{m}_1^2} - 1} \tag{4.1}$$

Where $\bar{m}_0, \bar{m}_1$ and $\bar{m}_2$ respectively as $\Sigma N_i L_i^0$, $\Sigma N_i L_i^1$ and $\Sigma N_i L_i^2$ (Ansys Fluent PBM, 2009)

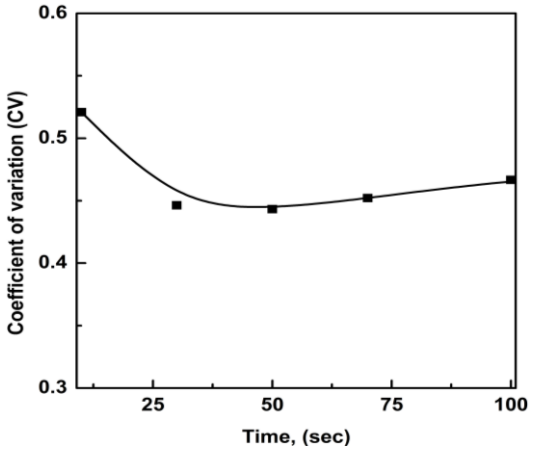

Fig. 4.43. Co-efficient of variation for crystal size 2×10^{-4} m.

The coefficient of variation (CV) is an important quality factor of crystals. CV of the crystal size is a measure of the spread of the size about the dominant crystal size. The larger the CV value the more is the 'spread' of the size distribution. For industrial crystallizers CV value lies between 30% and 50% (Dutta, 2009). Fig. 4.43 shows the CV value for crystal size 2×10^{-4} m is less than 50%.

Crystal growth is a layer by layer process and is occurred only at the face of crystal due to transport of solute from the bulk of the solution to that face (Perry, 2009). Growth of crystal is described as,

$$G = \lim_{\Delta L \to 0} \frac{\Delta L}{\Delta t} = \frac{dL}{dt} \tag{4.2}$$

where G is the growth rate over time interval t, (m/s).

The standard method of moments (SMM) is used, and the change in the mean crystal size with time is observed to characterize the growth of crystal. Fig. 4.44 shows change in mean crystal size and it is found that mean size is growing with time it is according to the theory that in supersaturated solution crystal size grows. Wei et al. 2001 have observed increase in mean crystal size in a semi-batch crystallizer.

To establish the relation of growth rate to the mean crystal size three different growth rates (1.8×10^{-8}, 2.6×10^{-8} and 3.3×10^{-8} m/s) have been used and for each growth rate, simulation has been carried out for 60 secs. Fig. 4.45 shows the variation of mean crystal size with growth rate. It is observed from the figure that with increase in growth rate the mean crystal size increases, which is obvious. This plot basically shows how the mean crystal sizes changes with growth rate.

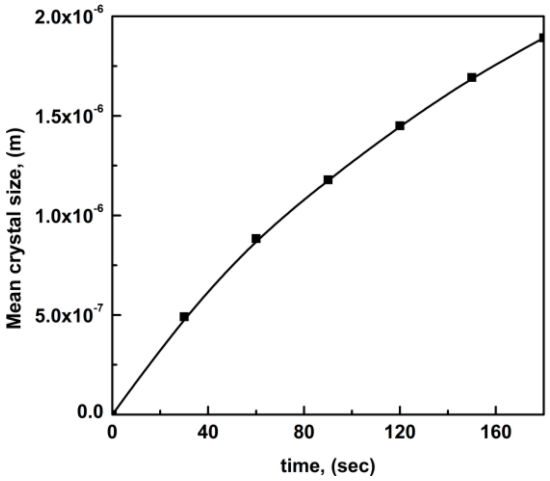

Fig. 4.44. Mean crystal size change with time.

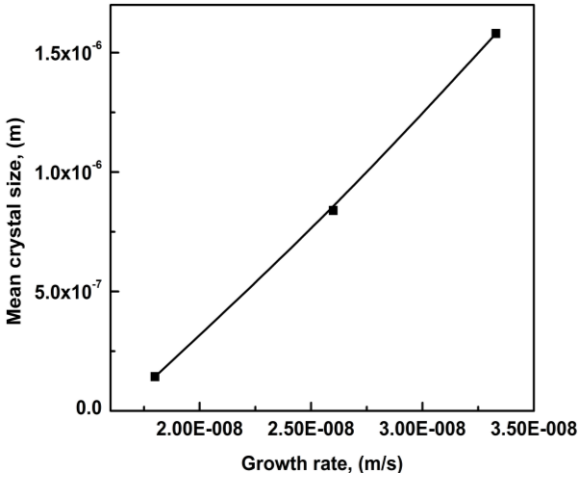

Fig. 4.45. Effect of growth rates on mean crystal size.

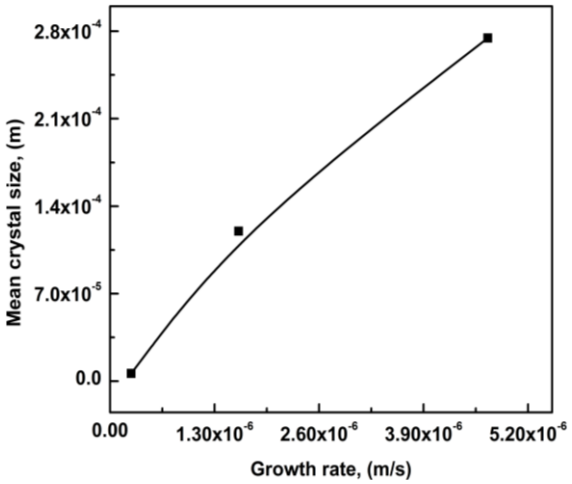

Fig. 4.46. Effect of growth rates 2.6×10^{-7}, 1.6×10^{-6} and 4.67×10^{-6} m/s on mean crystal size.

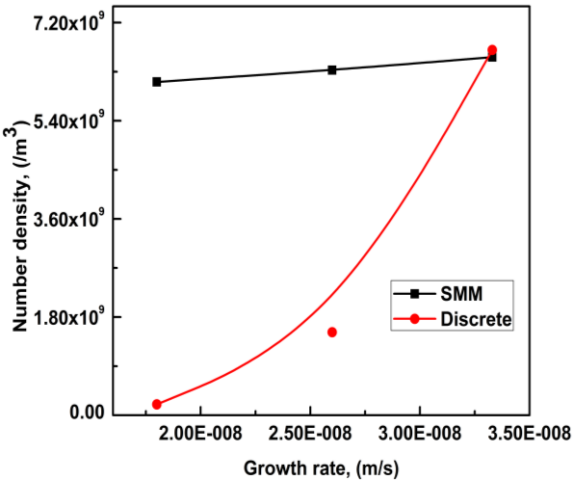

Fig. 4.47. Effect of growth rates 2.6×10^{-7}, 1.6×10^{-6} and 4.67×10^{-6} m/s on crystals.

Kramer et al. (2000) have carried out population density study for ammonium sulphate in FC crystallizer using compartmental method and simulation carried out in SPEEDUP simulation software package and found three different growth rates; 2.6×10^{-7}, 1.6×10^{-6} and 4.67×10^{-6} m/s at three different compartments of the crystallizer and found the mean

crystal size of 0.54 mm in the crystallizer. In the present work, simulation with the growth rates used by Kramer et al. (2000) has been done for NaCl system to find out the mean crystal size. From the simulation the maximum mean crystal size has been found to be 0.27 mm at growth rate of 4.67×10^{-6} m/s (Fig. 4.46). The difference in crystal size may be due to difference in the solubility of NaCl from ammonium sulphate.

The effect of different growth rates on crystals number density has been observed by using SMM and Discrete model (both methods used in population balance model). Fig. 4.47 shows variation of number density with growth rate obtained from the simulation using SMM and Discrete model. It is found that at low growth rates there is huge difference in crystals number density obtained by both the methods but at higher growth rate (3.3×10^{-8} m/s) the values are almost same. Again a difference may be observed at still higher flow rate. The Discrete method shows a very strong dependency of the number density on the growth rate, whereas the dependency in case of SMM is little.

CHAPTER-5

CONCLUSION AND FUTURE SCOPE

5.1. Conclusion

Computational studies have been carried out in the present work to understand hydrodynamics in isothermal and non-isothermal condition, solid volume fraction distribution, population density variation with time and mean crystal growth by using commercial CFD software Ansys Fluent 13 for Forced circulation (FC) evaporation crystallizer (height 2.13m and diameter 0.8m). The simulation has been carried out for different feed flow rates and inlet positions using different numerical models and different computational geometries. The outcome of the simulation has been summarized as;

Isothermal simulation; vapor volume fraction is more at center and solution volume fraction is more near the wall and both increase in there zone with increase in inlet flow rate and inlet height. Solution velocity magnitude is high near the wall (zero at the wall) at less at the center. The solution velocity is found to increase with inlet flow rate, which decrease slightly with elevation of inlet position. The maximum solution velocity is found to increase from 3.8 m/s to 9.374 m/s for increase in flow rate from 27.5 kg/s to 67.5 kg/s. The vapor and solution velocity magnitude is found to be same in the crystallizer. Pressure change is according to hydrostatic law, it increases with flow rate, the axial difference of solution static pressure is found to be more with at higher inlet height. Turbulence in flow field is found to increase with flow rate. The flow dynamics obtained from the present simulation differs from those obtained by Essemiani et al. (2004) for FC crystallizer. The reason may be because of tangential inlet in the present study to the radial inlet in the work of Essemiani et al. (2004).

Non-Isothermal simulation the vapor volume fraction gradually increases from feed to the top of the crystallizer and the vapor is completely separating from solution and free surface is formed. With increase in flow rate the vapor space shrinks due to increase in level of the solution, a vapor core is formed at the center which gradually extents to the solution outlet. With increase in inlet height the vapor space is found to shift upward. As obtained in case of isothermal simulation, here the solution velocity magnitude is high near the wall and less at the center, which increases with increase in flow rate and inlet height. Flow is observed more turbulent and non-uniform than the isothermal case.

Pressure is less in the upper region due to vapor phase occupying upper space. Pressure is found to increase with flow rate. The difference in solution static pressure also increases with increase in the elevation of inlet position. Solution temperature is more at the interface where phases separate. The solution temperature is found to decrease with increase in flow rate and the inlet position. Due to intense swirl flow free surface is not formed at higher flow rates and the magnitude of free surface deformation 7 cm (max.) which is less than that obtained by Essemiani et al. (2004).

Solid suspension, spatial distribution of particles are not uniform it is higher near the wall and low in center due to swirl motion. Particles of large size are less suspended than fines in the solution and the large sizes are present near the wall and in the bottom portion. Both flow rate and inlet position affect the suspension distribution in crystallizer. Better distribution of crystals is seen for higher flow rate of solution and its entry at a higher position.

Population density, at the beginning the population of crystals of size found to increase. After a while the population of smaller sizes decreases and larger sizes increase because of conversion of smaller crystals to larger ones and dissolution of smaller sizes to maintain supersaturation. The CV (co-efficient of variation) shows spread of the dominating crystal size distribution. For crystal size of 2×10^{-4} m it is less than 50% which is well within the range of industrial crystallizers (30% to 50%). It is observed that with increase in growth rate the mean crystal size and crystal number density both increases. At lower growth rates population density is different in case of SMM and discrete method but at higher flow rate studied they agrees, which seems to differ at still higher flow rate.

The simulation results show that the performance of FC crystallizer with tangential inlet is better than that with normal flow rate. The simulation successfully explains the behaviour of FC crystallizer.

5.2. Future scope

The future studies of this work may be;

- Variation in solution concentration to characterize viscous flow behaviour.
- Use of Lagrangian model for more exact description of particle flow.
- Crystallizer of different size may be studied to determine the effect of process scale.

- Using population balance model and UDF crystals growth and size variation may be studied.
- At different temperatures crystal growth may be observed for different components.

References

Al-Rashed, M., Wojcik, J., Plewik, R., Synowiec, P., & Kus, A., 2012. Multiphase CFD Modeling: Fluid Dynamics Aspects in Scale – up of a Fluidized - Bed Crystallizer. Chemical Engineering and Processing 63, 7-15.

Al-Rashed, M., Wojcik, J., Plewik, R., Synowiec, P., & Kus, A., 2009. Multiphase CFD Modeling-scale–up of a Fluidized - Bed Crystallizer. 19th European Symposium on Computer Aided Process Engineering, 695-700.

Ansys Fluent 12.0, 2009. Population Balance Module Manual. ANSYS, Inc. 7th main 1st block, Kormangala, Bengluru-560034, India.

Ansys Fluent 12.0, 2009. Theory Guide. ANSYS, Inc. 7th main 1st block, Kormangala, Bengluru-560034, India.

Ansys Fluent 12.0, 2009. User Guide. ANSYS, Inc. 7th main 1st block, Kormangala, Bengluru-560034, India.

Bamforth, A.W., 1965. Industrial Crystallization. The Grampian Press Ltd., 8-10 King Street, Hammersmith, London.

Bennett, R.C., 2000. Crystallization and Evaporation. The Engineering Handbook, CRC Press LLC, chapter -60, 1-18.

Bermingham, S.K., Kramer, H.J.M., Rosmalen, G.M.V., 1998. Towards On-Scale Crystalliser Design using Compartmental Models. Computers Chem. Eng. 22, 355-362.

Cubillas, P., Anderson, M.W., 2010. Zeolites and Catalysis, Synthesis, Reactions and Applications Vol.- 1. Wiley-VCH Verlag GmbH & Co. KGaA, Weinheim, Germany.

Dutta, B.K., 2009. Principles of mass transfer and separation processes. Prentice Hall Inc., 679-727.

Essemiani, K., Traversay, C.D., Gallot, J.C., 2004. Computational-fluid-dynamics (CFD) modelling of an industrial crystallizer: application to the forced-circulation reactor. Biotechnol. Appl. Biochem. 40, 235–241.

Ganesan, S., Tobiska, L., 2012. An operator-splitting finite element method for the efficient parallel solution of multidimensional population balance systems. Chemical Engineering Science 69, 59–68.

Gavhane, K.A., 2008. Mass transfer-IInd. 6th ed., Nirali Prakashan, 5.12-5.34.

GEA Messo, 2011. Crystallization in Theory and Practice. A company of GEA Group & member of GEA Evaporation & Crystallization, Friedrich-Ebert-Straße 134, Duisburg-47229, Germany.

GEA Process Engineering (India) Pvt. Ltd., 2013. Melt Crystallization. Block No.8, P.O. Dumad, Savil Road, Vadodra, India.

Geankoplis, C.J., 2007. Transportation process, separation process principles. 3rd ed., Prentice Hall Inc., 743-829.

Heath, A.R., Livk, I., 2006. Coupled Population Balance and CFD Model for a Continuous Gibbsite Crystalliser. 5th International Conference on CFD in the Process Industries CSIRO, Melbourne, Australia.

Jena, H.M., 2010. Hydrodynamics of Gas-Liquid-Solid Fluidized and Semi-Fluidized Beds. Ph.D. Thesis, National Institute of Technology, Rourkela.

Jones, A., Rigopoulos, S., Zauner, R., 2005. Crystallization and Precipitation Engineering. Computers and Chemical Engineering 29, 1159–1166.

Khanam, J., 2007. Crystallization-Pharmaceutical Engineering. Department of Pharmaceutical Technology Jadavpur University Kolkata-700032, India.

Kirk-Othmer Separation Technology Vol.-1, 2008. 2nd ed., Wiley. John Wiley & Sons, Inc., 632-685.

Kramer, H.J.M., Dijkstra, J.W., Verheijen, P.J.T., Rosmalen, G.M.V., 2000. Modeling of Industrial Crystallizers for Control and Design purposes. Powder Technology 108, 185–191.

Kougoulos, E., Jones, A.G., Wood-Kaczmar, M.W., 2006. A Hybrid CFD Compartmentalization Modeling Framework for the Scaleup of Batch Cooling Crystallization Processes. Chemical Engineering Communications 193, 1008-1023.

Leeuwner, M.J., Eksteen, J.J., 2008. Computational fluid dynamic modelling of two phase flow in a hydrocyclone. The Journal of the Southern African Institute of Mining and Metallurgy 108, 231-236.

McCab, W.L., Smith, J.C., Harriot, P., 2005. Unit Operations of Chemical Engineering. 7th ed., McGraw-Hill Companies, 929-963.

Mahdi, K.A., Al-Rashed, M.H., Alsairafi, A.A., Wójcik, J., 2009. CFD simulation of a Conical-Cylindrical crystallization unit using Multi-Phase Eulerian Model. 7th International Conference on CFD in the Minerals and Process Industries CSIRO, Melbourne, Australia.

Mersman, A., 2001. Crystallization Technology Handbook. 2nd edi., Marcel Dekker, Inc., 270 Madison Avenue, New York-10016, USA.

Moyers (Jr.), C.G. and Rousseau, R.W., 2009. Handbook of Separation Process Technology. John Wiley & Sons Inc., 578-641.

Perry, R.H., 2009. Perry's chemical engineer's handbook. 8th ed., McGraw-Hill Companies, chapter-18, 39-58.

Plewik, R., Synowiec, P., Wojcik, J., Kus, A., 2010. Suspension flow in crystallizers with and without hydraulic classification. Chemical Engineering Research and Design 88, 1194–1199.

Rein, P.W., Echeverri, L.F., Acharya, S., 2004. Circulation in Vacuum Pans. Journal American Society of Sugar Cane Technologists 24, 1-17.

Rielly, C.D., Marquis, A.J., 2001. A particle's eye view of crystallizer fluid mechanics. Chemical Engineering Science 56, 2475-2493.

Rodriguez, R., Wójcik, J., 2011. Modeling Of Starting Up Fluidized-Bed Crystallization Using Population Balance CFD Module. Department of Chemical and Process Engineering, Silesian University of Technology, Poland.

Seader, J.D., Henley, E.J., Roper, D.K., 2011. Separation Process Principles Chemical and Biochemical Operations. 3rd ed., John Wiley & Sons, Inc., 644-694.

Sha, Z., Oinas, P., Louhi-Kultanen, M., Yang, G., Palosaari, S., 2001. Application of CFD simulation to Suspension crystallization-factors affecting size-dependent classification. Powder Technology 121, 20–25.

Sun, Z., Li, Z., Sun, Z.Y., Song, F., Li, P., Wang, J., Yu, G., 2011. Study on Crystallization Process in an Industrial Continuous Draft Tube Baffle using. East China University of Science and Technology, Shanghai, China.

Svanoe, H., 1940. "Krystal" Classifying Crystallizer. Industrial and Engineering Chemistry 32, 636-639.

Swenson Technology, Inc., 2013. 26000 Whiting Way Monee, IL 60449-8060 USA.

Tangtonsakulwong, J., Flood, A., Chitsomboon, T., 2006. Flow Fields in a Mixed-Suspension Mixed-Product-Removal Crystallizer: A Numerical Analysis. Science Asia 32, 231-239.

Tavare, N.S., 1994. Mixing, Reaction and Precipitation: An Interplay in Continuous Crystallizers. Chemical Engineering Science 49, 5193-5201.

Veoila water solutions & technologies, 2013. L'Aquarena 1 place Montgolifire-94417, Maurice, France.

Wang, B., Xu, D.L., Xiao, G.X., Chu, K.W., Yu, A.B., 2003. Numerical study of gas-solid flow in a Cyclone separator. 3rd International Conference on CFD in the Minerals and Process Industries CSIRO, Melbourne, Australia, 371-376.

Wantha, W., 2006. Computational Fluid Dynamics Simulation of a DTB Crystallizer, Master of Engineering Thesis, Suranaree University of Technology, Thailand.

Wei, H., Zhou, W., Garside, J., 2001. Computational Fluid Dynamics Modeling of the Precipitation Process in a Semibatch Crystallizer. Ind. Eng. Chem. Res. 40, 5255-5261.

Wohlk, W., Hofmann, G., 1987. Types of crystallizers. International Chemical Engineering 27, 197-204.

Wojcik, J., Plewik, R., 2009. Hydrodynamic modeling of fluidized-bed crystallizers with use of the multiphase CFD method. Chemical Engineering and Processing 48, 1527–1533.

Zahra, L.T.J.P., 2012. CFD Modelling of the Behaviour of a Cylindrical Miniature Hydrocyclone. Ph.D. Thesis, University College - UNSW Australian Defence Force Academy School of Engineering and Information Technology, Australia.

Zheng, Q., Mao, Z.S., Yang, C., Zhao, C., 2006. Computational Fluid Dynamics Approach to the Effect of Mixing and Draft Tube on the Precipitation of Barium Sulfate in a Continuous Stirred Tank. Chinese J. Chem. Eng. 14, 713-722.

Zhu, Z., Wei, H., 2008. Flow Field of Stirred Tank used in the Crystallization Process of Ammonium Sulphate. Science Asia 34, 097-101.

Zuoliang, S., Qianqian, Z., Shouxiang, W., 2008. Study with Fluidized Bed Crystallizer with CFD simulation. Tianjin Key Laboratory of Marine Resources and Chemistry, Tianjin University of Science and Technology, 13th. Avenue, TEDA, Tianjin, China, 300457.

BIO-DATA

Name	Anis Bakhsh
Date of birth	26.05.1987
Permanent Address	In-front of Hind Tant House, Near of Bus Stand, Chhoti-Badoni Dist. Datia (M.P.), Pin code - 475686
E-mail ID	anis26bakhsh@gmail.com
Languages Known	Hindi, English

EDUCATIONAL QUALIFICATION

Examination	Discipline/ Specialization	School/college	Board/ University	Year of Passing	Percentile
M. Tech (Research)	Chemical Engineering	NIT Rourkela	National Institute of Technology Rourkela	2013	8.51 (CGPA)
B.E.	Chemical Engineering	IES, IPS Academy, Indore, M.P.	RGTU Bhopal	2010	62.34
HSSC	Maths, Physics, Chemistry	Govt. H.S. School Badoni, Dist. Datia, M.P.	Board of Secondary Education, M.P.	2005	62
HSC		Govt. H.S. School Badoni, Dist. Datia, M.P.	Board of Secondary Education, M.P.	2003	81

PROJECT DETAILS

M. Tech (Research)

- Modeling and Simulation of Forced Circulation Evaporation Crystallizer.

Conference

- Anis Bakhsh, H. M. Jena. Accepted paper “CFD analysis of hydrodynamic behavior in FC crystallizer” in “International Conference on Powder, Granule and Bulk Solids: Innovations and Applications”. November 28-30, 2013, Thapar University, Patiala, India.

NATIONAL INSTITUTE OF TECHNOLOGY
ROURKELA, ODISHA